Supercritical (and Subcritical) Fluid Behavior and Modeling: Drops, Streams, Shear and Mixing Layers, Jets and Sprays

Josette Bellan

Jet Propulsion Laboratory

California Institute of Technology

4800 Oak Grove Drive

MS125-109

Pasadena, CA 91109

josette.bellan@jpl.nasa.edu

Tel: (818) 354 6959

Fax: (818) 393 5011

October 20, 1999

Abstract

A critical review of recent investigations in the realm of supercritical (and subcritical) fluid behavior is presented with the goal of obtaining a perspective on the peculiarities of high pressure observations. Experiments with drops, isolated or in groups, streams, shear and mix-

ing layers, jets and sprays are tabulated and discussed as a precursor to forming a conceptual picture of fluid comportment. The physics of fluid behavior in the supercritical and subcritical regimes is discussed, and major differences between the observations in these two regimes are identified and explained. A variety of supercritical fluid models is then examined in the context of drop studies, and salient aspects of fluid behavior are identified. In particular, a model that has been validated with microgravity drop experiments is described and summarized; in this validated model, the differences in subcritical/supercritical comportment are interpreted in terms of lengths scales and it is this difference that is responsible for the traditional Lewis number expression no longer portraying the ratio of heat to mass transfer in supercritical fluids; instead, an effective Lewis number is recommended that gives a realistic estimate of the ratio of these length scales. Furthermore, the application of various fluid models to the description of supercritical fluid in various geometric configurations is discussed for conditions relevant to liquid rocket, Diesel and gas turbine engines. Such preliminary simulations performed with the validated fluid model have already reproduced some specific experimental features of supercritical fluid jet disintegration. Finally, comments are offered regarding future areas of research.

Contents

1 Introduction

Supercritical fluids are involved in numerous aspects of natural or industrial situations related to energy production or transfer. According to classical thermodynamic theory [1], a fluid is in a supercritical state when it is at a pressure **or** temperature exceeding its critical value; the value of the pressure, p, temperature, T, or molar volume, v, divided by its corresponding critical value (subscript c) is called the 'reduced' (subscript r) value. **When** $p_r > 1$ or $T_r > 1$, in the (p, T) plane

there is no longer the possibility of a two phase (i.e. gas/liquid) region and instead there is only a single-phase region [2]. The general term for the substance is fluid (neither a gas nor a liquid) and it is in a supercritical state. In the realm of natural situations, oil in underground reservoirs or volcanic lava are both supercritical fluids. In the realm of industrial processes, liquid rocket, Diesel or the new generation of gas turbine engines, all operate at supercritical conditions for the injected fuel. Although in all above examples the fluids are at supercritical conditions, the oil and lava have very different behavior than fuels in engines; this is because the natural and industrial examples above represent two extremes of supercritical fluids, the former having a high and the latter having a small molar volume. In this paper we will address only the behavior of fluids having small molar volume under supercritical conditions, although from the modeling point of view, providing that the equation of state (EOS) is correct, the same conservation equations can be used independently of the value of the molar volume.

Since most human experience is with atmospheric conditions phenomena, the physics of supercritical fluids is not intuitive. These fluids exhibit characteristics resembling both liquids and gases [3] in that they may have liquid-like densities but gas-like properties. The importance of using correct fluid properties is shown in Table 1 listing the percent difference in the thermal conductivity of fluid propane compared to that of the liquid at the same temperature. The calculations were performed using the plotted values of Reid et al. [3] (Fig. 10-5). Following the procedure for calculating conductivities at large p_r's knowing the conductivity at the same T_r but at a lower p_r (American Petroleum Institute [4], procedure 12A4.1), one can see that the difference increases with increasing p_r and T_r, that is with increased pressure and fluid heating.

Previous extensive reviews of supercritical studies (e.g. [5]) focussed primarily on experimental observations of hydrocarbon drops, and few details of modeling aspects were discussed; moreover, since no validated first-principles models of supercritical fluids were available, the reviews tended to be non-judgemental as to the effectiveness of the models in portraying reality, and therefore of

limited usefulness to the novice reader. The present review has a different emphasis in that both experiments (that are not necessarily restricted to drops) and theory are discussed to a similar extent, and a variety of species combinations including the LO_x/H_2 system (which is of practical importance in rocket propulsion) are analyzed. It turns out that because of the special thermophysical properties of the LO_x/H_2 combination, supercritical phenomena in this system tend to be enhanced, and the reason for it will be explained. Furthermore, given the recent success in first-principles modeling of both supercritical and subcritical fluids with the same formulation, one is now in a position to evaluate the necessary ingredients for obtaining an accurate theory of supercritical fluids, and thus to provide guidance to the novice reader.

This paper is organized as follows: First, the phenomenology of supercritical versus subcritical behavior is presented by examining observations of drops, shear layers, jets and sprays. Then, an extensive review of models from the last decade is performed with the goal of extracting the essence of the physics in each of the two regimes. A promising model is identified that has been validated with data over a significant range of (p, T), and its success is traced to the correct transport matrix, as well as to accurate EOS and transport properties. The implications of this model are discussed, and its preliminary application to the modeling of fluid disintegration is examined. Finally, in the concluding section the progress in the understanding of supercritical fluid behavior is summarized and comments on new avenues of research are offered.

Owing to the fact that the critical locus is a function of (p, T, Y_i) where Y_i is the mass fraction of species i, in this entire paper "subcritical" and "supercritical" refers to the situation with respect to the critical point (primarily the pressure) of an individual fuel species, and in the case of mixtures the reference is the fuel with the lowest critical pressure.

2 Experimental observations

Classical thermodynamics provides guiding rules (that are a consequence of the definition based on p_r and T_r) to differentiate between the subcritical and supercritical states. For example, it is well known that both the surface tension and the latent heat, being manifestations of the two phase regime, become null at and past the critical point [1]. In the supercritical regime, solubility effects become important and the heat of solvation becomes the relevant thermodynamic quantity for fluid interpenetration [1]. For this reason, a very precise semantics will be used in this entire review to remedy some of the inappropriate terminology used by habit in the literature. A special case is the appellation of "evaporation constant" or "evaporation rate" used indiscriminately under subcritical and supercritical conditions. Under true supercritical conditions there cannot be evaporation since the latent heat is null, and a surface cannot exist; therefore, the term "emission rate" and "emission constant" which are of more general meaning will be used here instead, with the understanding that in the subcritical regime the meaning is that of the classical terminology ('evaporation') which will be interchangeably employed.

Another thermodynamic fact is that the heat capacity at constant pressure becomes very large in the transcritical regime [1], this being an indication of the critical point being a singularity. It is also known that the critical point of a mixture is a function of the mixture fraction [1], [4], and that the critical locus (the ensemble of the critical points as a function of the mixture fraction) may be a nonmonotonic and convoluted curve [4], [1], according to the species in the mixture.

For many years it was assumed that because one can optically identify drop-like entities in the vicinity of fluid jets injected into surroundings at supercritical conditions (for the injected fluid), the injected fluid that was liquid under atmospheric conditions must remain liquid in the chamber (e.g. Mayer et al. [6]). This is a misconception since in fact optical measurements detect any large change in density (density gradients). Thus, the density ratio may be well below the $O(10^3)$

that characterizes its liquid/gas value, but the measurement will still identify a change in the index of refraction providing that the change is sudden (steep gradients). As shown by simulations of supercritical fluids (see Harstad and Bellan [7]), the density gradients may remain large during the initial stage of two supercritical fluids mixing, thus making them optically identifiable. Therefore, there is no inconsistency between the optical observation of 'drops' and 'ligaments' and the fluids (injected and surrounding) being both in a supercritical state. Another misconception is that data obtained with suspended drops immersed in surroundings at supercritical pressures are indicative of supercritical fluid behavior. This ignores the fact that suspended drops may have a surface tension, and this may be indicative of the drop fluid being vitiated at the location of contact with the suspending fiber, presumably due to the enhanced solubility (of the surrounding fluid) with increasing pressure; this would be evidence that the mixture at the point of contact between drop and fiber is subcritical rather than supercritical. Other physical mechanisms for the drop staying suspended on the fiber would be adhesion and wetting. None of these various possibilities has been discussed by experimentalists, and it is therefore difficult to fully understand the physics of drop suspension.

In the following, both drop and jet/spray experiments are considered because the information they provide supports the same conceptual picture which can then be used with some confidence as the baseline for building appropriate models. The experiments discussed here are listed in Table 3 in alphabetical author order, and are limited to experiments that were deemed to be relatively 'simple' so as to lead to as uncontroversial interpretation as possible. Therefore, experiments performed with multicomponent fuels (such as Diesel or liquid propellant gun fuels) in practical devices where there are many competing phenomena, although providing valuable information for other purposes, were either eliminated from or only succinctly presented in the present discussion. Similarly, not discussed are investigations focussing on drop ignition because the present review does not attempt to include any detailed high pressure, high temperature hydrocarbon chemistry as it is currently in infancy;

for the same reason, there will be only very limited discussions of high pressure microexplosion investigations.

2.1 Fluid drops

Existing single component high pressure experiments with fluid drops may be categorized in either evaporation/emission or combustion experiments, and further into normal or microgravity observations. From the point of view of understanding high pressure fluid physics, the advantage of evaporation/emission over combustion experiments is that the environment of the drop is easier to characterize since the surrounding pressure and temperature are known, being set by the observer. In contrast, in combustion experiments, unless the temperature of the flame (assuming to coincide with that of OH radical, although as discussed below, this could be questionable) region is provided, it is impossible to assess the environment of the drop and thus to infer accurate boundary conditions. None of the combustion studies reviewed in Table 3 provide such a measurement, and thus quantitative comparisons between those sets of data and simulations are currently impossible since kinetics of high pressure hydrocarbon reactions are currently unknown, and thus cannot be numerically simulated. However, high pressure combustion experiments can be valuable in providing qualitative trends that can be evaluated once the understanding from evaporation/emission observations is understood. Similarly, high pressure data obtained in microgravity is preferable to normal gravity data since buoyancy effects are minimized. However, microgravity data is not free of buoyancy effects as shown by Vieille et al. [8] who plotted the Grashof number, $Gr = (gd^3\rho^2/\mu^2)(\Delta T/T)$ versus pressure, where g is the gravitational acceleration, d is the drop diameter, T is the arithmetic mean temperature between the flame and the ambient temperature, ΔT is the difference between these two temperatures, ρ and μ are calculated at T, at the ambient pressure and at the composition of the ambient gas (since it is found that most of the induced fluid motion occurs outside the flame region). These plots show that for microgravity levels (i.e. g/g_0, where g_0 is the

normal gravity) of $10^{-2}, 10^{-4}$ and 10^{-6} one finds at a pressure of $\sim 10MPa$, $Gr = O(10^4), O(10^2)$ and $O(1)$, respectively. This means that in the context of high pressure physics even microgravity data must be interpreted with caution since it may also harbor buoyancy effects.

2.1.1 Microgravity emission/evaporation observations

The studies of Sato [9] and Nomura et al. [10] represent two unique examples of emissive observations in microgravity. Heptane drops of $0.7 - 1mm$ diameter were suspended from a $200\mu m$ fiber in a nitrogen environment and optical data was interpreted to yield the drop radius under the conditions listed in Table 3, encompassing both the subcritical and supercritical regime. Thus, the drop history was documented as a function of time, and it was observed that with increasing pressure the drop heat up time increases leading to the d^2 curve exhibiting increasing departures from the linear d^2 variation. In fact, in order to interpret and organize the data, Nomura et al. [10] felt compelled to correct the drop lifetime by subtracting the heat up period. When this was done, it was found that the drop lifetime decreased with the ambient temperature at all pressures, but that the dependence on pressure was different according to the range of temperatures: above $T_r \sim 1.2$, the lifetime decreased monotonically with pressure, while below ~ 0.8 the lifetime increased with pressure. The authors additionally suggest that there might be a temperature at which the drop lifetime is independent of the pressure. It should be pointed out that similar experiments were performed by Sato [9], however, the extensive parametric range of Nomura et al. [10] was not duplicated, except in normal gravity (see below). Qualitatively, Sato's results in the same parametric range are similar to Nomura's except that instead of an increasing lifetime with pressure at low T_r, a maximum is found in the supercritical vicinity of the critical pressure. Since Sato's additional normal gravity experiments were duplicated by other investigators (see below), providing credibility to his experimental method and setup, the speculation is that the difference between Nomura et al. 's and his results is due to buoyancy effects that become larger with increasing pressure (scaling as

p^2); these effects augment the emission rate which may the cause of the reduction in the lifetime at larger pressures and low temperatures.

It should be noted that even microgravity data must be interpreted cautiously. First, as discussed above, buoyancy effects may have persisted at the microgravity level of the experiments. For example, Nomura et al. [10] cite the average gravity of $10^{-2}g_0$ for parabolic flights and $10^{-3}g_0$ for drop towers during their experiments, but the time variation of this ratio is not provided. Since the emission rate is higher at the beginning of the experiment when the drop is larger, initial buoyancy effects may disproportionately influence the experiment. Moreover, Morin [11] recently calculated the influence of a $200\mu m$ suspending fiber on a drop temperature and found that it increases with increasing temperature or pressure; for drops of 1 mm diameter at 300 K, the heat flux from the fiber may be $\sim$ 7% and 10% of the heat provided by the surrounding nitrogen at 473 K and 0.1 MPa, and 673 K and 1 MPa, respectively. Despite these possible difficulties in interpretation, Nomura et al. 's and Sato's emission microgravity data remain a very valuable tool in assessing model validity because they represent the easiest interpretable situation that has experimentally been achieved so far.

2.1.2 Normal gravity emission/evaporation observations

Single component drops Early interest in single-drop high-pressure, supercritical experiments prompted investigators to perform studies in normal gravity and to interpret the emission rates thus obtained using various correlations developed under atmospheric conditions. For example, Brzustowski and Natarajan [12] find that 3 mm initial diameter aniline drops generally emitted according to the d^2- law at low pressures, but that the data became increasingly difficult to fit in this manner with increasing pressure. Parasitic buoyancy effects increased with pressure and it was difficult to determine whether the increased emission constant (the slope of d^2) at fixed ambient temperature was the result of the thermodynamics or the fluid mechanics (through buoyancy), or

of a combination of both. Observations of cold C_5H_{12} drops in mixtures of $O_2 - N_2$ or $O_2 - He$ at supercritical pressures are also mentioned by Natarajan and Brzustowski [13], however, the emphasis of that work being on combustion and on the derivation of Nusselt number correlations for heat and mass transfer, the details of the emission observations are not provided.

Savery [14] performed a series of high pressure experiments with water, Freon-13 and heptane drops in convective air at reduced pressures as large as 3.67 and observed that the quasi-steady drop temperature easily observable at low pressures is no longer observed at moderate ambient gas temperatures and reduced pressures grater than 1.5. This indicated that quasi-steady theories are no longer valid at supercritical pressures, a fact that is by now well established. Instead of the quasi-steady temperature, Savery [14] remarked a steadily increasing Freon-13 drop temperature that correlated well with the critical temperature of the mixture at the drop interface in the range of 1.5-1.8 reduced pressures (with respect to Freon-13). This steadily increasing drop temperature is consistent with the drop no longer being liquid, and therefore its temperature no longer being limited by the boiling point.

Some of the earliest suspended drop experiments were performed by Matlosz et al. [15] with C_6H_{14} drops emitting in N_2 or Ar at $p_r = 0.23 - 3.73$ at an ambient temperature of 548 K, with droplets in two diameter ranges, 0.72 - 0.91 and 1.42 - 1.78 mm. Drop temperatures and residual drop radii plotted on the same graph as a function of time showed that with increasing pressure the drop temperature becomes more elevated and does not reach a steady-state condition as it did at subcritical conditions; this unsteadiness is accompanied by a faster drop emission, as indicated by the reduced drop size at fixed time. Experiments performed in N_2 and Ar gave essentially the same qualitative result, however, since the pressures used in the two sets of experiments were not the same, it is difficult to draw conclusions regarding the supercritical emission time dependence on ambient fluid properties.

Suspended 1 mm C_7H_{16} drops in N_2 were examined by Sato [9] and the emission constant

was calculated from the d^2 plots at different T_r (with respect to C_7H_{16}) ranging from 0.55 to 1.4. When illustrated as a function of p_r, the emission constant exhibits a minimum in the supercritical vicinity of the critical pressure at T_r up to 0.8, but past this level the emission constant increases monotonically with pressure and furthermore, displays a rapid increase past the critical temperature. These observations were not physically explained, but were used to propose that the emission rate becomes maximum at a pressure exceeding that of the critical point, and that this point of maximum emission rate occurs at decreasing pressures with increasing ambient temperature. The observations of Chauveau et al. [16] for C_7H_{16} drops in air up to $p_r = 3.26$ and of Morin et al. [17] for C_7H_{16} drops in N_2 confirmed Sato's findings that the drop lifetime at $T_r < 1$ reaches a maximum in the supercritical vicinity of the critical pressure, and that it continuously decreases with pressure at $T_r > 1$. Methanol [18] emitting in dry air was found to behave similarly, and Chauveau et al. [18] speculated that this nonmonotonic dependence is due to the combined effects of the decreasing diffusivity with increasing pressure, thereby accumulating vapor near the drop surface and hindering emission, and to that of the increasing boiling point with pressure, thereby allowing the drop temperature to increase and reducing the heat transfer from the ambient to the drop.

The experiments of Chesnau et al. [19] with suspended LO_x drops in stagnant air, nitrogen or helium were all performed at subcritical conditions, but they are mentioned here both because of the present interest in LO_x, and also because the minimum in the emission constant with increasing pressure at low temperatures was not detected; instead, the emission constant continuously increased with pressure. However, the authors remark that their experiment was performed at supercritical rather than subcritical temperatures, and that for supercritical temperatures Sato [9] also found a monotonically increasing emission constant. Diagrams of d^2 for small reduced pressures [19] conformed to the linear d^2 variation, however, it was detected that the fiber seemed to have a strong influence on small drops whereas large drops suffered from strong buoyancy effects. Therefore, the

author's statement that the emission rate is strongly enhanced with increasing pressure should be considered as including all possible phenomena (not only thermodynamics) occurring at higher pressure and influencing drop emission. The authors' suggestion that the product ρD, where D is the binary diffusion coefficient, may no longer be constant under high pressure conditions is supported by the calculations of Harstad and Bellan [7] for the LO_x/H_2 system. Liquid oxygen drops in helium, and water and methanol drops in air behind shock waves were also studied by Anderson et al. [20], however, because the ambient temperature was not monitored, the results cannot be interpreted or compared with other observations or simulations.

Multicomponent drops The recent experimental observations of Stengele et al. [21] are unique in that binary fuel emission data is acquired and is compared with that obtained from single component drops of each species (C_5H_{12} and C_9H_{20}) entering the mixture. The two binary fuels considered were complementary in that the first component of the second fuel had the second component of the first fuel initial value of the mass fraction (mixture 1: $Y^0_{pent} = 0.3, Y^0_{non} = 0.7$; mixture 2: $Y^0_{pent} = 0.7, Y^0_{non} = 0.3$). The results are unfortunately plotted as a function of the distance travelled in the chamber and are thus difficult to interpret and inconclusive. For example, it is shown that for mixture 1 the drop velocity versus the distance decreases with increasing pressure, but so does the drop diameter; since in a higher pressure experiment the drop would take longer to arrive at a given location, the shorter distance travelled before disappearance does not necessarily imply that its emission is faster; a similar problem is encountered for data obtained for two different drop sizes of the same mixture. The situation becomes even more uncertain for mixture 2 for which drop velocities curves versus the distance at two different temperatures cross while the higher drop temperatures disappears at a shorter distance; compounding the difficulty in interpreting the data, comparisons between mixtures and single component species do not even illustrate velocity profiles, so that the affirmation that with increasing volatility the drop travels

a shorter distance before disappearance is inconclusive as far as evaporation time (which is the quantity of interest) is concerned. Although when designing combustion chambers the distance travelled by drops is of interest, in that practical configuration the influence of adjacent drops and turbulence will make the results of Stengele et al. [21] invalid. Further manipulation of the data by the authors is recommended to yield its very interesting potential information.

2.1.3 Microgravity combustion observations

Isolated single-component drops One of the first microgravity studies of high pressure drop combustion was that of Faeth et al. [22] in which suspended drops of $C_{10}H_{22}$ in room temperature $O_2 - N_2$ mixtures were observed in a free-fall apparatus ($\sim 1s$ of test time) at a reduced pressure of up to 6.87. Recorded drop temperatures past the ignition (i.e. appearance of a luminous flame in photographs) time showed an inflection point characteristic of the attainment of a wet-bulb state even at pressures that are about a factor of two larger than the critical decane value; this should not be interpreted as contradictory to the well-established fact that drop temperature unsteadiness prevails under supercritical conditions. Rather, it is clear that solubility effects might have continuously changed the composition of the drop, and therefore the value of the critical pressure for the conditions at the drop boundary may no longer be that of the unvitiated drop species. For considerably larger pressures than that critical for $C_{10}H_{22}$, the data showed that the drop temperature increased continuously with no evidence of steady-state, in agreement with the observations of Savery [14] for evaporating drops in normal gravity. In contrast to the emission (without combustion) results discussed above, Faeth et al. [22] found that the drop lifetime defined as the time between ignition and complete burning displayed a minimum in the neighborhood of the critical pressure of decane which was explained by the combined effect of the reduced mass diffusivity and the increased emission rate with increasing pressure. With increasing percentage of oxygen in the surrounding gas and at a large reduced pressure (~ 6.5), the drop lifetime was increasingly reduced which was

attributed to the larger drop temperature resulting from increased flame proximity. Similar results were obtained by Lazar and Faeth [23] with n-octane drops.

The study of Sato et al. [24] with suspended C_8H_{18} drops confirmed the existence of a minimum in the drop lifetime in the vicinity of the critical (octane) pressure. Similarly, Chauveau et al. [16] identified an increase in C_7H_{16} drop average burning rate and in the transient behavior of the instantaneous burning rate with increasing reduced pressure up to 0.65. Instantaneous CH_4O burning rates were also recorded by Chauveau et al. [18] for a reduced pressure of up to 0.62 and the three methods used to determine the drop diameter produced comparable results in that there was an almost linear increase of the average burning rate with pressure. The CH_4O study was extended by Vieille et al. [8] to a p_r of up to 1.15, and the same monotonic increase of the average burning rate with pressure was identified; results with C_7H_{16} for a $p_r > 2$ were too scattered to produce definite trends, but at lower p_r the same continuous increase as a function of pressure was obvious. From plots of normalized (by that observed at the critical pressure) burning rates versus the reduced pressure for CH_4O, C_6H_{14}, C_7H_{16} and C_8H_{18}, Vieille et al. [8] conclude that the subcritical trend of augmented burning rate with increased p_r is of general validity, whereas the supercritical part of the plot had enough scatter to prevent the emergence of a trend. However, it was obvious that the plot did not duplicate the maximum burning rate observed by either Faeth et al. [22] or Sato et al. [24] around the critical pressure. Although the discrepancy between these observations is not conclusively resolved, Vieille et al. [8] rightly call attention to the fact that not all microgravity experiments may be similar because the level of microgravity may not be the same, and in some situations buoyancy effects may not have been totally obliterated, as already discussed above. For example, the experiments of Vieille et al. [8] were conducted during parabolic flights in which the gravity is not as reduced as in the drop tower configuration of Sato et al. [24] where it is $\sim 10^{-5} g_0$. Consistent with these comments, Sato [9] shows plots of the burning rate constant for both C_7H_{16} and $C_{16}H_{34}$ where the constant monotonically increases for both species past the critical point, but

reaches a maximum only for the latter species in the vicinity of $p_r = 2$, the data for the former not being shown past ~ 1.2; these microgravity experiments were performed in a drop tower, but the microgravity level was not specified by the author.

One aspect that deserves comment is the fact that microgravity pure emission with no burning yields opposite trends than microgravity combustion regarding to the variation of the drop lifetime with p_r up to the critical point. In the former situation a nonmonotonic behavior was identified where for values of T_r above unity the lifetime decreased while for values below 0.8 it increased, whereas for the latter situation a consistent reduction was observed. This difference in trends highlights the difficulties in interpreting data in absence of information regarding the temperature magnitude and variation in the region surrounding the drop. One can only speculate that since the flame temperature is larger than the fuel critical temperature, the drop lifetime during combustion experiments follows the trends of the supercritical range of the pure emission observations: it decreases with p_r. For example, Sato [9] found that the emission time monotonically decreases with pressure up to $p_r = 1.4$ for C_7H_{16}, but that the burning time exhibits a minimum in the vicinity of the critical pressure. If a minimum drop burning lifetime truly exists in the neighborhood of the critical pressure, this may be attributed to the increase in the molecular correlation lengths in the vicinity of the critical point which reduces the molecular collision and thus reaction rates. As the pressure increases beyond the critical point, the correlation lengths decrease, and reactions become increasingly possible; this speculative discussion is valid independent of the differences in chemical schemes in the subcritical and supercritical regimes. These chemistry aspects have never been addressed in the context of hydrocarbon fuels, yet they are important to our elementary understanding of laminar drop combustion in pressure regimes containing the critical point.

Isolated multicomponent drops Suspended $C_7H_{16} - C_{16}H_{34}$ mixture drops having a 1mm initial diameter were observed burning in a free-fall experiment conducted in room-temperature air

by Mikami et al. [25];. the pressure range of the data was 1-6 MPa. The drops were suspended from a silica fiber of 125 μm diameter and experiments were performed in a drop tower providing 2.2 s of microgravity ($g/g_0 = 10^{-5}$). Although the results are presented primarily in terms of the burning lifetime, this quantity is not clearly defined except that it seems related to the drop size (not to the burning cessation time) and to a d^2 correction which is not presented. This burning lifetime was found to exhibit a minimum value at pressures well in excess of the critical pressure of either fuels, and the results were interpreted considering a ternary phase equilibrium system consisting of the two fuels and nitrogen. However, the relevance of the ternary system is questionable in a system of several components and assumes implicitly that the products of combustion do not attain the drop surface where they could dissolve into the fuel. Since the exact EOSs for CO_2 and H_2O are very different from that of N_2, the interpretation of the results can only be considered as a guideline for a more thorough analysis; it is well known [4] that small amounts of dissolved species can vastly change the critical point of a substance and since CO_2 has a large solubility, it is expected to be particularly influential on results stemming from such an analysis.

Interacting drops The studies of Mikami et al. [26] and Okai et al. [27] are distinctive in that the authors present microgravity ($g/g_0 = 10^{-5}$) data for two burning interacting drops and compare these observations with those from isolated drop studies both for C_7H_{16} and $C_{16}H_{34}$ single-component drops, and with mixtures of these fuels. The range of experimental pressures is 0.1 - 6 MPa in [26], corresponding to a p_r of 0.036 - 2.2 for n-heptane and 0.064 - 3.8 for n-hexadecane, and 1 - 3 MPa in [27] corresponding to 0.36 - 1.1 and 0.64 - 1.9, respectively. Because the critical locus for the $C_7H_{16} - C_{16}H_{34}$ mixture was not provided by the authors[26], [27], it is difficult to evaluate the p_r range for the binary fuels employed in the experiments, or the p_r range for each mixture which is characterized by a fixed $C_{16}H_{34}$ mass fraction; this difficulty is particularly due to the critical locus being not necessarily a monotonic function of the mixture fraction and having

possibly a multivalued aspect [4]. Therefore, the binary fuel data should be interpreted with caution, especially when comparing binary fuel drop results at fixed pressure for different mixture fractions because some mixtures may be subcritical, while others may be supercritical at the same pressure.

The Mikami et al. [26] experiment was performed with suspended millimeter diameter drops that were initially separated by a fixed distance which when nondimensionalized by the initial drop diameter (this ratio has previously been defined by Bellan and Cuffel [29] as the 'radius of the sphere of influence') was in the range 3.9 - 5.0; for this range of the sphere of influence, the flame surrounded the two drops in all experiments, indicating that there was drop interaction. Because the drop size decreases during combustion while the fibers remain at fixed positions, the radius of the sphere of influence increases during combustion, and accordingly there is less potential for drop interaction. Plots of the burning lifetime, defined as the duration between the appearance of a luminous flame and its disappearance, show that it is larger for two drops than for a single drop, and that it reaches a minimum with increasing pressure at approximately the same pressure as the single drop of the same composition; however, due to the data scatter the location of this minimum is unclear for some fuel compositions. A 'total interaction coefficient' defined as the ratio of the burning time in the two drop configuration to that of the single drop displayed a very slight maximum with increasing pressure for almost all mixtures, although the physical significance of this is not entirely clear; due to the longer heating time with increased pressure and a larger burning rate in the later stage, the authors state that this would suggest an increase in the interaction coefficient in the subcritical range, although this conclusion is not straightforward given the approximate manner for determining the drop lifetime. Following phenomenological arguments, Mikami et al. [26] conclude that under subcritical conditions the quasi-steady region around a drop decreases in extent with increasing pressure and that the radius of the sphere of influence at which drop interaction occurs decreases with increasing pressure. This last conclusion is substantiated by non-burning results of the validated model of Harstad and Bellan [30] discussed below, and can be considered as

circumstantial evidence for the reduction in the interaction coefficient of Mikami et al. [26]; however, the situation in the numerical study was different from that of the burning drop experiment and therefore the two sets of results are not entirely comparable. For example, in the numerical study of Harstad and Bellan [30] the reduced range of drop influence with increasing p_r could be traced to the reduction in the diffusion coefficient and the absence of evaporation at supercritical conditions; in the experimental study of Mikami et al. [26] although the diffusivity decreases with increasing pressure, the flame temperature changes in ways that have not been documented, and this effective far field boundary condition influences emission and thus the magnitude of the radius of the sphere of influence. Both findings that the total interaction coefficient displayed a minimum at a certain fuel composition, and that for most mixtures the burning lifetime exhibited a minimum at pressures well in excess of the critical pressure of either single-component fuels entering the mixture remain to be interpreted by the authors.

Three differences between the experimental conditions of Mikami et al. [26] and Okai et al. [27] are noteworthy: the latter data was obtained in a mixture of nitrogen and 0.12 mole fraction of oxygen rather than air in order to improve the quality of the visual observations, the initial radius of the sphere of influence was varied to determine its influence as a function of pressure, and the pressure range was narrower, 1 - 3 MPa . Similarly to Mikami et al. [26], Okai et al. [27] do not calculate the critical locus of the binary mixture (same mixture as in [26]) and therefore cannot determine whether the experiments are performed in the subcritical or supercritical regime for the mixture. However, because the maximum observation pressure only slightly exceeds the larger critical pressure of the two fuels, the authors assume that their optical measurements are in the subcritical range. Okai et al. [27] focus on the three stages of binary drop combustion (the more volatile fuel vaporization, a size plateau due to necessary drop heating before further evaporation, and less volatile fuel vaporization, see [28]) which they also identify with increasing pressure; however, the plateau is less pronounced with increasing pressure and understandably occurs sooner with

increasing initial mass fraction of the less volatile fuel. The drop lifetime consistently decreased with increasing pressure and displayed a maximum as a function of the less volatile fuel mass fraction; as the pressure increased this maximum shifted towards higher values of the mass fractions, and generally the graphs exhibited less variation in the drop lifetime for different values of the less volatile fuel mass fraction. Moreover, the initial drop separation distance was shown to have a weaker influence on the drop lifetime with increasing pressure, in agreement with the observations of Mikami et al. [26]. Although all these results were qualitatively explained, there is currently no theory able to make similar predictions for burning drops, mainly due to lack of validated high pressure kinetics.

2.1.4 Normal gravity combustion observations

Many investigators have discussed the difficulty in interpreting normal gravity drop experiments, even at atmospheric pressure, since the accurate evaluation of buoyancy effects is not straightforward. Indeed, the correction usually applied to augment the emission rate in the presence of buoyancy involves a coefficient that must be determined through 'calibration' with data; thereby rendering the application of this method pointless for uncontroversial understanding of the physics. The situation becomes exacerbated with increasing pressure since, as already mentioned, buoyancy effects are proportional to p^2. Moreover, the density variation induced by a flame will additionally enhance buoyancy. Thus, in normal gravity and at high pressure, buoyancy effects will be important but the quantitative extent of their influence is not easily assessable without considerable detailed data extraneous to the classical d^2 and emission rate plots.

Nevertheless, even in absence of such extraneous data, some limited insight may be obtained from normal gravity observations of burning drops in high pressure surroundings. The early study of Brzustowski and Natarajan [12] was performed with 2-2.5 mm diameter suspended aniline drops in reduced pressures up to 1.05, and in $O_2 - N_2$ mixtures at different initial temperatures up to a

reduced temperature of 1.54. Even at $p_r \sim 0.28$ the data displayed too much scatter to be correlated by the d^2- law, which is an indication of increasing problems in data interpretation at larger pressures. In fact, flames at increased values of p_r had very different appearances: at $p_r = 0.56$ the flame was so opaque (presumably due to soot formation) that the drop could not be seen, whereas at a value of 1.05 the flame is again devoid of particulates. The phenomenological explanations of the differences between these two combustion modes were convoluted and not readily connected to essential physics. Further comparisons between 1.2 mm suspended C_5H_{12} drop combustion at p_r of 0.44 and 1.26 by the same authors [13] were more precise and relatable to essential physics: for example, it was observed that at the higher pressure the drop was less clearly defined and non-spherical, implying that it was no longer liquid (a density gradient of $\sim O(10^3)$) but rather fluid (a density gradient $\sim O(10)$, for example). Other differences were a shorter near wake for the higher p_r, but a more elongated far wake, and a large reduction in the near wake opacity. Careful evaluations of the applicability of classical drop burning models prompted the authors to state that they were not applicable to moderate or high pressure not because the drop emission model was invalid, but because the oxidation processes of the emitted fuel were not reproducible by the models. It appears that thermal expansion of the drops at high p_r was not detected, and the emission rate of burning drops (not to be confused with the burning rate since flames did shortly persist after the drop disappearance) could be correlated with the linear d^2 variation. Additionally, the data reduction problems that were faced, in absence of precise values for the parameters entering the functional forms were thoroughly discussed by the authors.

A variety of alcohol and alkane drops were used by Canada and Faeth [31] in 6.3 - 19.0 mm diameter porous sphere experiments under natural convection conditions at pressures up to 10.1 MPa. Because of soot deposits on the porous sphere during experiments with alkanes at pressures of 3 - 6 MPa, near critical burning conditions data were obtained only for experiments with CH_4O and C_2H_6O. Dimensional alkane burning rates (the exact definition of the burning rate is not provided)

sharply increased with pressure up to the vicinity of the critical point, after which the increase was considerably more gradual (these results were later duplicated by Kadota and Hiroyasu [32]). Although the burning rate for alcohols also increased with pressure, the data contains too much scatter to allow a definite trend concerning its augmentation rate. When normalizing the burning rate by the empirical convection correction known as the Spalding correlation, the burning rate seemed to be independent of pressure for several hydrocarbons and porous sphere sizes, and this was attributed by the authors to the offsetting effects of the enthalpy rise and the reduced heat of vaporization. Therefore, the raise of the burning rate with pressure was viewed as being entirely due to convective rather than kinetic effects; this conjecture has neither been confirmed nor dismissed by currently available data. Drop surface temperatures showed a sharp elevation with pressure for alkanes, but data was not available past the critical point due to soot obscuration; alcohol data was reliable at supercritical pressures, and it was observed that the temperature elevation with pressure was more gradual.

Kadota and Hiroyasu [32] observed n-heptane, n-decane, n-dodecane, n-hexadecane, iso-octane and light oil drops at reduced pressures as large as 1.5, and even 2.7 for oil, and carefully documented the drop temperature. Confirming the earlier normal gravity pure emission observations of Savery [14], the drop temperature no longer reached a steady state as a function of time as the pressure increased, but instead exhibited an inflection point and it continuously increased at pressures past the critical point of the fuel. Introducing the concept of final temperature defined as that at the end of the emission process (but determined from the temperature measured near the inflection point), Kadota and Hiroyasu [32] found this final temperature to increase with p_r and become constant under supercritical conditions. For all fuels, the combustion lifetime, defined as the time from the appearance of the flame to its disappearance, displayed an abrupt reduction with p_r up to the critical point, after which the reduction was only gradual. The authors commented on the difference between their findings and those of microgravity combustion experiments where the

combustion lifetime increased at supercritical pressures, and attributed their own results to the predominant effect of buoyancy. Interestingly, Kadota and Hiroyasu [32] remarked that there seem to be three distinct regimes of different dependency of the combustion lifetime and burning rate upon p_r. The first regime, where $p_r < 0.3$, is characterized by the lifetime decreasing and the burning rate increasing with increasing pressure according to a similar power law; these results are similar to those of [16] for C_7H_{16} and [18] for CH_4O. In the second regime situated in the $0.3 \leq p_r \leq 1$ range, the abrupt decrease in the combustion lifetime was accompanied by a marked increase in the burning rate constant, but apparently the functional form was dissimilar from the first regime. Furthermore, in the supercritical regime, there was a slight decrease in the combustion lifetime with increasing pressure, but a considerable increase in the burning rate constant, suggesting that there is a difference between the emission and combustion lifetimes. Similarly, Vieille et al. [8] found a continuous increase in the burning rate constant of C_7H_{16} and CH_4O for pressures past the critical point.

These supercritical results were contradicted by Sato et al. [24] who found that for C_8H_{18} drops the burning rate constant decreases with pressure at supercritical pressures for p_r as high as 1.5, but this contradiction with the results of Kadota and Hiroyasu [32] or those Canada and Faeth [31] is surprisingly not mentioned. Moreover, Sato et al. [24] found that the linear d^2 variation holds over both the subcritical and supercritical pressure regimes and that when nondimensionalized by the microgravity burning rate, the normal gravity burning rate is a continuously increasing function of p_r. Since both the Kadota and Hiroyasu [32] and the Sato et al. [24] investigations were observational, with physical explanations provided only through already established subcritical correlations, it is difficult to determine the reason of the contradictory behavior at supercritical pressures for apparently similar, suspended, millimeter size, hydrocarbon drops burning in air. Sato [9] extended the observations of Sato et al. [24] to other hydrocarbons (n-heptane, n-decane, n-hexadecane, methyl alcohol and ethyl alcohol) and observed a similar decrease of the burning

rate constant with increasing pressure past the critical point. Moreover, Sato [9] observed a slight increase in the burning lifetime of the drop (defined, similarly to Kadota and Hiroyasu [32], as the time between ignition and flame disappearance) past the critical point which is also in contradiction with the findings of Kadota and Hiroyasu [32] who observed a gradual decrease past p_r. This minimum in the burning time occurred independently of the percentage of O_2 in the mixture, however its value was naturally larger with decreasing O_2.

Currently, the discrepancies between the findings of Sato et al. [24] and Sato [9], and those of Kadota and Hiroyasu [32] and Vieille et al. [8] resulting from similar experiments with sometimes the same hydrocarbon species, remain unexplained. Compounding the difficulties encountered in interpreting the results is the fact that the data is usually incomplete in that it is restricted to plots of d^2 and a burning rate constant or drop lifetime obtained by removing the information associated with the drop heating. Temperature and species profiles at several times would have enabled a better comparison among experiments and offered the possibility of understanding the source of these contradictory results.

Drops composed of mixtures of C_7H_{16} and $C_{16}H_{34}$ were observed burning at pressures up to 2 MPa in room temperature air by Niioka and Sato [33] with the purpose of ascertaining whether previous atmospheric pressure findings [28] showing a three-staged drop combustion can be extended to higher pressures. As mentioned earlier, the three stages consisted in an initial period of preferential volatile gasification, a transition period devoted to drop heating and a final period of gasification of the less volatile component. The results were primarily observational, showing that the kink in the d^2 profiles (i.e. a switch to a decreased slope) that is symptomatic of the transition period attenuates with increasing pressure. The drop lifetime, which was not clearly defined, was found to display a minimum around the critical pressure of the more volatile species, but this result was not explained. Despite the valuable findings regarding the distinction between the region of microexplosive burning due to heterogeneous nucleation which occurs at low pressures

and that of disruptive burning due to hypothesized homogeneous nucleation which occurs at high pressures, given the controversy existing even on the single-component data, one must await further developments in the understanding of supercritical mixtures to venture into a meaningful review of multicomponent fuel combustion.

2.2 Fluid shear layers, jets and sprays

Experiments with fluids emerging from an orifice into a chamber containing another fluid are more apt at portraying the situation in a combustion chamber, although the data may present more interpreting difficulties. In this configuration, the distinction between jets and sprays is purely a question of intent in the experiment: jets are discussed when the intent is to study the fluid column disintegration, whereas sprays are discussed in the context of following drops (fluid parcels) that have already separated from the incoming fluid jet. In the following the distinction between jets and sprays will carry this connotation, with the emphasis being on whether or not the experiment was performed under burning conditions. Similar to the above distinction between emission which is a phenomenon operative at all pressures and evaporation which is a purely subcritical process, here we distinguish between atomization which is a purely subcritical process and relies upon the existence of a surface that must break up, and disintegration which is a process that may occur whenever there is a boundary that may not necessarily be a tangible surface. All experiments discussed below are listed in Table 3 and we note that all were performed under normal gravity conditions.

2.2.1 Shear and mixing layer evolution

Interest in the physics of density stratification induced Brown and Roshko [34] to investigate shear layers at higher than atmospheric pressures. Using a pressurized (up to 10 atm) experimental facility they compared the spreading angle from a nitrogen - air mixing layer at 7 atm where the

density ratio was considered to be close to unity, to that of a nitrogen - helium flow in 4 atm where the density ratio was changed by switching the location of nitrogen from top to bottom. The stratification effects on the development of the mixing layer were only modest: a large (factor of 7) increase in ρ_2/ρ_1 (the subscripts 1 and 2 refer to the upper and lower streams, respectively) resulted only in a factor of 2 decrease in the spreading angle. More extensive sets of data are necessary for model validation.

2.2.2 Disintegration and emission/evaporation experiments

One of the earliest experimental studies of sprays under high pressure conditions was that of Sankar et al. [35] for a shear-coaxial configuration at pressures as high as $\sim 0.7MPa$. However, since the working fluid was water and the surrounding fluid was air, this means that the entire range of experimental conditions was well below the critical point (see Table 2). Measurements performed over 0.1- 0.69 MPa revealed that the drop size resulting from atomization yielded increasing drop sizes with increasing pressure. This result was attributed to the identified decrease of the relative shear velocity with increasing pressure, and therefore to potentially decreasing secondary atomization. Experiments with water in air for largely subcritical conditions were also conducted by Krülle and Mayer [36] who observed surface waves which they tracked using high speed cinematography; their illustrations show a highly convoluted spray interface that becomes increasingly devoid of ligaments with increasing chamber pressure (the authors also list test conditions for liquid nitrogen into gaseous nitrogen but do not present the associated results, explaining the reason for the omission of these experiments in Table 3). Confirming these findings were the observations of Jasuja and Lefebvre [37] with aviation kerosene; not only were larger drops detected with increasing pressure, but their velocity distribution was considerably more uniform than at low pressures. The increased drop size with pressure was tentatively explained by the reduction in relative velocity between fuel and atomizing air that occurs as a result of the higher chamber pressure.

Birk et al. [38] also performed water disintegration experiments (in nitrogen rather than air [35]) but the pressure and temperature ranges were considerably higher and well into the supercritical regime (see Table 3). Additional species used working fluids were ethanol, nitromethane, and two formulations of hydroxylammonium nitrate (HAN) based Liquid Gun Propellant; however, since the critical properties of Liquid Gun Propellants (LPGP) are unknown, these experiments are not listed in Table 3. The experiments were carefully conducted and documented in order to identify global differences between visual aspects at various operating conditions; in particular, the chamber temperature and pressure as a function of time were recorded and presented. Water injected through a 1 mm circular orifice apparently disintegrated into large drops, however, neither nitromethane nor ethanol, also injected into supercritical conditions, exhibited the formation of these large drops. The authors do not provide an explanation for this apparently different behavior, but mention that visual aspects of these latter sprays (intermittent segmentation, 'corkscrewing' and deviations of the spray axis from its nominal centerline) differ substantially from those familiar under subcritical conditions. Visual comparisons of spray X-ray records for non-evaporating, subcritical evaporation, transcritical and supercritical conditions conducted by Birk et al. [39] clearly showed marked differences among the different situations: this observational study with methyl iodine (chosen because of its desirable properties matching the experimental technique) jets concludes that the jet core is not well defined under supercritical conditions, but it is rather the region of the flow where there is a large concentration of working fluid. Conducting evaporative experiments where both the pressure and the temperature were above the critical point of the working fluid, the authors detected (under this new definition of the core) an increased core penetration with increasing pressure which they speculatively attributed to the attainment of the critical temperature in close proximity to the injection location, and therefore to a slow jet disintegration that could produce a longer core. These authors also investigated the difference between full cone and annular jets and detected in the latter a cylindrical shell composed of streamwise ligaments which, when magnified, exhibited the helical

structure identified in the cores of full cone sprays. This aspect of behavior is consistent with the shell behaving locally as the shear layer at the surface of full cone sprays. An unexplained peculiarity of supercritical annular sprays was a inward collapse of the shell close (1-2 shell diameters) to the injection location and a further spatial divergence which occurred closer to the injection point with increasing ambient pressure and temperature. The theoretical prediction of such behavior remains a challenge in that it is obviously not only the supercritical aspect of the spray that must be fully mastered, but also the turbulence and geometrical features that must be faithfully described.

The difference between subcritical and supercritical jet behavior were also examined by Mayer et al. [40], [41], [42], and by Chehroudi et al. [43]. The latter authors further interpreted their jet spatial growth results in terms of an empirical, intuitive equation that reasonably correlated the results over almost four orders of magnitude for the density ratio of the chamber to injectant fluid, and they also analyzed the fractal nature of the jet boundary [44]. Although the presented correlation [43], [44] reproduced in Fig. 1 is meant to be only an engineering tool, it intuitively incorporates the effect of the jet to surrounding fluid density ratio on the jet disintegration and spatial evolution. Indeed, all these studies reported a remarkable difference in the outcome of the fluid disintegration according to the surrounding pressure: whereas in the subcritical regime ligaments and drops were observed, in the transcritical regime atomization was inhibited, and further in the supercritical regime the subcritically identified ligaments were replaced by thin threads of fluid extruding from the jet in the near field, followed by big chunks of irregularly shaped fluid in the far field. The fuel threads were seen to disappear very quickly, dissolving into the surrounding fluid. This shows that atomization theories based upon Rayleigh-Taylor and/or Kevin-Helmholtz instabilities are no longer applicable to supercritical situations where there is no longer a surface tension; instead, the fluid behavior is determined by turbulence and diffusional mixing. With increasing chamber pressure, the dark core region was observed to decrease in length and thickness, therefore contradicting the observation of Birk et al. [39] that were also made at supercritical

pressures, although at much larger temperatures; the cause of this difference may be the diminished chamber fluid density at larger temperatures which would allow the existence of a longer jet core. The similarity of the supercritical and gaseous jets is further confirmed by the fractal analysis [44] which compares the fractal dimension of the Chehroudi et al. [43] jets at increasing pressures with those of a turbulent water jet, a disintegrating water jet in the second wind-induced regime, an axisymmetric gaseous jet, a gaseous boundary layer and a plane gaseous mixing layer. Not only Chehroudi's results (see Fig. 2) depict an increasing fractal dimension with p_r, but they also showed a transition form quantitative agreement with the water breakup results to that with gaseous layers and jets, and show that the dimension is smaller in the upper limit than the dimension of the turbulent water jet. This valuable analysis isolates the unique aspects of supercritical jets and suggests that to capture their physics one must invoke all high supercritical thermodynamic features in the context of turbulence.

The recent results of Oschwald et al. [45] of liquid nitrogen disintegration in gaseous hydrogen at $p_r = 1.17$ and $T_r = 2.13$ (with respect to the injected fluid) constitute the first quantitative, rather than pictorial, evidence of the difference in jet disintegration as a function of the injected jet temperature and of the coaxial fluid velocity. While the velocity of the annular flow is shown to have little influence on the density distribution in the chamber, decreasing the LN_2 initial temperature induces sharper gradients; however, in the absence of data at the same radial locations for all experimental conditions, it is difficult to determine the final impact of the LN_2 initial temperature on fluid disintegration.

2.2.3 Burning sprays and jets

The study of Birk et al. [38] was conceived to determine some of the chemical kinetic aspects of two HAN based LGP propellants, LGP1845 and LGP1898, the latter being notoriously more reactive than the former. Although the authors consider that the visual observation of conical spray outlines

indicates the existence of a surface and therefore are clear evidence that the experiments were performed in the atomization regime, this assertion is debateable since, as will be discussed below, strong density gradients persist at supercritical conditions and can be mistakenly identified with surfaces, although they may be in fact mere boundaries with no physical tangibility. This statement holds for any fluid parcel, including drops which may be fluid instead of liquid and still be optically identifiable. In this respect, the observation of large drops [38], interpreted as being the result of coalescence, may be only the effect of supercritical fluid disintegration which, as discussed above, yields large size parcels of fluid in contrast to the small drops resulting from atomization. During these experiments [38], the length of the spray penetration distance defined as the location where the spray is totally converted to gaseous products (but in the present interpretation being merely the location where one can no longer identify a strong density gradient) is considered an indication of the speed of the chemical reaction. This definition is also debatable since density gradients may not be identifiable at supercritical conditions once the fluids have dissolved into each other and therefore may not be indicative of chemical mechanisms. To determine which scenario is valid one would need to have available the critical locus of the mixture for the entire range of operating temperature and pressures; this critical locus is unfortunately not available for these complicated monopropellant/air combinations. Given these uncertain definitions, the [38] conclusions regarding the similarity of chemical time scales for different propellants will not be discussed here; and neither will interpretations based upon intensity histograms ensuing from OH radical based spectroscopy be discussed since there is currently no information that this radical is indeed an indicator of flames at high pressure (spectroscopists affirm, however, that due to the increased number of collisions at higher pressures, OH survival diminishes which naturally makes more difficult to detect, but also increases their potential of being good flame indicators). Instead, we will only note that the increased chamber temperature during experiments with LGP1898 correlates with the visual observation of more extensive regions of high luminosity, indicating a more robust reaction than

with LGP1845.

The investigations of Mayer and Tamura [40] and of Ivancic et al. [46] are devoted to LO_x/H_2 combustion, an experiment particularly difficult given the explosive nature of the mixture. Comparable with the optical features discussed by Birk et al. [38], Mayer and Tamura [40] also detected intermittent jet segmentation at locations upstream of that of LO_x disintegration into large lumps. Visual features of the burning jet exhibited the asymmetries and snake-like oscillations with amplitudes of several jet diameters reminiscent of the features observed by Birk et al. [38]. Both spark photography and OH emission indicate that most of the combustion occurs in the mixing zone between the two fluids and that in fact the flame seems to be located at the boundary between the two fluids. Immediately after ignition the flame attaches itself to the LO_x post and it is in the intense recirculating region behind the LO_x post that a strong flame continues to reside during the entire period of observation. In fact the influence of the post wake can be tracked many jet diameters downstream where it continues to control fluid mixing and combustion. The hydrogen injection temperature had only a marginal effect on mixing when compared to the chamber pressure. The authors conclusion is that these features of behavior are considerably different from those observed in subcritical regimes, and that liquid core and drop tracking modeling approaches using specified drop distribution functions are inappropriate to describe the phenomena in the supercritical regime. The new models must incorporate formulations describing the jet disintegration in thread-like manner at its boundary, the downstream disintegration of the jet into lumps, the dissolution of these lumps in the surrounding turbulent fluid concomitant with chemical reaction. Although this modeling task is currently very challenging, considerable progress has been made towards the ultimate goal, as will be discussed in the next section.

3 Modeling of subcritical/supercritical fluids

The present discussion is limited to studies conducted in the last decade since the large number of publications in this area would otherwise make this review prohibitively long. Investigations older than a decade are mentioned only when pertinent to the understanding of those performed within the last decade. Paralleling the available data, most models of supercritical fluids were constructed for drops, with few attempts at modeling fluid jets and sprays. Moreover, this review is devoted to formulations intended to capture the fundamental physics of supercritical behavior, and does not consider empirical models. All models reviewed are listed in Table 4. Although some listed studies focus on modeling of high pressure hydrocarbon burning drops or sprays, the results from such investigations are necessarily approximate since validated high pressure kinetics are presently lacking for the majority of fuels. Westbrook and Dryer [47] found that flame speeds were pressure dependent in the form of a power law and that the exponent was increasing with pressure, however, there is currently only scant information about these exponent values according to the reactants. This lack of high-pressure hydrocarbon kinetics is almost never mentioned in the listed combustion studies, with the exception of Shuen and Yang [48] and Daou et al. [49], and most of the investigations adopt reaction schemes that are either of the generic one step irreversible form or a subcritically validated extended scheme. In the light of the above, all good agreement between combustion simulations and equivalent observations should be considered fortuitous.

3.1 Salient physics of subcritical/supercritical behavior

The physics of subcritical/transcritical/supercritical fluid states is generally described in classical thermodynamics textbooks [1], [2] although neither of these states necessarily obeys the thermodynamic equilibrium assumption that is a fundamental hypothesis of thermodynamics. The reason for this classical thermodynamics description is the traditional lack of a framework for naturally

integrating non-equilibrium processes in the fluid description; Keizer's relatively recent fluctuation-dissipation theory [50], [51] now elegantly mitigates the previous formalism gap. The viewpoint of fluctuation-dissipation theory is intermediate to that of continuum and molecular-level approaches and allows the modeling of transport processes totally consistent with non-equilibrium thermodynamics, which continuum theory [52] does not address. For example, continuum theory does not give relationships between fluxes and forces for a general fluid; it is customary within the continuum formulation to extend the kinetic theory of rarified gases to describe more general cases (as in [52]). Within the formalism of Keizer's fluctuation-dissipation theory [50], [51], the mass diffusivity and thermal diffusivity appear in elements of a transport matrix that relates the gradients of the chemical potentials and of the temperature to the molar and heat fluxes that appear in the conservation equations. However, relating these elements to measurable thermal conductivities and diffusivities is not a straightforward process, as shown by the derivation of Harstad and Bellan [53], because one must insure that their definitions converge to those of kinetic theory in the limit of low pressure. However, once such association is made, the measured transport properties can be used, and in particular the effective diffusivity naturally becomes null at the critical point (see below). Umemura [54] arrived at this conclusion about the diffusivity through phenomenological arguments regarding the effective mass diffusivity, and further used an empirical factor to insure that this condition is met [55], [56], a feature that is missing in the vast majority of models (see discussion below). However, there is no need for this feature of the effective diffusivity to be artificially introduced as it naturally appears in the validated model of Harstad and Bellan [53].

Any accurate model of fluid behavior over a wide range of pressures and temperatures encompassing the critical point must capture the following aspects of behavior for two fluids one of which is a liquid at atmospheric conditions: At subcritical conditions, evaporation of the more volatile liquid must occur and we note that evaporation is a non-equilibrium process which is well described by the Langmuir-Knudsen kinetic law [57]; for isolated evaporating drops at atmospheric conditions,

the classical d^2-law must be satisfied. Condensation may also occur under appropriately favorable conditions. As the surrounding pressure is progressively elevated, the fluid density increases and solubility of one fluid into the other becomes increasingly important. At the critical point, which is a thermodynamic singularity, the effective mass diffusivity, the surface tension and the latent heat of the liquid vanish, and the heat capacity at constant pressure, C_p, the isentropic compressibility, κ_s, and the thermal conductivity, λ, become infinite. At this thermodynamic singularity the correlation lengths become very large and it is well known that the integral conservation equations may not be necessarily convertible to a differential form; this implies in particular that the Navier-Stokes equations become increasingly invalid as the critical point is approached, and therefore any model of the critical/transcritical regime using the Navier-Stokes equations must be carefully scrutinized for inconsistencies. Once the pressure is above the critical point of the liquid, the fluids acquire transport properties that are very different from those at subcritical conditions, and the Soret and Dufour effects may become particularly important in the transport matrix.

3.2 Modeling of drops

Listed in Table 4 are drop models classified according to the fluids employed and to the thermodynamic conditions of the far field (subscript ∞). Moreover, notable aspects of the models are listed (in short form) as well. Since there are investigators who made many contributions to the advancement of the state-of-the-art, the table is presented as collections of these contributions under the name of the senior author ("co." standing for "collaborators") with the exact references given in a separate column and listed at the end. This presentation enables the reader to follow the progression of a group's modeling efforts as the listing is the time sequence of the group's contributions. For isolated contributions the table listing reverts to the name of the authors as listed in the reference.

3.2.1 Drops in stagnant surroundings

Emitting drops Perhaps the most abundant supercritical modeling literature is that devoted to isolated emitting drops; this state is understandable since such a model is prerequisite to modeling the considerably more complex situations of drops emitting in convective flows and that of burning drops.

More than a decade ago, Curtis and Farrell [60] accounted for real gas effects in their formulation of a transient model of drop emission in far field conditions above the critical pressure but near the critical temperature, and performed calculations for C_8H_{18} drops in N_2. Beside the implicit assumption that Soret and Dufour effects are negligible, the authors did not include the specifics of high pressure transport properties and also assumed that there is an interface which is thermodynamic equilibrium between the drop and its surroundings. Both of these assumptions are unwarranted, practically forcing the drop to be liquid; it is thus not surprising that the authors find that the drops never reach the critical temperature during their lifetime. No data were available for model validation, but results from the model indicated that subcritical and supercritical drop behavior are significantly different which is in agreement with early models previously cited by Givler and Abraham [5]. Further progress by the same authors is distinctive from all modeling studies with the exception of those of Sui and Chen [61] and Harstad and Bellan [7], [30], [62], [53], in that Soret and Dufour effects were included in a model that was otherwise similar to the original model [60]. The value of the thermal diffusion factor for each of the binary systems of species considered (see Table 4) were calculated using a best fit curve correlating data from Grew and Ibbs [63] as a function of the ratio of the molecular weights of the two species through

$$\alpha_T = 2.3842 \times 10^{-2} + 0.2482 \log_{10}(m_1/m_2) \qquad (1)$$

where m_i are the molecular weights. However, we note that eq. 1 is not an antisymmetric rela-

tionship (i.e. $\alpha_{T,12} = -\alpha_{T,21}$) as the theory states [53] it should be, thereby being fundamentally incorrect. Additionally, the thermal diffusion factor is in reality a function not only of the m_i 's, but also of p, T and Y_i, the mass fraction of species i. Rosner [64] discusses these dependencies in detail and shows that the isotopic approximation whereby α_T is a function of $(m_1 - m_2)/(m_1 + m_2)$ (note the antisymmetry) is not even a good the first order representation of the thermal diffusion factor for $(m_1 - m_2)/(m_1 + m_2) > 0.5$ as it considerably underestimates its value (see Fig. 3 reproduced from [64]). Nevertheless, the investigation of Curtis and Farrell [65] has the merit of considering the thermal diffusion effect in the context of fluid drops, attempting to identify a reasonable value for the thermal diffusion factor and discussing its importance. The detailed model validations presented by the authors address primarily the subcritical regime which is well represented, but it is noteworthy that the supercritical C_7H_{16} in N_2 simulations are compared with data for the wet bulb temperature, a quantity that has no meaning under supercritical conditions since the drop temperature never reaches a steady-state before disappearance [66], [53]; in fact the drop temperature should continue to increase throughout the drop lifetime because it is no longer constrained by the boiling point.

Concomitant with the above studies, Chiang and Sirignano [67] formulated a theory of drop emission at high pressure, however, no real gas or solubility effects were included and it is unclear if the transport properties were consistent with the high pressure conditions meant to be portrayed; the model was exercised in the low pressure regime for liquid drops, consistently with its assumptions. The regime of supercritical pressures for LO_x/H_2 and C_6H_{14}/air was further investigated by Delplanque and Sirignano [68] with a constant density model in which the mixture is approximated by a gas with average properties. Moreover, the transport properties did not include high pressure effects and solubility effects were again neglected. Although real gas effects were modeled, the isobaric heat capacity was obtained from an ideal gas relation, possibly being inconsistent with the equation of state. Since no scientific basis was presented for all these drastic approximations, no

comments will be made regarding the results from these simulations. A similar model is that of Tsukamoto and Niioka [69] who simulated C_7H_{16} in N_2.

Another set of investigations exploring high pressure conditions is that of Jia and Gogos [66], [70] who derived the conservation equations for a liquid-gas system under the assumption of thermodynamic equilibrium neglecting Soret and Dufour contributions but including real gas effects and high pressure properties. The difference between the two formulations [66], and [70] is that in the latter the high pressure solubility effects are included. The latter simulations show [70] that neglecting solubility at high pressure results in the underestimate of the drop lifetime, or more dramatically in the break down of the solution by failing to predict the correct vapor-liquid equilibrium. The model was exercised for C_6H_{14} in N_2 for pressures of approximately 0.1-10 MPa and temperatures 500-1250K and the simulations showed that in the low temperature regime ($\sim$ 500 K) the drop lifetime increased with pressure, reaching a maximum at 600 K, further showing little sensitivity to the pressure and finally at 1250 K decreasing with pressure. The temperature at the assumed drop surface was found to become rapidly uniform at 0.1 MPa, consistent with the classical theory [52], but to rise with time and increase with pressure, consistent with high pressure thermodynamics. Since comparisons with drop experiments were not performed it is difficult to assess the quantitative value of the model; however, qualitatively it is certain that predictions from this model conform to expected or observed features of drop behavior.

Undoubtfully, Yang [71], [72] has been with his collaborators among of the most prolific investigators of supercritical phenomena. The earlier contributions of this group have been documented elsewhere [5] and therefore the focus is here on their latter contributions only. Shuen et al. [71] formulated the conservation equations in integral form assuming negligible Soret and Dufour effects, as well as the fact that the drop is liquid and is surrounded by gas, and the transport properties were calculated accordingly; the employed EOS was a simple correction of the perfect gas relation. The assumption of liquid and gas at very high pressures is always questionable since it is the fluid

state that then prevails. At the drop surface solubility effects were ignored and thermodynamic equilibrium was assumed if the critical conditions did not prevail. These approximations might compromise the accuracy of the results, in particular as it is found for C_5H_{12} drops in air that the drop reaches the critical temperature at the critical pressure, a situation which, as we discuss below, is highly unlikely. Moreover, time variation of d^2 were shown to exhibit a linear variation in agreement with the atmospheric pressure behavior that the theory emulates, but comparisons are not conducted with the porous sphere burning rate data of Canada and Faeth [31] (in fact measuring the rate at which the fuel is emitted from the drop) for the same species; although the experiment and simulations do not represent exactly the same configuration, such comparisons with experiments could have been interesting, particularly since in both cases the surface temperature and emission rate are available over a wide range of ambient pressures. Consistent with the observations of Canada and Faeth [31], Shuen et al. [71] find that the gasification rate increases continuously with pressure from the subcritical and well into the supercritical regime. The same model was used by Yang et al. [72] to investigate the emission of LO_x drops in stagnant H_2 at supercritical pressures, but the assumption of a liquid drop whose surface coincides with the radial location of the critical temperature was used and solubility effects are again neglected. The results recover the existence of a wet bulb temperature in the subcritical regime but strangely show the same phenomenon at supercritical conditions and additionally a lower surface temperature as the pressure increases. There may be several reasons for this disconcerting result, one of which is the inappropriate choice of the definition of the drop surface (given the other correct concepts described by the authors, it is inferred that the meaning of "surface" was really "boundary" without necessarily having a material attribute since only the temperature was there at the critical mixing conditions); the definition of the drop boundary certainly influenced the findings on the drop lifetime which displays a minimum past the critical pressure. However, the d^2 variation exhibits the well known linear variation in the subcritical regime but assumes a positive curvature in the supercritical regime quite different from

the nonlinear variation found by Harstad and Bellan [73] for the same species and configuration and resembling more the results of Harstad and Bellan [74] for clusters of polydisperse LO_x drops in quiescent H_2.

Anticipating this difficulty of defining a drop boundary in a coherent manner, Haldenwang et al. [75] devote an important part of their study to discussions of an appropriate definition. While most of the simulations are conducted assuming that the drop has a material surface separating a liquid drop from a gas and the surface is defined by the condition of phase equilibrium, calculations are also performed by identifying the surface with the critical locus in order to compare the results with those of Yang et al. [72]. The model of Haldenwang et al. [75] neglects Soret and Dufour effects, contains an inconsistent (with the EOS) calculation of C_p and is deficient in calculations of the transport properties for the conditions of the study; therefore the ensuing results should be critically analyzed. However, not surprisingly, the drop lifetime obtained by using each of the two definitions varies widely, which is a very believable outcome. As it will be discussed below, there is an uncontroversial manner in which one can define a drop boundary that is not necessarily a surface, so that it can be consistent with optical data. The earlier work of Sanchez-Tarifa et al. [76] which is not reviewed here, as well as Haldenwang et al. [75] both allude to this correct definition, but curiously, neither one of them adopts it.

An intriguing model is that of Sui and Chen [61] in that it includes real gas effects, high pressure transport properties, and strangely, it contains Soret but no Dufour effects. The model is exercised for the heaviest gas, sulfur hexafluoride, in nitrogen, which is a system that has no practical application in combustion. The results and associated discussion are scant and there are no comparisons with equivalent drop experiments making it difficult to assess the validity of the formulation for the species and conditions for which it was exercised.

In all modeling studies discussed above, it is only the thermal conductivity, λ, and the viscosity, μ, that may have been calculated accounting for high pressure effects. The mass diffusivity, D_m,

always presented a problem in that an equivalent protocol to that established [3] for calculating λ and μ for a single species fluid or mixtures over a wide range of p and T does not exist for calculating D_m. The Takahashi [77] procedure to calculate D_m at high pressure for even a binary mixture relies upon a correction of the low pressure value. However, Umemura [54] was the first to realize that matching fluxes at the drop boundary while it is at the critical point requires that the mass diffusivity be null; it is noteworthy that there is nothing insuring theoretically that this condition is satisfied in the Takahashi [77] correction which in fact displays distinct non null values of $(D_m p)_r$ at the critical point (see Fig. 1 in [77]). Lacking an appropriate procedure for calculating D_m, Umemura and Shimada [55], [56] multiplied D_m by an empirical factor to insure its consistent value at the critical point and studied drop emission [55] as well as some linear acoustic aspects during this process [56]. Despite this careful consideration of the correct value of D_m, the model suffers from the omission of the diffusional mass terms that multiplied by the molar enthalpies supplement the thermal conductivity term to form the heat flux, this omission being equivalent to effectively assuming that the C_p 's of all species are equal (in this respect being similar to the model of [68]), and from the lack of Soret and Dufour terms. The results from the simulations are primarily used to establish maps of drop behavior in the (p, T) plane according to the initial drop temperature. In the absence of experimental validation, and considering the approximations described above, it is difficult to evaluate the merit of these results.

An empirical factor for correcting the mass diffusivity at the critical point was also used by Lafon and Habiballah [78] in a model where thermal diffusion effects were neglected, thermodynamic equilibrium was assumed at the drop surface and solubility effects appear to have been neglected. However, real gas effects are considered outside of the assumed liquid drop, and transport properties first calculated from kinetic theory are empirically corrected for high pressure effects. Simulations performed for LO_x drops in H_2 at supercritical conditions show all the attributes of the subcritical regime in that the d^2 variation is almost linear, without displaying an initial size increase that may

sometimes occur due to drop heating (drops initially at 90 K are immersed into H_2 at 1000 K), and the drop surface temperature reaches a wet bulb which exhibits a maximum $\sim$ 8 MPa. The validity of these predictions remains to be evaluated by comparisons with experiments.

Discerning the need for a model incorporating all aspects of supercritical behavior and of a systematic evaluation of various thermodynamic or transport contributions to the accurate portrayal of supercritical phenomena, Harstad and Bellan developed a fundamental theory of fluid drop behavior under supercritical conditions [7]. This model was further extended to include subcritical conditions and was validated [53] with the microgravity observations of Nomura [10] over the entire data range of (p, T). The model of Harstad and Bellan [7] is based on Keizer's fluctuation-dissipation theory [50] which has the distinct advantage of formally accounting for non-equilibrium processes as well as naturally relating fluxes and forces for a general fluid, a relationship that continuum theory does not provide. Fluctuation-dissipation theory allows the modeling of transport processes totally consistent with nonequilibrium thermodynamics and its main result is the form of the transport matrix which includes two terms for each of the molar and heat fluxes; the molar flux is the sum of Fickian terms and the Soret term, whereas the heat flux term is the sum of the Fourier term and the Dufour term. In Harstad and Bellan's formulation [7], [53] the conservation equations are valid for a general fluid, and no assumption is made regarding the existence of a material interface between the drop and its surroundings; instead, this information is expected to evolve as a result of the calculations rather than being an input. Anticipating the comparisons with experimental data [53], the drop boundary is defined to be the location of the maximum density gradient because this is what is optically measured in an experiment. Moreover, Harstad and Bellan [7], [53] included in their model real gas EOSs and transport properties valid over the entire subcritical/supercritical range. Special attention was devoted to the correct definition of λ from the transport matrix to obtain consistency with the kinetic theory in the low pressure limit [53]. Unlike in all existing models, the ambiguity of the correct value of D_m at the critical point did not arise at all since the

Fickian terms are proportional to the product $\alpha_D D_m$ where $\alpha_D(p, T, Y_i)$ is the mass diffusion factor whose null value is a necessary condition characterizing the critical point (see detailed explanation below). As for the calculation of D_m, its value is found from an interpolated curve spanning the entire fluid range and converging to the liquid and gas limit at the appropriate conditions [7]. As constructed, the model contains no adjustable constants; however, the value of the thermal diffusion factor is unknown for the C_7H_{16} in N_2 set of species used in the experiment of Nomura et al. [10]. To compound the difficulty in determining the value of the thermal diffusion factor, Harstad and Bellan [53] show that one may define the thermal diffusion factor in two different ways, each one being associated with one definition of the heat flux; the two forms of the heat flux are called the Irwing-Kirkwood (IK) and Bearman-Kirkwood (BK), respectively [79], and the associated thermal diffusion factors are correspondingly named $\alpha_{IK,ij}$ and $\alpha_{BK,ij}$. However, $\alpha_{IK,ij}$ and $\alpha_{BK,ij}$ are not independent, and in fact they are related through a thermodynamic function [53] as follows:

$$\alpha_{BK,ij} = \alpha_{IK,ij} - \alpha_{h,ij} \tag{2}$$

where

$$\alpha_{h,ij} \equiv (m_i m_j/m)(h_i/m_i - h_j/m_j)/(R_u T), \tag{3}$$

and $\lim_{p\to 0}(\alpha_{BK,ij}) = \alpha_{KT,ij}$ where $\alpha_{KT,ij}$ is the kinetic theory value, h_i is the molar enthalpy and R_u is the universal gas constant. The $\alpha_{IK,ij}$ term enters the expression of the Dufour term in the IK form of the heat flux, whereas $\alpha_{BK,ij}$ enters the expression of the Dufour term in the BK form of the heat flux and of the Soret term in the mass flux. Since high pressure thermal diffusion factor values for the C_7H_{16} in N_2 are not available, Harstad and Bellan [53] used part of Nomura et al.'s [10] data to determine $\alpha_{BK,ij}$ and they further performed model validations with the $\alpha_{BK,ij}$ thus determined. Figures 4-7 and Table 5 (K is the emission rate based on the maximum slope of the curves in Figs. 4-8), all reproduced from [53] show the remarkable agreement

between simulations and data given the facts that: (1) the experiment was that of a suspended drop whereas the simulations were for a free floating drop, (2) the level of microgravity might have been insufficient to eliminate Grashof number effects, as discussed above, and (3) the determination of $\alpha_{BK,ij}$ in the simulation was necessarily approximate. When this model was exercised for the drop sizes of interest in Diesel and gas turbine engines, the ensuing results showed that the d^2 variation is nonlinear for pressures just in excess of atmospheric and that past an initial heat up regime the drop's size might even increase at supercritical conditions; the duration of the heat-up period increased with far field pressure similarly to the experimental observations. As the pressure was increased, d^2 became nonmonotonic with time, with a slope whose magnitude increased as a function of time. Thus, the drop underwent initially a heating period during which its size may increase, followed by a period during which the size was continuously reduced. A detailed analysis of the ρ, T and Y_i profiles revealed that the temperature relaxes first while the mass fraction relaxes last in agreement with the known fact that the Lewis number, Le, is larger than unity. However, it was also shown that the classical calculation of the Lewis number is no longer valid at supercritical conditions and an effective Lewis number, Le_{eff}, was defined and calculated [62]; these novel ideas will be discussed in a subsection below.

The only study of bicomponent drops in a stagnant one component environment at high pressure is due to Stengele et al. [80]. In their model the drop is assumed to be a liquid whose surface is in thermodynamic equilibrium with its surroundings, and the diffusion limit model of the conservation equations is used. The paper is unclear on the calculation of the drop fluid enthalpy, and thus on the computation of the latent heat, and therefore it is impossible to determine if the heats of solvation are neglected in the boundary condition at the drop surface; the species concentration of the gas dissolved into the drop is calculated from the phase equilibrium condition. In the governing equations for the drop surroundings, the Soret and Dufour contributions are neglected and an average C_p is used for the mixture, thereby compromising further the interest of the simulations.

Although a real gas EOS was used to describe the domain surrounding the drop, the fact that C_p was independently calculated from the EOS could introduce inconsistencies into the model. Transport properties were calculated assuming the drop to be a liquid and the surrounding to be gaseous, and in particular the Takahashi [77] method was employed to obtain the diffusivity. The model was exercised for a $C_7H_{16} - C_{12}H_{26}$ mixture (which was assumed ideal) in N_2 with results showing a d^2 variation that becomes linear past an initial heat up time (in contrast with the results of [53]) during which the drop's size even increases at supercritical conditions (in agreement with the results of [53]). At a low far field temperature the drop lifetime exhibited a maximum in the supercritical regime, however, at a high temperature no such maximum was found and the lifetime continuously decreased. It is unfortunate that subsequent experiments from the same group [21] were conducted for different species and thus did not allow a comparison between their previous predictions and data. Other predictions of the model would also have been interesting to evaluate including the prediction that the internal concentration distribution is a very weak function of the far field pressure and that the temperature has a greater influence of the on both drop lifetime and composition. Comparing the predictions with the observations of Nomura et al. [10] for C_7H_{16} in N_2 who found that the drop lifetime decreased monotonically with p at T_r in excess of ~ 1.2 while it increased with p at T_r below ~ 0.8, the trends are different; however, since the experiments were performed for a single component hydrocarbon which is one of the two alkanes used in the simulation, the comparison is not necessarily appropriate.

Burning drops One of the earliest investigations of drop combustion in a supercritical environment is due to Shuen et al. [71] who used their above discussed drop model in conjunction with a single step reaction kinetics to simulate combustion. Since the reaction rates were determined at atmospheric conditions [47] and devoid of pressure effects, the authors rightly warn readers about the doubtful aspect of the kinetics and recommend cautious interpretation of their results from C_5H_{14}

in air calculations. The primary qualitative conclusion from this study is that diffusion processes are very likely controlling the combustion process; this is understandable since diffusion has a much longer characteristic time than kinetics.

Tsukamoto and Niioka [69] applied their drop model presented above to the study of C_7H_{16} in air ignition and also chose the atmospheric kinetic rates of Westbrook and Dryer [47] for performing their simulations. Their study epitomizes the reluctance in this review to discuss papers concerned with high pressure ignition: the rates used in the Tsukamoto and Niioka's [69] investigation are probably even less valid than if used for high pressure combustion studies since Westbrook and Dryer [47] derived their rate constants for well developed flames. However, the primary qualitative conclusions from the Tsukamoto and Niioka [69] study seem reasonable: Small drop ignition is controlled by the chemical reaction, whereas large drop ignition is controlled by emission processes. Considering that the burning rate (i.e. the drop disappearance rate under burning conditions, see Section 2.1.3 for single drops) decreases with increasing pressure, their conclusion is that the ignition time of these large drops might not decline with increasing pressure. Other studies on ignition do exist, but due to the rudimentary understanding of this phenomenon (this being the reason of not reviewing observations of high pressure drop ignition), they are best relegated to a further review which must await substantial progress in this area.

Lafon and Habiballah [78] also used a one step reaction to portray LO_x combustion in H_2, and qualitatively compared their results with known observations from high pressure hydrocarbon combustion. The difference between their prediction of the drop and combustion lifetimes declining with p_r, and the hydrocarbon combustion observations of Faeth et al. [22] who found a minimum in the drop lifetime in the vicinity of the critical point is attributed by the authors to the smaller stand-off ratio (flame radial location divided by drop radius) in the former LO_x/H_2 combustion situation. Moreover, Lafon and Habiballah [78] find that the drop lifetime is equal to the combustion lifetime which is interpreted as being a consequence of the smaller stand-off ratio preventing fuel

accumulation between drop and flame, and thus resulting in the drop disappearance coinciding with the end of burning. Far field temperature variations show a monotonic decrease of the drop lifetime with pressure which is qualitatively similar to that observed in the experiments reviewed earlier in this paper (see Section 2.1.3 for single drops).

Liquid oxygen combustion in hydrogen is also the subject of the investigation conducted by Daou et al. [49], but by difference from the Lafon and Habiballah [78] model is that here the reaction scheme is detailed and involves radicals; nevertheless, a similar uncertainty is associated with these kinetics as well since, as acknowledged by the authors, it has not been validated at the high pressures prevailing in rocket combustion chambers. Circumventing the possible occurrence of two phases, the drop is always assumed to be in a supercritical state but the properties used are those of low pressure gases. The model lacks Soret and Dufour effects but includes a real gas EOS; however, the presentation of the formulation in unclear regarding the inclusion of solubility effects. The drop boundary (erroneously called "interface") is assumed to be at the location of an initially prescribed value for either T, or ρ or Y_{LO_x} and it is claimed that these three different definitions are nearly equivalent for the prediction of the drop lifetime. However, the results used to compare the three definitions of the drop boundary clearly indicate that solubility effects are not considered which leads to unphysical results. For example, the three definitions of the boundary are either $Y_{LO_x} = 0.99$ or $T = 91$ K (the initial drop temperature was 90 K and the ambient one was 1000 K), or ρ equal to the initial density at the drop boundary. First, due to solubility effects Y_{LO_x} will eventually relax everywhere to be < 0.99, but this does not mean that a drop boundary does not exist. Second, due to the relaxation process there is no guarantee that the density will be anywhere equal to its initial value at the drop boundary. Finally, under supercritical conditions the drop temperature will increase everywhere beyond the initial value. Moreover, since the due to the large Lewis number the T profile relaxes first while the Y_{LO_x} profile relaxes last, it is clear that the three definitions cannot be equivalent. As discussed in the preceding section on emitting

drops, the only definition which can be physically validated is that based on the density gradient. Given these problems in the drop boundary definition, the results must be interpreted cautiously; in particular, the d^2, based on the temperature definition of the boundary, shows no initial drop size increase due to drop heating for all conditions and displays a linear variation with time that is characteristic to the subcritical regime. Since the combustion simulations are performed with an uncertain kinetic model coupled to this problematic emission model, and since no experimental validation is presented, the ensuing results will not be discussed.

Lewis number calculations for all pressures and temperatures The Lewis number is a measure of the importance of heat diffusion, D_T, to the mass diffusion, $Le \equiv D_T/D_m$, where traditionally $D_T = \lambda/(nC_p)$ with n being the molar density and C_p being the molar heat capacity. Therefore Le provides an indication of what process controls a phenomenon through a comparison of length scales, or equivalently of time scales, and because of that it has an engineering as well as a scientific relevance. For example, in gases usually $Le = O(1)$ which means that heat and mass diffusion proceed at similar rates, whereas in liquids $Le = O(10) - O(100)$ indicating that heat diffusion is faster than mass diffusion. Supercritical fluids being neither gases nor liquids, they are expected to fit in the intermediary regime of the above values. However, in the supercritical regime one must question the traditional definition of D_T and D_m both of which are based upon the binary mixture concept at atmospheric conditions. Indeed, for a binary mixture there is only a single mass diffusion coefficient which provides a single characteristic length scale, and at atmospheric conditions the molar and heat flux are well described by the Fick and Fourier laws, respectively. The question is whether the same definition applies for multicomponent mixtures or under supercritical conditions. The analysis and results of Harstad and Bellan [62] provide an answer for binary mixtures under supercritical conditions and further explain the different relaxation times of the T, ρ or Y_i profiles observed during numerical simulations. Moreover, they also provide guidance in understanding the

source of the dissimilarity between the behavior of various binary mixtures.

The point of departure for the derivation of Le_{eff} is the observation that characteristic lengths of mass and thermal diffusion can be immediately defined only when the differential operators for the two variables Y_1 and T are uncoupled because the diffusion term in the equation for each variable contains only derivatives of that variable; then, the diffusion matrix whose elements are the coefficients of the molar and heat gradients is diagonal. In that situation, one defines the traditional Le as the ratio of the diffusive length scales of the temperature and mass fractions and the ratio is calculated using the coefficients of the diffusive terms. In the more general situation where the flux matrix

$$\begin{aligned} J = &\quad A_J \frac{\partial Y_1}{\partial r} \quad + B_J \frac{\partial T}{\partial r} \quad + C_J \frac{\partial p'}{\partial r} \\ q = &\quad A_q \frac{\partial T}{\partial r} \quad + C_q \frac{\partial Y_1}{\partial r} \quad + B_q \frac{\partial p'}{\partial r} \end{aligned} \tag{4}$$

is given by the general diffusion matrix containing Soret and Dufour terms additional to the Fick and Fourier ones, the differential operators for the two variables are no longer uncoupled because in each equation the diffusion term contains derivatives of **both** variables. Here J is the molar flux, q is the heat flux, r is the radial coordinate and

$$A_J = (m/m_1) n D_m \alpha_D \tag{5}$$

$$B_J = (m_2/m) n D_m X_1 X_2 (\alpha_{IK} - \alpha_h)/T \tag{6}$$

$$C_J = (m_2/m) n D_m (m_1 m_2 X_1 X_2/m)(v_1/m_1 - v_2/m_2)/(R_u T) \tag{7}$$

$$A_q = \lambda + (\alpha_{IK} - \alpha_h)\alpha_{IK} R_u n D_m X_1 X_2 \tag{8}$$

$$C_q = [m^2/(m_1 m_2)] n D_m \alpha_D \alpha_{IK} R_u T \tag{9}$$

$$B_q = n D_m \alpha_{IK} (m_1 m_2 X_1 X_2 / m)(v_1/m_1 - v_2/m_2) \tag{10}$$

where X_i is the molar fraction and v_i is the molar volume. The differential operators are now coupled, and this coupling prohibits a simple definition of appropriate diffusion length scales for heat and mass transfer. In order to find again the appropriate characteristic length scales, one must diagonalize the differential operator representing the species and energy equations. For this purpose, Harstad and Bellan [62] construct Shvab-Zeldovich-like variables [52] that are combinations of Y_1 and T. Whereas in the traditional Shvab-Zeldovich formalism for transient combustion in a diffusive-convective system, linear combinations of variables are used in conjunction with a series of assumptions to eliminate the reaction term from all but one equation and render the conservation equations easier to solve, in the present context, the combined variables are defined to diagonalize the operators of the differential equations. Once this matrix is diagonalized, an effective mass diffusivity, D_{eff} and thermal conductivity, λ_{eff}, can be defined as the eigenvalues of the matrix, and these quantify departures from D_m and λ :

$$\rho D_{eff} = \alpha_D D_m (1 - X_1 X_2 \alpha_{BK}^2 R_u n D_m \sigma) \tag{11}$$

$$\lambda_{eff} = \lambda + X_1 X_2 \alpha_{BK}^2 R_u n D_m (1 + n D_m \alpha_D C_p \sigma) \tag{12}$$

where σ is the positive root of an algebraic equation [62]. Since the second term in eq. 11 and the third term in eq. 12 are both positive, it is apparent that the diffusivity is diminished whereas the thermal conductivity is enhanced.. These new effective transport coefficients form the basis of the Le_{eff} definition, $Le_{eff} = \lambda_{eff}/(n C_p D_{eff})$. Le and Le_{eff} plots for the validated C_7H_{16} in N_2

database of Nomura et al. [10] are reproduced from Harstad and Bellan [81] and are illustrated in Fig. 8a-8d for the high temperature (745 K) and in Fig. 9a-9d for the low temperature (445 - 495K) calculations.

Figures 8a and 8b show results from the 0.1 MPa simulations, whereas Figs. 8c and 8d portray parallel results at 2 MPa; in both simulations the pressure is in the subcritical regime and the temperature is 745 K. Inspection of the plots shows that for a pure mixture at subcritical conditions Le and Le_{eff} have the same values in regions of weak gradients, thereby validating the model for Le_{eff}. Quantitative and qualitative differences appear in mixture regions where gradients are important, and L_{eff} can be as much as a factor of 2 larger than Le. With increasing pressure, while still in the subcritical regime, these differences become larger indicating that the estimate provided by Le regarding the relative importance of heat and mass diffusional scales deteriorates as the pressure increases. Similar plots of Le and Le_{eff} appear on Fig. 9 (a - d) for the low temperature simulations validated above. Figures 9a and 9b are for the same pressure as in Figs. 8c and 8d (2 MPa), but at 445 K, whereas Figs. 9c and 9d are for 5 MPa (supercritical pressure) and 495 K. For the low temperature, subcritical pressure Le and Le_{eff} are in close agreement (Figs. 9a and 9b), again validating the Le_{eff} model, and comparisons with Figs. 8c and 8d show that as expected, the lack of strong heating in Figs. 9a and 9b decreases the gradients and increases the agreement of Le and Le_{eff}. However, even at low heating, under supercritical pressure conditions L_{eff} becomes substantially different from Le as shown in Figs. 9c and 9d. Mistakenly, Le indicates that the drop is gaseous ($Le < 1$), whereas Le_{eff} correctly indicates that the drop is a dense gas with properties approaching those of a liquid ($Le_{eff} > 1$). This comparison emphasizes the importance of an appropriate model for the determination of the ratio of heat to mass diffusional scales. Fortuitously, the far field boundary conditions of the simulations (taken to be those of the data) presented in Figs 8 and 9 allowed the uncoupling of the pressure and temperature effects on the Le versus Le_{eff}. The combined effect of pressure and temperature on the values of Le and

Le_{eff} was further explored by Harstad and Bellan [53] who showed that with increasing (p, T) the discrepancy between the two estimates becomes substantially larger than shown here.

One issue worth emphasizing is the dependence of the ratio Le_{eff}/Le on the species in the mixture (and of course on the initial conditions). The magnitude of the reducing or enhancing terms depends upon α_{BK} which is of course species specific. Moreover, it is also noteworthy that even if the thermal diffusion factor term were negligible, the fact that $D_{eff} \propto \alpha_D$ means that the diffusivity is reduced because of nonideality rendering $\alpha_D < 1$. Such diffusion departures from the usual, subcritical behavior were discussed by Cussler [82] who points out that diffusion coefficients may approach a null value near and above the critical condition. In contrast, all these effects are milder for the C_7H_{16}/N_2 system, primarily because the difference in the molar enthalpies between the two species is not as large as for LO_x/H_2.

This Lewis number enhancement is also intimately related to solubility effects in the drop and with emission effects in the drop surroundings since it is precisely the coexistence of two species at one location that gives rise to the reducing/enhancement terms (see eqs. 11 and 12). Of course, this contribution will be considerably more important outside of the drop; inside the drop these effects will be initially reduced, despite the large temperature gradients, by the lack of second species, whereas once the second species becomes appreciably dissolved, the temperature gradient will be more relaxed, reducing again this contribution; we recall that the mass fraction gradient is initially null in the drop and assumes finite values only relatively late in the drop lifetime.

3.2.2 Drops in convective surroundings

Emitting drops Few investigators ventured into the realm of drops in convective flows under supercritical conditions and the reason is easy to understand. Under subcritical conditions drops have a tangible surface and the drag force is a straightforward concept. This is no longer the case for drops in supercritical conditions which may not have a surface, in which case drag is not an

appropriate concept.

One model that bypassed this difficulty was that of Lee et al. [83] who studied a drop suddenly injected into an initially quiescent environment having assumed the immediate existence of a potential flow around the drop upon injection and the initial formation of a vortex sheet at the drop surface (the correct semantics would have been "drop boundary"). This arbitrary assumption implied that the flow was entirely induced by the vorticity and allowed a simplified mathematical treatment and the calculation of the evolution of this vortex sheet. The initial drop boundary appeared increasingly distorted with time, yielding a mushroom-like shaped drop; these results, however, remain to be validated. Such an experiment might be difficult to perform since the absence of a unidirectional flow in the calculation would be hard to duplicate.

The realistic configuration of a supercritical LO_x drop in a H_2 stream was treated by Hsiao et al. [84]. The fluid model employed was similar to that developed by Yang and his collaborators [71], [72] except that a single phase was here assumed to exist with the differences between drop and surroundings accounted by the properties of the fluid. Illustrated results from the simulations showed a critical mixture composition locus that became increasingly distorted, with a shape similar to that of a bubble rising in a flow. As the flow velocity increased, the shape of the critical mixture composition locus gradually changed from a mushroom-like (with the cap facing the incoming flow) to a crescent-like, whereas with increasing p the shape became more convoluted and closer to that of a mushroom. For all these calculations, the critical mixture temperature and the critical mixture composition never coincided, with the former always enclosing the latter. The critical mixture temperature boundary did not exhibit the strong deformation of that of the critical mixture composition, and instead assumed an increasingly elliptical shape with increasing time, far field velocity or pressure. These profiles seem reasonable since under far field supercritical conditions the temperature profile will relax faster than that of the mass fraction. Although the absence of a material surface prevented the authors from truly calculating a drag coefficient, the critical

temperature locus (which is geometrically more regular) was chosen to evaluate the equivalent of C_D. This calculation was performed by evaluating the drag force as the product of the acceleration of the drop's center of gravity by its mass; we note that both of these quantities are arbitrarily defined and therefore it is difficult to give too much credence to the concept of drag under such conditions.

Delplanque and Sirignano [85] assumed the existence of a material surface on a LO_x drop initially at 100 K immersed in H_2 at approximately 10 MPa and 1000K. The focus of that model was on the boundary-layer stripping effects for a drop in convective flow in the transcritical regime. However, as it was discussed in the Introduction, the assumption of a material surface is erroneous under the conditions of this study since once either p_c or T_c are exceeded, the conditions are supercritical and therefore a material surface can no longer exist; since boundary-layer theory holds only in circumstances where a material surface is present, the premise of the study seems invalid. Moreover, solubility effects were considered negligible and it is unclear if transport properties were appropriately calculated at the elevated pressure of the simulations. Since the conceptual picture of the formulation is at fault, the conclusions regarding the effect of boundary-layer stripping on the drop lifetime and drop heating will not be discussed.

The latest contribution to the study of drops in convective, supercritical situations is due to Gogos and Soh [86] who applied their model to C_6H_{14} in N_2 in both micro- and normal gravity. The drop was assumed to be liquid despite the maximum far field pressure of $\sim$ 10 MPa which is substantially above the p_c of the fuel, as apparently the mixture was always below its critical point; in fact the calculations were stopped when either the residual radius was 20% or the critical point was reached. The axisymmetric conservation equations were solved including real gas effects, mixture non-ideality, solubility effects and variable properties for the two phases, but no Soret or Dufour effects. Comparisons between the drop lifetime predictions and the normal gravity data of Matlosz et al. [15] show that the agreement is reasonable at low and moderate pressures, but it

deteriorates as the pressure augments, and at the highest pressure considered the results overpredict the data by a factor of two. The increasing disagreement with increasing pressure could be due both to the difference between the suspended drop configuration of the experiment and the free floating drop of the simulation, as well as to the neglect of the thermal diffusion which becomes increasingly important with increasing pressure.

Burning drops Recently, Daou and Rogg [87] have claimed to study convective burning of fuel pockets at supercritical pressures, however, the proposed model contains the perfect gas EOS, constant C_p as well as constant transport properties, all for a gas, and therefore the formulation is clearly inadequate to portray supercritical conditions in many respects, even without accounting for the unjustified flame sheet approximation used to describe burning.

The lack of investigations of isolated burning drops in convective flows perhaps epitomizes the corresponding lack of fundamental information regarding hydrocarbon reaction rates in supercritical environments which combined with the uncertainties in treating the momentum transfer between what is optically identified as a drop and its surrounding, make an accurate formulation currently impossible. This topic area represents one of the challenges of future research.

3.2.3 Conclusions from drop models

Considering the physics of supercritical behavior presented in Section 3.1, and comparing it to the above drop models, one can immediately identify several major features that have been generally erroneously modeled.

First, in most studies, with the exception of Harstad and Bellan [7], [53] the drop boundary (which is not necessarily a surface), was empirically identified with the locus of the critical temperature ([49], [84], etc.), or with the locus of thermodynamic equilibrium (most papers listed in Table 4). This identification is erroneous in the context of model validation because optical measurements

of drop size detect the density gradient, which albeit being reduced under supercritical conditions from its two phase value, still exists and can be substantial. The fact that the location of this density gradient may be different from that of the critical temperature is immediately apparent since the temperature relaxes in a shorter characteristic time than the density, as discussed above. Moreover, attainment of the critical temperature is insufficient to the existence of a tangible surface since it is both the temperature and pressure that must attain the critical value at the given composition. In other studies, the existence of a critical locus of the mixture was assumed (see Table 4) by hypothesizing that the drop remains liquid, however, this is hypothesis is not necessarily correct; the existence of a surface which may be either one of phase equilibrium or the critical locus must be a result of the calculation, not an assumption. It is even possible to obtain situations where due to the difference in composition between the drop and its surroundings two different supercritical states coexist on the two sides of the drop boundary (identified with the observable point of maximum density gradient) as found by Harstad and Bellan [88]; however, this is not an indication that the critical point for the particular composition is reached at a locality between these two conditions (which could be physically located between the two grid point) because p_c and T_c might not occur at the same location. Under these conditions, assuming the existence of the critical locus is tantamount to forcing the density gradient to coincide with the critical locus, which is correct only if the critical locus is indeed attained; however, this cannot be a hypothesis, but rather a result. Finally, identifying the drop boundary with the locus of thermodynamic equilibrium is inconsistent since as long as there is drop emission, there cannot be thermodynamic equilibrium.

Second, although Umemura [54] reached the conclusion that the diffusivity must be null at the critical point using physical arguments involving species fluxes at the drop boundary, most models do not include this effect; exceptions where empirical models have been included are the formulations of Umemura and Shimada [55], [56], and of Lafon and Habiballah [78]. However, none of these investigators, including Umemura [54], realized that it is not the mixture diffusivity

as calculated from the corresponding states models using mixing rules, but the **effective** mixture diffusivity that becomes null at the critical point. This is because the effective mixture diffusivity is the product of the mixture diffusivity and the mass diffusion factors, α_{Dij}, which are null at the critical point as they are the derivatives of the Gibbs function, $\alpha_{Dij} = \beta X_i(\partial^2 G/\partial X_i \partial X_j)_{p,T,X_k}$ for all $k \neq i,j$ where $\beta \equiv 1/(R_u T)$; and by definition [89] the critical point occurs when both the determinant of the second derivatives of G, $|\,\overline{\overline{U}}\,|$, and that of the second derivatives of G combined with the first derivatives of $|\,\overline{\overline{U}}\,|$ are null. Alternately, the mass diffusion factors may be readily computed from the chemical potential, μ_i, as

$$\alpha_{Dij} \equiv \beta X_i \partial \mu_i / \partial X_j = \partial X_i / \partial X_j + X_i \partial \ln \gamma_i / \partial X_j \tag{13}$$

for $i \in [1,N]$, $j \in [1,N-1]$ where N is the number of species and $\gamma_i = f_i/(X_i f_i^0)$ is the activity coefficient where f_i is the fugacity [53]; any other empirically imposed value can only be inconsistent with thermodynamics over a range of pressures, temperatures and mass fractions. The relationship 13 correctly indicates that at low pressures, where the perfect gas EOS holds, the mass diffusion factors have unity values whereas departures from unity occur with increasing pressure as shown by Harstad and Bellan [53]; basically, with increasing pressure there are amplified departures from mixture ideality [53]. In fact the occurrence and maintenance of sharp density gradients is directly associated with the faster (than the mass fractions) temperature relaxation and the effective diffusivity reduction: once the temperature becomes uniform, the Soret contribution to the molar fluxes vanishes, and the reduction in the effective diffusivity with increasing pressure decreases the molar flux; this diminished molar flux prevents changes in the density and thus explains the large density gradient. Of course, no confusion between mixture diffusivity and effective mixture diffusivity occurs if the values used are from data since in an experiment such distinction cannot be made and what it is the effective diffusion coefficients that are measured. However, using molecular theories (i.e. kinetic theory), or models for calculating high-pressure diffusivities based upon these theories

with high pressure corrections based on reduced parameters [77] can lead to incorrect results, unless the model has been validated for the particular set of species under consideration; otherwise there is no guarantee that the correct values are attained.

Quantitative validation and interpretation of numerical results by comparison with data cannot be performed if these modeling aspects are incorrectly treated. Moreover, solubility effects must always be included at high pressures because otherwise the drop heating and thus its size will be inaccurately predicted.

3.3 Modeling of groups of drops (arrays, clouds and clusters)

Snyder et al. [90] performed a simple evaluation of the nondimensional radius of the sphere of influence in liquid rocket engines and concluded that its value is about 3-6. Therefore, although single drops are the first step in the understanding of supercritical sprays, it is the more realistic situation of groups of drops that is immediately pertinent to the practical applications. The difference between the behavior of an isolated drop and that of a drop in a group of many drops results from drop interactions which determine the magnitude of the far field variables (p, T, Y_i) for each drop.

Stagnant conditions outside the group of drops Jiang and Chiang [91], [92], [93] devote several investigations to the study of drop interaction in a monodisperse cloud using the model of Bellan and Cuffel [29] to couple the drops. The single drop model is devoid of Soret and Dufour terms but includes real gas effects. The drop is assumed liquid and all properties inside the drop are accordingly calculated, whereas the surrounding fluid is assumed to be a gas with equivalent gas transport properties. Thermodynamic equilibrium prevails at the drop surface, and solubility effects are included. Additionally, the C_p in the gas phase is not calculated from the adopted Soave-Redlich-Kwong EOS, but is independently calculated, thereby possibly introducing inconsistencies.

The Takahashi method [77] is used to calculate binary gas phase diffusivities which, as discussed above, is a questionable method near the critical point. The model is exercised for the C_5H_{12}/N_2 system for pressures as large as $\sim$ 6 MPa and temperatures as high as 1250 K; given the critical characteristics of both C_5H_{12} it is certain that the drop is no longer a liquid at the most elevated pressure. The coupling between the drops includes the assumption that the cluster is adiabatic on a global basis [91], and therefore that its size remains constant while naturally the pressure varies inside the cluster. This latter aspect of pressure variation during a single simulation makes comparisons with experiments and other models at best qualitative since all observations and most other existing simulations were performed at constant pressure. In fact, plots of the pressure nondimensionalized by the initial pressure show small declining excursions from unity for a relatively low initial temperature ($T_r = 1.06$), except for the initially atmospheric pressure where an increase is observed due to the strong evaporation, however, all conditions exhibit an asymptotic trend to unity; at a higher initial temperature ($T_r = 2.13$) the declining excursions from unity are greater, in particular being also displayed by the atmospheric case. The dilute cluster results [91] at a relatively low initial temperature ($T_r = 1.06$) show a maximum in the drop life time as a function of initial pressure but for high initial temperatures ($T_r \gtrsim 1.6$) a monotonic decrease with increasing initial pressure is obtained instead. While this latter result reminds that of Nomura et al. 's [10] for single suspended hydrocarbon drops at constant pressure, the result for the lower temperature cannot be compared to those of [10] since those were for $T_r \lesssim 0.8$ and $T_r \gtrsim 1.2$. For dense clusters of drops the drop lifetime was found to decrease monotonically with initial pressure over the entire range of initial temperatures investigated, $T_r \geqslant 1.06$. Examination of the results showed that the linear variation of d^2 was obeyed only for dilute clusters and only at low pressures. Generally, it was concluded that with augmenting pressure, drop interactions become less important.

Jiang and Chiang also studied moving drops [92], [93] and calculated mass ejection from the cloud, although the formulation of the cluster boundary conditions is lacking from the paper, and

there is thus an uncertainty as to the exact model for heat and mass transfer through the cloud boundary. Consistent with their hypothesis of a liquid drop even at high p_r, a drag law governs the individual drop motion and the usual empirical correlation enhancing heat transfer to the drops under convective conditions [52] is used. When the initial temperature of the interstitial gas in the cloud is equal to that of the cloud surroundings [92], the results show that the mass ejection from the cloud decreases substantially at high pressures, thereby making cloud envelope flames improbable. For clouds initially cooler than their surroundings [93], the authors state that a cited critical mixture temperature corresponding to the conditions at the drop surface is never reached, although why this temperature should be the same for all cases, while presumably the surface composition is different, is not explained. Since the critical state of a mixture depends upon (p, T, Y_i), the meaning of their conclusion is uncertain; just as difficult to accept is their hypothesis that the drops are (initially) liquid at $p_r \simeq 1.8$.

Harstad and Bellan [30], [62] base their monodisperse drop cluster calculations on the single drop model described in [7] and couple the drops in the cluster through conservation equations based on the same fluid model. The heat and mass transfer between cluster and its surroundings are modeled through an equivalent Nusselt number and it is shown that the results of the calculations are not sensitive to its value over three orders of magnitude. Simulations performed for both the LO_x/H_2 [30] and the C_7H_{16}/N_2 [62] system at a given far field pressure show that the size of the cluster is also found to be a very weak parameter, consistent with the lack of sensitivity to the Nusselt number. Parametric studies performed for the LO_x/H_2 system for various drop proximities show that the most important cluster effect is the progressive accumulation in the interstitial part of the cluster of a non-negligible amount of LO_x with decreasing drop interdistance. The effect of drop proximity decreases with increasing pressure in that the behavior of the fluid drops in a very dense gas becomes increasingly similar to a pure diffusion process. For given initial drop proximity, an increase in pressure was found to eventually result in increased smearing of the gradients, a desirable

aspect because it promotes interdiffusion; this result is exactly the opposite of what is obtained for isolated fluid drops [7]. Also studied was the impact of the fluid drop size on the mass fraction distribution within the cluster: larger fluid drops were shown to have a larger characteristic time and to evolve similarly to the smaller drops except that the evolution time is proportionally stretched. These results, therefore, agree with the well-known design practice of trying to atomize the LO_x jet into the smallest possible size fluid drops. The trends were similar for the C_7H_{16}/N_2 system except that due to the peculiarities of the LO_x/H_2 system, supercritical features are enhanced for the latter. In both cases it was shown that L_{eff}, as defined above, increases with increasing pressure and decreasing temperature, and that closer drop proximity results in it exhibiting sharper peaks due to the increased gradients of the dependent variables.

The issue of the d^2 variation in polydisperse clusters of drops was addressed by Harstad and Bellan [74] in the context of LO_x/H_2 using the model in [30] as a building block for the polydisperse model. The interstitial pressure, temperature and LO_x mass fraction were found insensitive to the value of the thermal diffusion factor (within an appropriate range of values) up to 40 MPa where a modest sensitivity was apparent. What was found to control the magnitude of the interstitial quantities was the value of the cluster Nusselt number, however, an order of magnitude increase in the Nusselt number reduced the drop disappearance time only by a small fraction, thus reflecting the diffusive nature (large characteristic times) of the situation. Under all conditions of this study, encompassing 6-40 MPa and a LO_x/H_2 mass ratio of 4-12, the variation of d^2 was not linear and the curves consistently exhibited a small but definite positive curvature. Since for the C_7H_{16} isolated drops in N_2 a consistently negative curvature was found [53], the conclusion is that the d^2 variation is both species and configuration dependent and caution about making hasty inferences from one system of species or configuration to another was recommended. Comparisons of results from a binary size cluster of drops containing a much larger proportion of small drops with those from a monodisperse cluster where the drop size was the surface based average of the two size

classes, showed that although the interstitial quantities may be well predicted by a monodisperse approximation, the lifetime of the cluster was significantly underestimated. All these LO_x/H_2 results displayed departures from the perfect gas law and mixture ideality epitomizing the supercritical conditions. For example, the compression factor exhibited values $O(10^{-1})$ inside the drop which significantly depart from the $O(10^{-3})$ for liquids and $O(1)$ for perfect gases, whereas the mass diffusion factor decreased as low as 0.2, considerably deviating from the ideal mixture unity value. Therefore, the assumption of a drop in a liquid state for either $T_r > 1$ or $p_r > 1$, that is under supercritical conditions with respect to the fuel, made by Jiang and Chiang [91], [92], [93] may be totally erroneous.

Convective conditions outside the group of drops The difference of behavior between an isolated drop and drops in an array was explored by Delplanque and Sirignano [58] in the transcritical regime. The supercritical model used is that of [68] whereas the array model is that described by Delplanque [94], and the emphasis of the investigation is on the effect of pressure and velocity oscillatory conditions on drop emission and combustion. In this formulation, drops are continuously injected into the combustion chamber where they vaporize and change the environment of the surrounding drops. The reaction is basically uncoupled from the oscillatory field by prescribing these fields and assessing the response of the drop evaporation to these prescribed fields. Since the model is based upon the problematic high pressure fluid description of [68], the accuracy of the results upon addition of the convective effects remains in question.

3.4 Modeling of streams, shear and mixing layers, jets and sprays

The recent experimental information regarding supercritical spray disintegration, which is now understood to be a process essentially different from subcritical atomization [40], [44], poses a new challenge: that of modeling fuel jet disintegration into the threads and chunks observed in the

experiments. Such a successful model coupled to an accurate drop model [53] would prove a very powerful simulation tool.

3.4.1 Streams

As with the isolated drop studies, Umemura [54] made an early contribution to the model development in this more idealized configuration of a one-dimensional, plane fluid undergoing combustion in isobaric conditions. The fuel is initially assumed to be and to remain liquid, and the oxidizer is assumed to be gaseous. The equations are devoid of Soret and Dufour effects, the heat capacities are implicitly averaged, thermodynamic equilibrium is assumed to hold at the fuel surface and the flame is hypothesized to be infinitely thin. Considering all these drastic assumptions, and that the species used in the calculation were not the same as those in the experiments, it is not surprising that the C_4H_{10} in N_2 gasification simulations, and that the calculated C_4H_{10} in air combustion lifetimes duplicate only qualitatively the similar $C_{10}H_{22}$ data of Faeth et al. [22]. Although the model formulated by Umemura [54] is essentially qualitative, one very important aspect is quantitative: the realization that the mass diffusivity must be null at the critical point. The importance of this issue cannot be overstated since, as already discussed above, null effective mass diffusivities represent a necessary condition for being at the critical point. On the other hand, any model of mass diffusivity issued from kinetic theory will not conform to this condition; moreover, as discussed above, even pressure corrected mass diffusivities, such as Takahashi's [77] might not posses this important feature.

3.4.2 Shear and mixing layers

High pressure shear and mixing layers have been studied only recently owing to the paucity of data to guide the models; the fact is that there is virtually no detailed experimental information on turbulence development in supercritical mixing/shear layers. An exception is the study of density

stratification effects in spatially evolving high pressure mixing layers of Brown and Roshko [34] discussed earlier in this review. However, those observations were certainly insufficient for developing a well founded turbulence model. For this reason, Oefelein and Yang [95] used classical atmospheric pressure turbulence models to develop a Large Eddy Simulation (LES) model describing mixing and combustion of LO_x and H_2, where the latter stream had the larger velocity. The employed high pressure fluid model is that developed by Yang and his collaborators and discussed in Section 3.2 above, and includes real gas EOSs, high pressure λ and μ, whereas the mass diffusivity is calculated by interpolating between the gas and liquid regime by using a linearly weighted combination based on the mixture feed fractions. As explained in Section 3.2, this calculation of the mass diffusivities by no means guarantees the attainment of a null value at the critical point. The Subgrid Stress (SGS) turbulence model is that of Erlebacher et al. [96] using the assumption of scale similarity and incorporating compressibility effects, but based on intuition and data obtained from atmospheric turbulence. The combustion model is represented by a comprehensive twenty four step kinetic mechanism involving nine species using published reaction rates that have been validated in the 300-3000 K temperature range and at several pressures for pressure dependent reactions. The results indicate that the density gradient dominates the evolution of the layer and that the mass diffusion rate greatly diminishes near the critical point.

The same dominating effect of the density gradient was found in the Direct Numerical Simulations (DNS) of Miller et al. [97] of a C_7H_{16}/N_2 three-dimensional (3D) shear layer based on the validated all-pressure fluid model of Harstad and Bellan [53]. In contrast to the investigation of Oefelein and Yang [95], here the emphasis was on developing high pressure SGS models based on supercritical fluid turbulence using the same protocol employed as that at atmospheric pressure: DNS pursued to turbulence transition would provide the necessary database to the development of SGS models which in turn will allow calculations using LES. The results in [97] represent the first step towards this goal as they describe a pretransitional shear layer. One of the most important

aspect of the results worth emphasizing is that even at this early stage of the simulation, the flow visualization qualitatively agrees with the observations of a N_2 jet in N_2 of Chehroudi et al. [43] at supercritical conditions. Essentially, the simulations show the development of regions of strong density gradients which are optically detected as the wispy fluid threads evolving from the boundary of the jet. This distinctive feature is not exhibited by density unstratified mixing layers and can be considered to be representative of supercritical mixing layers, as discussed by [43], thereby providing credibility to the simulations in [97]. Although jets and shear layers are not identical fluid dynamical configurations because of the additional azimuthal component of the velocity in the former, for the purpose of qualitative comparisons, the jet mixing region (as different from its core) behaves comparably to a mixing layer. Moreover, an additional difference between the experiment and the simulations is that the former is concerned with a spatial evolution whereas the latter explores a temporal evolution. Nevertheless, distinctive visual features are well known to be common to spatial and temporal layers at atmospheric conditions, and the expectation is that this commonality persists at higher pressures. Because of the large density stratification, and because of the presence of these strong density gradient regions, transition to turbulence is expected to be delayed; not only is it more difficult to entrain the heavy, slower stream fluid, but also any small turbulent scales formed will bounce off these strong density gradient regions which act similarly to material boundaries and thus hinder transition to turbulence. Simulations towards transition are in progress at the time of writing of this paper.

3.4.3 Jets

An extensive computational effort was undertaken by Yang et al. [98] to simulate the combustion of a LO_x cylindrical (axisymmetric) jet in a $H_2 - He$ mixture. The calculations were steady, the Soret and Dufour effects were neglected, viscous dissipation was assumed insignificant, the LO_x jet was assumed to have a material surface which was a locus of thermodynamic equilibrium, the

perfect gas EOS was used for the $H_2 - He$ mixture while for LO_x the density was calculated as a polynomial of T, and combustion was described either using the chemical equilibrium approximation or a detailed H_2/O_2 kinetics, although it is not mentioned if the reaction rates were validated for the high pressure used in the calculation. It is difficult to reconcile the simplistic treatment of the EOS with the effort in modeling elevated pressure transport properties, or with the introduction of solubility effects which may be inconsistent with the chosen EOS. Under these circumstances, the excellent agreement between the measured and the predicted both oxygen mole fraction and centerline temperature at approximately 3 and 7 MPa are either fortuitous or indicate that for reasons that are not discussed all of the above drastic assumptions are justified. Just as worrisome is the shown insensitivity of the oxygen mole fraction at both 3 and 7 MPa to the calculation of the mass diffusion coefficient (constant versus the Takahashi [77] method) whose variation, as discussed earlier in this review, plays a dominant role in truly determining the supercritical behavior.

The numerical simulations of Ivancic et al. [46] represent an attempt at calculating the evolution of a LO_x jet in H_2 at 6 MPa. A two-dimensional (2D) steady calculation was conducted which included the $k-\varepsilon$ turbulence model and real gas EOS and properties, with the combustion modeled based on the chemical equilibrium assumption. Since it is well recognized that supercritical fluid models must be transient, the authors acknowledge that it is not surprising to find that the drastic steady hypothesis (compounded by the 2D approximation) yields results that are at variance from the observations in that they do not predict the correct thickness of the OH zones or their radial distance to the centerline of the combustor.

3.4.4 Sprays

The ultimate goal of drop and other fluid dynamical configuration modeling is to enable the eventual simulation of an entire spray, including the fluid disintegration leading to the fluid drops , threads or chunks of fluid that provide the fuel available for combustion. Although there currently is no

such validated model, attempts at reaching this very important goal have already been made.

Chegini et al. [99] have investigated the dynamics and mixing of a LO_x stream in a channel in the presence of air at a pressure in excess of the p_c of O_2 but at a temperature below its T_c. The assumption is made that the LO_x jet, initially at 105 K, has disintegrated upon contact with the atmospheric temperature air into fluid drops devoid of surface tension, and therefore the Redlich-Kwong EOS is used to account for real gas effects. The Nukiyama-Tanasawa relationship, which is valid only at atmospheric pressures, is used to fit the drop size distribution based upon a Weber and a Reynolds number; inexplicably, the Reynolds number is based on the air velocity (instead of the relative velocity) but the LO_x viscosity, and the Weber number is based on the free stream velocity without mention of which surface tension is used to define it. This last issue is very important since the Weber number based on the LO_x (the fluid disintegrating) surface tension is infinite owing to the null surface tension, as noted by the authors. Moreover, despite the drops having no surface tension, their dynamics is controlled in the model by the drag force, a concept which is entirely associated with the existence of a material interface. Furthermore, a similarity model for heat and mass transfer based on the Ranz-Marshall correlation, a subcritical relationship, is used to describe the fluxes into the drop. Additionally, Soret and Dufour effects are neglected. The results focus on the difference in the prediction of a given size drop trajectory induced by an isothermal versus a nonisothermal treatment of the heat transfer inside the drop, but one must be skeptical about the findings considering the numerous subcritical aspects of the model (in fact the entire model is based on subcritical physics with the exception of the EOS).

The early model of Mayer et al. [6] did not benefit from their more recent observations of fluid jet disintegration [40], [41], [42] and thus it conventionally considered the interaction between liquid drops and a surrounding gas flow, including possible drop breakup and dispersion. The drops were followed in a Lagrangian manner based upon equations of motion governed by the drop drag force with a subcritical relationship for the drag coefficient, and the drop interaction with the flow was

modeled using an integral time scale based on the Lagrangian autocorrelation; since a single value was chosen for this time scale based on a $k-\varepsilon$ model, the flow was assumed turbulently homogeneous. Moreover, turbulence was hypothesized to be stationary and isotropic. Extensive results were presented illustrating drop dispersion and turbulent velocity versus position, as well as drop velocity-diameter correlation. The turbulent drop dispersion and drop energy compared reasonably well with experimental observations, however, all the data were from subcritical experiments while the title of the paper stated that the study was conducted for typical rocket engine conditions (the exact conditions of the simulations were not given in the paper). Based upon all discussions above, considerably more effort is necessary to model a supercritical spray.

The most comprehensive supercritical spray simulation to date is that of Oefelein and Yang [59] who performed a LES using as a building block the fluid model developed in [84] in conjunction with the subcritically developed SGS model of Erlebacher et al. [96]. Although the drops were followed in a Lagrangian manner, the drag coefficient was corrected from its subcritical value by a factor obtained from the supercritical model in [84] which calculated an equivalent drag force based on the critical temperature isocontour of fluid drops in a convective flow. The simulation configuration is that of a dilute LO_x spray at 100 K injected at the trailing edge of a splitter plate and flowing between two H_2 co-flowing streams at 1000 K at pressures of approximately 0.1, 10 and 40 MPa. The drops, injected at the local gas velocity, are not followed individually but rather as 'computational parcels' chosen according to a sampling technique. The results highlight the influence of the pressure on the spray evolution. For example, it is found that the coupling between the spray and its surroundings increases with pressure due to the enhanced turbulent diffusion and to the variations in the gas phase structures stemming from changes in composition. Additionally, the simulations showed that both mixing and dispersion become stronger functions of the SGS fluctuations and of the large scale coherent structures of the flowing H_2 with increasing pressure, indicating that an accurate, supercritically based SGS model (and we note again that the model in

[59] is subcritically based) is crucial to obtaining quantitatively validated predictions. The precursor of such a model is the DNS described in [97], and the SGS model is currently under development by Bellan and collaborators, as discussed above.

4 Conclusions

A critical review of the literature has been presented with the goal of distilling the essence of supercritical fluid behavior in a variety of physical configurations; subcritical fluid behavior was reviewed only with respect to similarities to or differences from that encountered under supercritical circumstances. The classical definition of the supercritical regime was adopted whereby a liquid becomes a supercritical fluid if either of its critical pressure or temperature is exceeded. The review was restricted to studies whose contribution was geared to enhancing the fundamental understanding of fluids typically used in liquid rocket, gas turbine or Diesel engines; this restricts the review to fluids whose molar volume is large under supercritical conditions. The emphasis of the review was on the fluid dynamics, the thermodynamics and the transport properties, with negligible mention of detailed chemical processes; this choice was dictated by the dearth of validated detailed kinetic mechanisms of ignition and combustion for engine fuels at supercritical pressures.

An extensive examination of experiments was offered and these were categorized according to the geometric configuration and to the influence of gravity upon the observations. Data obtained in microgravity was considered easier to interpret and therefore took precedence over that in normal gravity which inherently included convective effects. Even nominal microgravity data was scrutinized according to the level of microgravity in the experiment, as previous analysis showed that Grashof effects may persist well into what is sometimes considered the microgravity regime. In the context of drop experiments a distinction was made between evaporation which is by definition a subcritical effect and emission which may occur independent of the number of phases; to enable

an integrated analysis of data, 'emission' was selected to represent the most general situation. A survey of the drop emission microgravity data has shown that there is still no consensus regarding the variation of the square of the drop diameter under supercritical conditions, the drop diameter being determined from optical measurements. And neither is there a complete agreement as to the variation of the drop lifetime as a function of pressure or as a function of temperature well past the critical point. Ascertaining these issues is a high priority since they represent the foundation for understanding more complex experiments and developing rigorous models. Burning drop data was shown to be generally incomplete in that no situation is characterized to the extent that it can be used for model validation. The same comment is valid for multicomponent drops in either emitting or burning situations. Therefore, these two research areas offer opportunities for further studies.

It is only recently that observations of fluid jet disintegration under supercritical conditions have shown that this process is fundamentally different from the much studied subcritical liquid atomization. Instead of the subcritical wave formation at the surface of the liquid resulting from the relative velocity between the liquid and gas, ensuing in the subsequent Kevin-Helmholtz instability and the further breaking of the liquid sheet, under supercritical conditions the fluid disintegrates in a remarkably different fashion. The optical data shows wispy threads of fluid emanating from the jet boundary and dissolving into the surrounding fluid. A survey of these experiments was presented and thoroughly discussed. The existing information is of qualitative nature and considerable more work is necessary to create databases appropriate for uncontroversial model validation.

Complementing the experiment examination, a parallel review of supercritical fluid models was presented. Aspects specific to supercritical fluids such as intrinsic transient behavior, the lack of a material surfaces, real gas equations of state, mixture non-ideality, increased solubility, Soret and Dufour effects and high pressure transport properties were all addressed when evaluating the accuracies of existing models. Moreover, misconceptions about the salient features of supercritical behavior were specified, and a microgravity validated fluid model was discussed. Investigations of

isolated drops were distinguished from those of groups of drops, and studies in stagnant surroundings were differentiated from those in convective ones. Although considerably more scarce, models of streams, shear and mixing layers, jets and sprays have also been surveyed. In contrast to the drop models, some of these latter formulations contain turbulence models which makes them of considerable more interest for practical applications. Despite the fact that these turbulence models are all subcritically based and that spray models follow drops in a Lagrangian manner based upon the incorrect concept of drag, these imaginative studies pave the way to accurate future models. The necessary, but currently lacking, ingredients of these future models are species specific thermal diffusion factors, multicomponent diffusivities valid over a wide range of pressures and temperatures, and supercritically based turbulent models. Work is already in progress in all these areas and we shall witness in the future exciting new developments.

ACKNOWLEDGMENT

This study was conducted at the Jet Propulsion Laboratory and sponsored by the National Aeronautics and Space Administration (NASA), Marshall Space Flight Center under the direction of Mr. Klaus Gross, and Glenn Research Center under the direction of Dr. Daniel Bulzan, by the Air Force Office of Scientific Research under the direction of Dr. Julian Tishkoff and by the Army Research Office under the direction of Dr. David Mann, the latter two under an interagency agreement with NASA. The author would like to thank Dr. Kenneth G. Harstad of the Jet Propulsion Laboratory for numerous enlightening discussions elucidating the physics of supercritical fluids.

References

[1] Prausnitz, J., Lichtenthaler, R. and de Azevedo, E., *Molecular Thermodynamics for Fluid-phase Equilibrium*, Prentice -Hall, Inc., 1986

[2] Hirshfelder, J. O., Curtis, C. F. and Bird, R. B., *Molecular Theory of Gases and Liquids*, John

Wiley and Sons, Inc., 1964

[3] Reid, R. C., Prausnitz, J. M. and Polling, B. E., *The Properties of Gases and Liquids*, 4th Edition, McGraw-Hill Book Company, 1987

[4] American Petroleum Institute, *Petroleum Refining Data Book*, American Petroleum Institute, 5th ed., 1992

[5] Givler, S. D. and Abraham, J., Supercritical droplet vaporization and combustion studies, *Prog. Energy Combust. Sci.*, **22**, 1-28, 1996

[6] Mayer, W., Labani, R. and Krülle, G., Theoretical investigations of droplet flow under typical coaxial injector flow conditions in cryogenic rocket engines, AIAA 92-3121, presented at the AIAA/SAE/ASME/ASEE 28th Joint Propulsion Conference, Nashville, TN

[7] Harstad, K. and Bellan, J., Isolated fluid oxygen drop behavior in fluid hydrogen at rocket chamber pressures, *Int. J. Heat Mass Transfer* **41**, 3537-3550, 1998

[8] Vieille, B. Chauveau, C, Chesnau, X, Odeïde, A and Gökalp, I., High pressure droplet burning experiments in microgravity, *26th Symp. (Int.) on Combustion*, 1259-1265, 1996

[9] Sato, J., Studies on droplet evaporation and combustion in high pressures, AIAA 93-0813, 31st Aerospace Sciences Meeting, Jan. 11-14, Reno, NV, 1993

[10] Nomura, H., Ujiie, Y., Rath, H. J., Sato, J. and Kono, M., Experimental study on high pressure droplet evaporation using microgravity conditions, *26th Symp. (Int.) on Comb.*, 1267-1273, 1996

[11] Morin, C., Studies on the influence of pressure and temperature on the vaporization of hydrocarbon droplets, Ph.D. thesis Centre National de la Recherche Scientifique, Orléans, France, 1999

[12] Brzustowski, T. A. and Natarajan, R., Combustion of aniline droplets at high pressures, *Can. J. Chem. Eng.*, 194-201, 1966

[13] Natarajan, R. and Brzustowski, T. A., Some new observations on the combustion of hydrocarbon droplets at elevated pressures, *Comb. Sci. and Tech.*, 2, 259-269, 1970

[14] Savery, C. W., Experimental studies of the vaporization of droplets in heated air at high pressures, NASA CR-7254, 1969

[15] Matlosz, R. L., Leipziger, S. and Torda, T. P., Investigation of liquid drop evaporation in a high temperature and high pressure environment, *Int. J. Heat Mass Transfer*, 15, 831-852, 1972

[16] Chauveau, C., Chesnau, X. and Gökalp, I., Burning characteristics of n-heptane droplets, AIAA 93-0824, 31st Aerospace Sciences Meeting, Reno, NV., 1993

[17] Morin, C., Chauveau, C. and Gökalp, I., Studies on the influence of pressure and temperature on the vaporization of n-heptane droplets, ILASS-Europe 1999

[18] Chauveau, C., Chesnau, X. and Gökalp, I., High pressure vaporization and burning of methanol droplets in reduced gravity, AIAA 94-0430, 32nd Aerospace Sciences Meeting, Reno, NV., 1994

[19] Chesnau, X, Chauveau, C, and Gökalp, I., Experiments on high pressure vaporization of liquid oxygen droplets, AIAA 94-0688, 32nd Aerospace Sciences Meeting, Reno, NV., 1994

[20] Anderson, T. J., Winter, M. and Haas, M., Observation of droplet/shock interactions in a supercritical environment, AIAA 94-0557, 32nd Aerospace Sciences Meeting, Jan. 10-13, Reno, NV, 1994

[21] Stengele, J., Prommersberger, K., Willmann, M. and Wittig, S., Experimental and theoretical study of one- and two- component droplet vaporization in a high pressure environment, *Int. J. Heat Mass Transfer*, 42, 2683-2694, 1999

[22] Faeth, G. M., Dominicis, D. P., Tulpinsky, J. F. and Olson, D. R., Supercritical bipropellant droplet combustion, *12th Symp. (Int.) on Comb.*, 9-18, 1969

[23] Lazar, R. S. and Faeth, G. M., Bipropellant droplet combustion in the vicinity of the critical point, *13th Symp. (Int.) on Comb.*, 801-811, 1971

[24] Sato, J., Tsue, M., Niwa, M. and Kono, M., Effects of natural convection on high-pressure droplet combustion, *Combust. and Flame*, 1990, **82**, 142-150

[25] Mikami, M., Habara, O., Knon, M. Sato, J. Dietrich, D. L. and Williams, F. A., Pressure effects in droplet combustion of miscible binary fuels, *Comb. Sci. and Tech.*, 124, 295-309, 1997

[26] Mikami, M., Kono, M., Sato, J. and Dietrich, D. L., Interactive effects in two Droplets combustion of miscible binary fuels at high pressure, *27th Symp. (Int.) on Comb.*, 2643-2649, 1998

[27] Okai, K, Tsue, M., Kono, M., Mikami, M., Sato, J., Dietrich, D. L. and Williams, F. A., Strongly interacting combustion of two miscible binary fuel droplets at high pressure in microgravity, *27th Symp. (Int.) on Comb.*, 2651-2657, 1998

[28] Wang, C. H., Liu, X. Q. and Law, C. K., Combustion and microexplosion of freely falling multicomponent droplets , *Combust. Flame*, 56(2), 175-197, 1984

[29] Bellan, J. and Cuffel, R., A theory of non-dilute spray evaporation based upon multiple drop interaction, *Combust. Flame*, 51, No. 1, 55-67, 1983

[30] Harstad, K. and Bellan, J., Interactions of fluid oxygen drops in fluid hydrogen at rocket chamber pressures, *Int. J. Heat Mass Transfer*, 41, 3551-3558, 1998

[31] Canada, G. S. and Faeth, G. M., Fuel droplet burning rates at high pressures, *14th Symp. (Int.) on Comb.*, 1345-1354, 1973

[32] Kadota, T. and Hiroyasu, H., Combustion of a fuel droplet in supercritical gaseous environments, *18th Symp. (Int.) on Comb.*, 275-282, 1981

[33] Niioka, T. and Sato, J., Combustion and microexplosion behavior of miscible fuel droplets under high pressure", *21st Symp. (Int.) on Comb.*, 625-631, 1986

[34] Brown, G. L. and Roshko, A., On density effects and large structure in turbulent mixing layers *J. Fluid Mech.* 64(4), 775-816, 1974

[35] Sankar, S. V., Wang, G., Brena de la Rosa, A., Rudoff, R. C., Isakovic, A. and Bachalo, W. D., Characterization of coaxial rocket injector sprays under high pressure environment, AIAA 92-0228, 30th Aerospace sciences Meeting, Jan. 6-9, 1992, Reno, NV

[36] Krülle, G. and Mayer, W., Injection, atomization and mixing of propellants in liquid rocket engines using coaxial injectors, *Proc. of ICLASS 1994*, Rouen, France

[37] Jasuja, A. K. and Lefebvre, A. H., Influence of ambient pressure on drop size distributions in dense sprays, *25th Symp. (Int.) on Comb.*, 345-352, 1994

[38] Birk, A., McQuaid, M. and Bliesener, G., Reacting liquid monopropellant sprays - experiments with high velocity full cone sprays in 33 MPa, 500° C nitrogen, Final Report ARL-TR-17, 1992

[39] Birk, A., McQuaid, M. and Gross, M., Liquid core structure of evaporating sprays at high pressures - flash X-ray studies, Proc. of ICLASS-94, pp.459-466, 1994; also Final Report ARL-TR-901, 1995

[40] Mayer, W. and Tamura, H., Propellant injection in a liquid oxygen/gaseous hydrogen rocket engine", *Journal of Propulsion and Power*, 12(6), 1137-1147, 1996

[41] Mayer, W., Schik, A., Schweitzer, C. and Schäffler, M., Injection and mixing processes in high pressure LOX/GH2 rocket combustors, AIAA 96-2620, presented at the AIAA/SAE/ASME/ASEE 32nd Joint Propulsion Conference, Lake Buena Vista, FA, 1996

[42] Mayer, W., Ivancic, B., Schik, A. and Hornung, U., Propellant atomization in LOX/GH2 rocket combustors, AIAA 98-3685, presented at the 34th AIAA/ASME/SAE/ASEE Propulsion Conference, Cleveland, OH, 1998

[43] Chehroudi, B., Talley, D. and Coy, E., Initial growth rate and visual characteristics of a round jet into a sub- to supercritical environment of relevance to rocket, gas Turbine, and Diesel engines, AIAA 99-0206, 37th Aerospace Sciences Meeting, Reno, NV, 1999

[44] Chehroudi, B., Talley, D. and Coy, E., Fractal geometry and growth rate changes of cryogenic jets near the critical point, AIAA 99-2489, 35th AIAA/ASME/SAE/ASEE Joint Propulsion Conference, Los Angeles, CA, 1999

[45] Oschwald, M., Schik, A., Klar, M. and Mayer, W., Investigation of coaxial LN2/GH2-injection at supercritical pressure by spontaneous Raman scattering, AIAA 99-2887, 35th AIAA/ASME/SAE/ASEE Joint Propulsion Conference, Los Angeles, CA, 1999

[46] Ivancic, B., Mayer, W., Krülle, G. and Brüggemann, D. Experimental and numerical investigation of time and length scales in LOX/GH_2- rocket combustors, AIAA 99-2211, 35th AIAA/ASME/SAE/ASEE Joint Propulsion Conference, Los Angeles, CA, 1999

[47] Westbrook, C. K. and Dryer, F. L., Simplified reaction mechanisms for the oxidation of hydrocarbon fuels in flames, *Comb. Sci. and Tech.*, 27, 31-43, 1981

[48] Shuen, J-S. and Yang, V., Combustion of liquid-fuel droplets in supercritical conditions, AIAA 91-0078, 29th Aerospace Sciences Meeting, January 7-10, Reno, NV, 1991

[49] Daou, J., Haldenwang, P. and Nicoli, C., Supercritical burning of liquid oxygen (LOX) droplet with detailed chemistry, *Combust. Flame*, 101, 153-169, 1995

[50] Keizer, J., *Statistical Thermodynamics of Nonequilibrium Processes*, Springler-Verlag, New York, 1987

[51] Peacock-Lopez, E. and Woodhouse, L., Generalized transport theory and its application to binary mixtures, in *Fluctuation Theory of Mixtures*, Advances in Thermodynamics, Vol. 2, Eds. Matteoli, E. and Mansoori, G. A., Taylor and Francis, 301-333, 1983

[52] Williams, F. A., *Combustion Theory*, Addison-Wesley,1965

[53] Harstad, K. and Bellan, J., An all-pressure fluid drop model applied to a binary mixture: heptane in nitrogen, accepted for publication in *Int. J. of Multiphase Flow*, 1999

[54] Umemura, A., Supercritical liquid fuel combustion, *21st Symp. (Int.) on Comb.*, 463-471, 1986

[55] Umemura, A. and Shimada, Y., Characteristics of supercritical droplet gasification, *26th Symp. (Int.) on Comb.*, 1621-1628, 1996

[56] Umemura, A. and Shimada, Y., Linear acoustic characteristics of supercritical droplet vaporization, *27th Symp. (Int.) on Comb.*, 2659-2665, 1998

[57] Bellan, J. and Summerfield, M., Theoretical examination of assumptions commonly used for the gas phase surrounding a burning droplet, *Combust. Flame*, 33, 107-122, 1978

[58] Delplanque, J-P. and Sirignano, W. A., Stability influence of transcritical LOX droplet vaporization in an idealized rocket combustor, AIAA 93-0231, 31st Aerospace Sciences Meeting, Reno, NV, 1993

[59] Oefelein, J. C. and Yang, V., Analysis of transcritical spray phenomena in turbulent mixing layers, AIAA 96-0085 34^{th} Aerospace Sciences Meeting, Reno, NV., 1996

[60] Curtis and Farrell, P. V., Droplet vaporization in a supercritical microgravity environment, *Acta Astronautica*, 17(11/12), 1189-1193, 1988

[61] Sui, P-C. and Chen, L-D., Heat and mass diffusion in binary systems composed of supercritical and subcritical fluids, AIAA 97-3046, 33rd AIAA/ASME/ASAE/ASEE Joint Propulsion Conference, 1997

[62] Harstad, K. and Bellan, J., The Lewis number under supercritical conditions, *Int. J. Heat Mass Transfer,* **42,** 961-970, 1999

[63] Grew, K. E. and Ibbs, T. C., *Thermal Diffusion in Gases*, Cambridge University Press, Cambridge, 1952

[64] Rosner, D. E., Thermal (Soret) diffusion effects on interfacial mass transport rates, *Physico-Chemical Hydrodynamics*, 1, 159-185, 1980

[65] Curtis and Farrell, P. V., A numerical study of high-pressure droplet vaporization", *Combust. Flame*,90, 85-102, 1992

[66] Jia, H. and Gogos, G., Investigation of liquid droplet evaporation in subcritical and supercritical gaseous environments, *Journal of Thermophysics and Heat Transfer*, 6(4), 738-745, 1992

[67] Chiang, C. H. and Sirignano, W. A., Axisymmetric vaporizing oxygen droplet computations, AIAA 91-0281, 29th Aerospace Sciences Meeting, Reno, NV, 1991

[68] Delplanque, J-P. and Sirignano, W. A., Numerical study of the transient vaporization of an oxygen droplet at sub- and super-critical conditions, *Int. J. Heat Mass Transfer*, 36(2), 303-314, 1993

[69] Tsukamoto, T. and Niioka, T., Numerical simulation of fuel droplet evaporation and ignition under high temperature and high pressure, *Prog. Astro. Aero.*, 152, 263-279, 1993

[70] Jia, H. and Gogos, G., High pressure droplet vaporization; effects of liquid-phase solubility, *Int. J. Heat Mass Transfer*, 36(18), 4419-4431, 1993

[71] Shuen, J-S., Yang, V. and Hsiao, G. C., Combustion of liquid-fuel droplets in supercritical conditions, *Combust. Flame*, 89, 299-319, 1992

[72] Yang, V., Lin, N. and Shuen, J-S., Vaporization of liquid oxygen (LOX) droplets in supercritical hydrogen environments, *Combust. Sci. and Tech.*, **97**, 247-270, 1994

[73] Harstad, K. and Bellan, J., The d^2 variation for isolated LOX drops in hydrogen and n-heptane drops in nitrogen at subcritical/supercritical conditions, in preparation

[74] Harstad, K. and Bellan, J., The d^2 variation for polydisperse clusters of LOX drops in hydrogen at supercritical conditions, submitted for publication, 1999

[75] Haldenwang, P., Nicoli, C. and Daou, J., High pressure vaporization of LOX droplet crossing the critical condition, *Int. J. Heat Mass Transfer*, **39**(16), 3453-3464, 1996

[76] Sanchez-Tarifa, C., Crespo, A. and Fraga, E., A theoretical model for the combustion of droplets in supercritical conditions and gas pockets, *Astron. Acta*, 17, 685-692, 1972

[77] Takahashi, S., Preparation of a generalized chart for diffusion coefficients of gases at high pressures, *Journal of Chemical Engineering (Japan)*, 1974, **7**, 417- 420

[78] Lafon, P. and Habiballah, M., Numerical analysis of droplet vaporization and burning under high-pressure conditions, AIAA94-2909, 30th AIAA/ASME/SAE/ASEE Joint Propulsion Conference, June 27-29, Indianapolis, IN, 1994

[79] Sarman, S. and Evans, D. J., Heat flux and mass diffusion in binary Lennard-Jones mixtures, *Phys. Rev.* **A45**(4), 2370-2379, 1992

[80] Stengele, J. Bauer, H.-J. and Wittig, S., Numerical study of bicomponent droplet vaporization in a high pressure environment, ASME paper 96-GT-442, 1996

[81] Harstad, K. and Bellan, J., A validated all-Pressure fluid drop model for binary mixtures: heptane in nitrogen, AIAA 99-206, Joint AIAA/ASME/SAE Propulsion Meeting, Los Angeles, CA, June 20-23, 1999

[82] Cussler, E. L., *Diffusion. Mass transfer in fluid systems*, Cambridge University Press, 1984

[83] Lee, H. S., Fernandez-Pello, A. C., Corcos, G. M. and Oppenheim, A. K., A mixing and deformation mechanism for a supercritical fuel droplet, *Combust. Flame*, 81, 5-58, 1990

[84] Hsiao, G. C., Yang V. and Shuen, J. S., Supercritical vaporization and dynamics of liquid oxygen (LOX) droplet in hydrogen stream, AIAA 95-0383, 33rd Aerospace Sciences Meeting, Reno, NV, 1995

[85] Delplanque, J-P. and Sirignano, W. A. Boundary-layer stripping effects on droplet transcritical convective evaporation, *Atomization and Sprays*, 4, 325-349, 1994

[86] Gogos, G. and Soh, S. H., Subcritical and supercritical evaporation within a natural convection environment, presented at the Joint Meeting of the United States Sections, The Combustion Institute, March 15-17, 1999

[87] Daou, J. and Rogg, B., Convective burning of gaseous fuel pockets and supercritical droplets, *Combust. Flame*, 115, 145-157, 1998

[88] Harstad, K. and Bellan, J., Numerical simulations of polydisperse clusters of n-heptane drops in nitrogen, in preparation

[89] Peng, D-Y. and Robinson, D. B., A rigorous method for predicting the critical properties of multicomponent systems from an equation of state", *AIChE J.*, 23(2), 137-144, 1977

[90] Snyder, R., Herding, G., Rolon, J. C. and Candel, S. Analysis of flame patterns in cryogenic propellant combustion, *Comb. Sci. and Tech.*, 124, 331-370, 1997

[91] Jiang, T. L. and Chiang, W-T., Effects of multiple droplet interaction on droplet vaporization in subcritical and supercritical pressure environments", *Comb. Flame*, 97, 17-34, 1994

[92] Jiang, T. L. and Chiang, W-T., Vaporization of a dense spherical cloud of droplets at subcritical and supercritical conditions, *Combust. Flame*, 97, 355-362, 1994

[93] Jiang, T. L. and Chiang, W-T., Transient heating and vaporization of a cool dense cloud of droplets in hot supercritical surroundings, *Int. J. Heat Mass Transfer*, 39(5), 1023-1031, 1996

[94] Delplanque, J-P., Liquid oxygen droplet vaporization and combustion: Analysis of transcritical behavior and application to liquid rocket combustion instability, PhD thesis, University of California, Irvine, Department of Mechanical Engineering, 1992

[95] Oefelein, J. C. and Yang, V., Analysis of hydrogen-oxygen mixing and combustion processes at high-pressures, AIAA 96-0085 35^{th} Aerospace Sciences Meeting, Reno, NV., 1997

[96] Erlebacher, G., Hussaini, M. Y., Speziale, C. G. and Zang, T. A,. Toward the Large Eddy Simulation of compressible turbulent flows, *J. Fluid Mech.*, 238, 155-185, 1992

[97] Miller, R. S., Harstad, K. and J. Bellan, J.,Direct numerical simulations of supercritical fluid mixing layers applied to heptane nitrogen, submitted for publication to *J. Fluid Mech.*, 1999

[98] Yang, A-S., Kuo, K. K. and Hsieh, W. H., Supercritical evaporation and combustion of liquid oxygen in an axisymmetric configuration, *Progress in Astronautics and Aeronautics*, 166, 439-480, 1996

[99] Chegini, H., Chaturvedi, S. K. and Kondic, N., Heat and mass transfer from a supercritical LOX spray, *Int. Comm. Heat Mass Transfer*, 18, 767-778, 1991

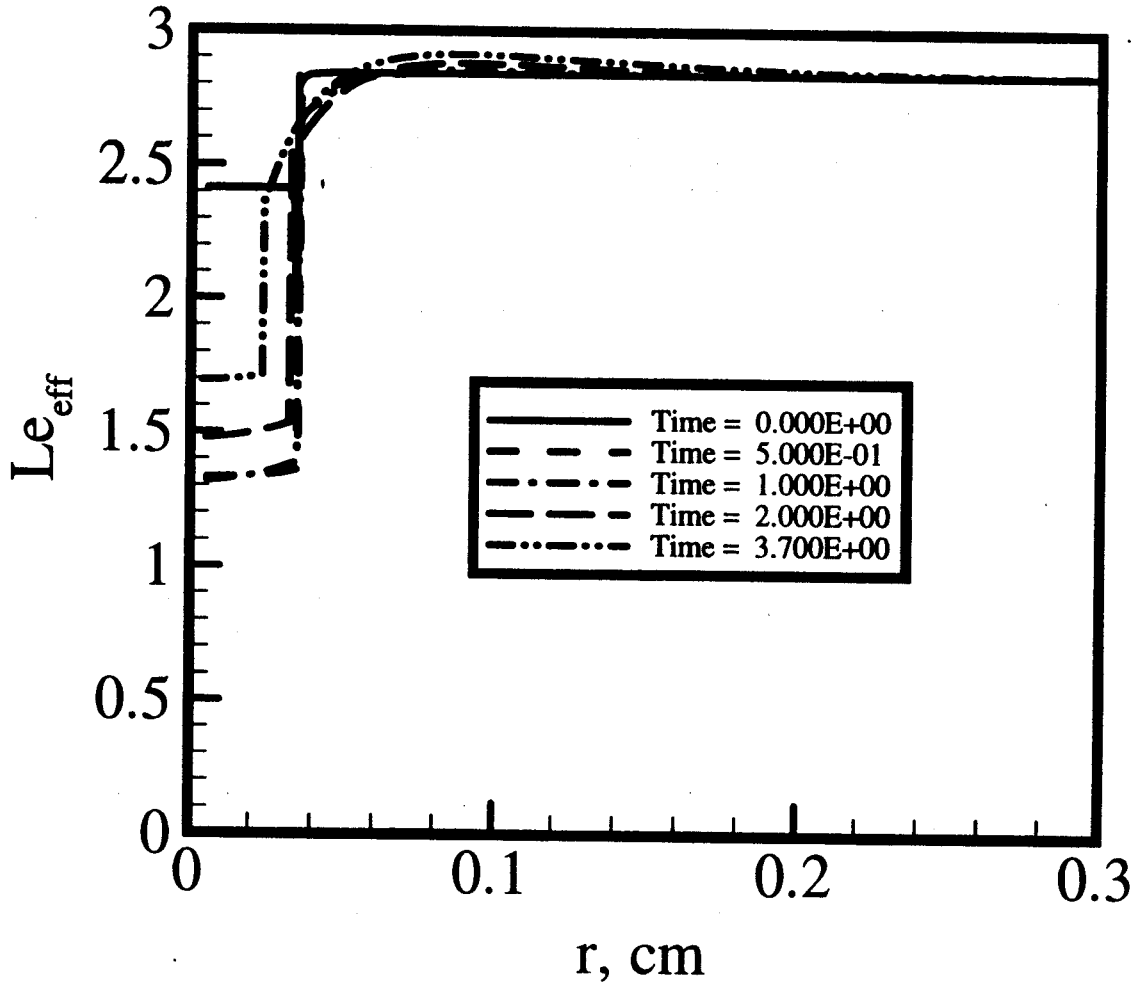
3
2.5
2
1.5
1
0.5
0
0
0.1
0.2
0.3
Le_{eff}
r, cm
Time = 0.000E+00
Time = 5.000E-01
Time = 1.000E+00
Time = 2.000E+00
Time = 3.700E+00

Fig 9d

		$T_r(T)$	
$p_r(p)$	$0.81(300K)$	$0.86(320K)$	$0.92(340K)$
$2.35(100bar)$	10%	13.5%	13.5%
$7.06(300bar)$	25%	32%	35%

Table 1: Percent error in the calculation of thermal conductivity for propane if calculated for a liquid instead of a fluid. T_r and p_r are the reduced values of temperature and pressure, respectively.

Species	$p_c(MPa)$	$T_c(K)$
water	22.064	647.0
air	3.766	132.5
nitrogen	3.39	126.2
oxygen	5.043	154.6
hydrogen	1.313	33.2
helium	0.227	5.2
nitromethane	5.87	588.0
n-butane	3.784	425.1
n-pentane	3.364	469.7
n-hexane	3.010	507.7
n-heptane	2.76	540.3
n-octane	2.493	568.9
iso-octane	2.57	543.9
n-nonane	2.29	594.6
n-decane	2.104	617.7
n-dodecane	1.824	658.2
n-hexadecane	1.57	722.0
methanol	8.092	512.6
ethanol	6.137	513.9
1-propanol	5.170	536.8
methyl iodine	7.366	528.0
aniline	5.24	503.0
light oil	1.5	743.0
Freon-13	3.87	302.0
Refrigerant 113	3.38	487.0
sulfur hexafluoride	3.77	318.7

Table 2: Critical pressure and temperature of the species discussed in this paper. The chemical formula corresponding to the species names appear in Table 3.

References	Config.	Fluids	p, MPa	p_r	T, K	T_r
Anderson, T. J. et al., 1994 [20]	drops$_n^e$	LO_x in He H_2O and CH_4O in air	4.1-5.86 0.1	0.81-1.16 0.004/0.01	300 300	1.9 0.46/0.6
Birk, A. et al., 1992 [38]	sprays^{d,co}	H_2O in N_2 C_2H_6O in N_2 CH_3NO_2 in N_2	28-33 28 28-33	1.27-1.50 4.56 4.77-5.62	293-803 753 753	0.45-1.24 1.46 1.28
Birk, A. et al., 1995 [39]	circ./ann. jets^d	CH_3I in N_2 or in mixtues ofH_2O, O_2, H_2, N_2 and/or Ar	6.48-13.79 1.38-13.79	0.88-1.87 0.187-1.87	293-623 293-2225	0.55-1.18 0.55-4.21
Brzustowski, T. A. and Natarajan, R., 1966 [12]	drops$_n^{e,co}$	aniline in $N_2 + O_2$ mixtures	0.69-5.51	0.132-1.05	446-773	0.87-1.54
Canada, G. S. and Faeth, G. M., 1973 [31]	drops$_n^{co}$	CH_4O, C_2H_6O, $C_3H_8O, C_5H_{12}, C_7H_{16}$, $C_{10}H_{22}$ in air	up to 10.1	calc. using Table 2	300	calc. using Table 2
Chauveau, C. et al., 1993 [16]	drops$_{n,m}^{e,co}$	C_7H_{16} in air	0.1-9	0.04-3.26	300	0.56
Chauveau, C. et al., 1995 [18]	drops$_{n,m}^{e,co}$	CH_4O in air and N_2	up to 9	up to 1.2	300	0.59
Chesnau, X. et al., 1994 [19]	drops$_n^e$	LO_x in air, N_2 or He	0.1- 3	0.02-0.59	300	1.94
Chehroudi, B. et al., 1999 [43]	jets^d	N_2,in N_2, or $CO + N_2$ He in N_2, O_2 in N_2	0.77-9.19 0.77-9.19 0.77-9.19	0.23-2.74 3.39-40.5 0.15-1.8	300 300 300	2.37 57.7 1.94
Faeth, G. M. et al., 1969 [22]	drops$_m^{co}$	$C_{10}H_{22}$ in $N_2 + O_2$ mixtures	0.69-14.45	0.33-6.87	300	0.49
Ivancic et al. [46]	jets$_n^{co}$	LO_x in H_2	6	1.19	n.a.	n.a.
Jasuja, A. K. and Lefebvre, A. H., 1994 [37]	spray^d	aviation kerosene in air	0.1-1.2	n.a.	300	n.a.
Kadota, T. and Hiroyasu, H., 1981 [32]	drops$_n^{co}$	$C_7H_{16}, C_8H_{18}, C_{10}H_{22}$, $C_{12}H_{26}, C_{16}H_{34}$, and light oil in air	0.1-4.05	calc. using Table 2	n.a.	n.a.
Krülle, G. and Mayer, W., 1994 [36]	spray^d	H_2O in air	$\sim$ 0.1-2	0.004-0.1	300	0.46
Lazar, R. S. and Faeth, G. M., 1971 [23]	drops$_n^{co}$	$C_8H_{18}, C_{10}H_{22}$ in air	up to 7.1	calc. using Table 2	300	calc. using Table 2

Table 3: Experimental conditions for the references discussed in this paper. The pressure and temperature refer to the chamber conditions. Both p_r and T_r are calculated by dividing the chamber (p, T) values by the critical values of the fluid in the drop, jet or spray. The superscript co indicates a combustion whereas e indicates an evaporation/emission experiment. For jets or sprays, the superscript d indicates break-up or disintegration (a general term valid for both subcritical and supercritical conditions). The subscripts n and m refer to normal and microgravity experiments, respectively. For jets and sprays all experiments were performed in normal gravity.

References	Config.	Fluids	p, MPa	p_r	T, K	T_r
Matlosz, R. L. et al., 1972 [15]	drops$_n^e$	C_6H_{14} in N_2 and Ar	0.69-11.25	0.23-3.73	548	1.08
Mayer, W. and Tamura, H., 1996 [40]	spray^{d,co}	LO_x in air, H_2	1-10	0.2-1.98	150-300	0.97-1.94
Mayer, W. et al., 1996 [41]	jets^{d,co}	LO_x in H_2 LN_2 in He	1-10 2-5	0.2-1.98 0.59-1.47	150-300 275	0.97-1.94 2.18
Mayer, W. et al., 1998 [42]	jets^{d,co}	LN_2 in N_2 LN_2 in He	2-4 1-6	0.59-1.18 0.29-1.77	300 280	2.38 2.22
Mikami, M. et al., 1997 [25]	drops$_m^c$	C_7H_{16}, $C_{16}H_{34}$, and mixtures of the two in air	0.1-6.0	0.036-3.8; n.a. for mixtures	300	0.4-0.55; n.a. for mixtures
Mikami, M. et al., 1998 [26]	drops$_m^c$ (single/two interacting)	C_7H_{16}, $C_{16}H_{34}$, and mixtures of the two in air	0.1-6.0	0.036-3.8; n.a. for mixtures	300	0.4-0.55; n.a. for mixtures
Morin, C. et al., 1999 [17]	drops$_n^e$	C_7H_{16} in N_2	0.1-10	0.36-3.6	293-973	0.54-1.8
Natarajan, R. and Brzustowski, T. A., 1970 [13]	drops$_n^{e,co}$	C_5H_{12} in $O_2 + (N_2$ or $He)$	0.47-4.45	0.14-1.32	588.5	1.34
Niioka and Sato, 1986 [33]	drops$_n^c$	C_7H_{16}, $C_{16}H_{34}$, and mixtures of the two in air	0.1-2.0	0.036-1.27; n.a. for mixtures	300	0.4-0.55; n.a. for mixtures
Nomura, H. et al., 1996 [10]	drops$_m^e$	C_7H_{16} in N_2	0.1-5.0	0.036-1.8	398-765	0.74-1.41
Okai, K. et al., 1998 [27]	drops$_m^{co}$ (single/two interacting)	C_7H_{16}, $C_{16}H_{34}$, and mixtures of the two in $N_2 - O_2$ (0.12 mole fraction)	1.0-3.0	0.36-1.9; n.a. for mixtures	300	0.4-0.55; n.a. for mixtures
Oschwald et al., 1999 [45]	jets$_n^e$	LN_2 in H_2	4	1.17	270	2.13
Sankar, S. V. et al., 1992 [35]	sprays^d	water in air	up to 0.69	0.03	300	0.46
Sato, J. et al., 1990 [24]	drops$_{n,m}^{co}$	C_8H_{18} in air	up to 10.0	up to 4.0	n. a.	n. a.
Sato, J., 1993 [9]	drops$_{n,m}^{e,co}$	C_7H_{16} in N_2; $C_{16}H_{34}$ in air	up tp 15	up to 5.43	297-756	0.55-1.4
Savery, C. W., 1969 [14]	drops$_n^e$	water in air $CClF_3$ in air C_7H_{16} in air	2.03-6.08 2.93-6.89 0.1-10.13	0.09-0.28 0.76-1.78 0.036-3.67	358-416 310-422 310-422	0.55-0.64 1.03-1.40 0.57-0.78
Stengele, J. et al., 1999 [21]	drops$_n^e$	C_5H_{12}, C_9H_{20} and mixtures of the two in N_2	2-4	0.6-1.73; n.a. for mixtures	500-650	0.84-1.38; n.a. for mixtures
Vieille, B. et al., 1996 [8]	drops$_{n,m}^{co}$	CH_4O, C_2H_6O, C_6H_{14}, C_8H_{18} in air	up to 11.2	up to 4.5	300	0.53-0.59

Table 3: Cont'd.

Group	Ref.	Config.	Species	$p_\infty; T_\infty$	Real gas EOS	S/D effects	High p λ and μ	Turb. model	Comments on model
Bellan and co.	[7]	$drop^{e}_{nc,s}$	LO_x in H_2		yes	yes	yes	no	
	[30]	$cluster^{e}_{nc,s}$	LO_x in H_2		yes	yes	yes	no	
	[62]	$drop^{e}_{nc,s}$; $cluster^{e}_{nc,s}$	LO_x in H_2; C_7H_{16} in N_2		yes	yes	yes	no	
	[53]	$drop^{e}_{nc,s}$	C_7H_{16} in N_2	0.1-10; 445-800	yes	yes	yes	no	validated w. microgravity data
	[97]	shear layer	C_7H_{16} in N_2	6; 900,1000	yes	yes	yes	no	2D & 3D DNS
Chegini et al.	[99]	spray^{e}	LO_x in H_2	13.7; 311	yes	n.a.	n.a.	$k-\varepsilon$	Lagrangian drop tracking; subcrit. C_D
Daou and co.	[49]	$drop^{co}_{nc,s}$	LO_x in H_2	10; 1000-2500	yes	no	no	no	
	[75]	$drop^{e}_{nc,s}$	LO_x in H_2	8; 500-2500	yes	no	yes	no	phase eq. or crit. locus at surface
Farrell and co.	[60]	$drop^{e}_{nc,s}$	C_8H_{18} in N_2	2.53-4.98;	yes	no	no	no	phase eq.
				550-1138					
	[65]	$drop^{e}_{nc,s}$	$R113$ in N_2 C_7H_{16} in N_2 $C_{12}H_{26}$ in N_2	1-2; 550-600 5; 300-800 5.2-6; 744-975	yes	yes	no	no	phase eq.
Gogos and co.	[66]	$drop^{e}_{nc,s}$	C_6H_{14} in N_2	0.1-10.1; 500 to 1250	yes	no	yes	no	phase eq.;w/o solubility or viscous dissip.
	[70]	$drop^{e}_{nc,s}$	C_6H_{14} in N_2	same; to 1500	yes	no	yes	no	w. solubility
	[86]	$drop^{e}_{nc,s}$	C_6H_{14} in N_2	0.69-10,3; 548	yes	n.a.	n.a.	no	
Jiang and Chiang	[91]	$cluster^{e}_{nc,s}$	C_5H_{12} in N_2	0.1-6; 500-1250	yes	no	yes	no	w/o solubility; phase eq.
	[92]	$cluster^{e}_{nc,s}$	C_5H_{12} in N_2	0.5-6; 1000	yes	no	yes	no	
	[93]	$cluster^{e}_{nc,s}$	C_5H_{12} in N_2	0.5-6; 500-2000	yes	no	yes	no	phase eq.
Lafon and Habiballah	[78]	$drop^{e,co}_{nc,s}$	LO_x in H_2	1-20; 1000	yes	no	yes	no	phase eq.
Lee et al.	[83]	$drop^{e}_{c,ns}$	n.a.	n.a.	no	no	no	no	potential flow around drop; initial harm. vortex sheet at surface

Table 4: Features of models discussed in this paper. The pressure and temperature refer to the far field conditions and are in MPa and K, respectively. "EOS" stands for Equation of State. "S/D" stands for Soret/Dufour. A 'cluster' is defined to be a cluster of spherical drops. The superscripts e and co refer to emission and combustion conditions, respectively. The subscripts nc, s and ns refer to non-convective, spherical and non-spherical, respectively. Additionally: "calc." stands for "calculated; "crit." stands for "critical" ; "cst." stands for "constant"; "diff." stands for "diffusivity"; "dissip." stands for "dissipation"; "DNS" stands for Direct Numerical Simulation"; "eq." stands for "equilibrium"; "harm." stands for "harmonic"; "n.a." stands for "not available"; "w." stands for "with"; "w/o" stands for "without".

Group	Ref.	Config.	Species	$p_\infty; T_\infty$	Real gas EOS	S/D effects	High p λ and μ	Turb. model	Comments on model
Mayer and co.	[6]	spray_c^e	LO_x/H_2	n.a.	no	no	no	yes	drops tracked as if liquid
	[46]	jet_c^{co}	LO_x/H_2	6; n.a.	yes	n.a.	n.a.	yes	steady model; chemical eq.
Sirignano and co.	[67]	drop_c^e	LO_x/CH_4	1000	no	no	n.a.	no	phase eq.; w/o solubility
	[68]	$\text{drop}_{nc}^{e,co}$	LO_x/H_2; C_6H_{14}/air	1-20; 1500 0.1; 1500	yes	no	no	no	constant density; w/o solubility; no viscous dissip; mixt. approx. by gas with average properties
	[58]	drop_c; array_c^{co}	LO_x/H_2+ H_2O	10; 1000	yes	no	n.a.	no	same as above
	[85]	$\text{drops}_{c,s}^e$	LO_x/H_2	10; 1000	yes	no	n.a.	no	w/o solubility; phase eq. at the drop surface
Stengele et al.	[80]	$\text{drop}_{nc}^{e,co}$	C_7H_{16}+ $C_{12}H_{26}/N_2$	0.1-4; 800-2000	yes	no	yes	no	phase eq. at the drop surface; drop diffusion limit model
Sui and Chen	[61]	drop_{nc}^e	F_6S/N_2		yes	S yes; D no	yes	no	phase eq. at the drop surface
Tsukamoto and Niioka	[69]	$\text{drop}_{nc,s}^{e,co}$	C_7H_{16}/N_2	0.1-9; 800-1000	yes	no	yes	no	

Table 4: Cont'd.

Group	Ref.	Config.	Species	$p_\infty; T_\infty$	Real gas EOS	S/D effects	High p λ and μ	Turb. model	Comments on model
Umemura and co.	[54]	stream^{e,co}	C_4H_{10}/N_2 C_4H_{10}/air	2.84-15.1; 132-660	yes	no	yes	no	phase eq. at the drop surface; $Le = 1$; same, cst. C_p for the two species
	[55]	drop$^{e}_{nc}$	n.a./N_2	n.a.	yes	no	yes	no	empirical factor to get null diff. at the crit. point
	[56]	drop$^{e}_{nc}$	n.a./N_2	n.a.	yes	no	yes	no	phase eq. at the drop surface; empirical factor to get null diff. at the crit. point
Yang A-S. et al.	[98]	stream^{e,co}	LO_x in He; LO_x in H_2 + He	3, 6.8; 300, n.a.	no	no	yes	no	steady model; no visc. dissip.; phase eq. at the drop surface; w. differential diff.;
Yang . V. and co.	[71]	drop$^{e,co}_{nc}$	C_5H_{12} in air	0.5-14; 1000	yes	no	yes	no	phase eq. at the drop surface; w/o solvability
	[72]	drop$^{e}_{nc}$	LO_x in H_2	0.5-25; 1000	yes	no	yes	no	same as above
	[84]	drop$^{e}_{c,ns}$	LO_x in H_2	10-40; 1000	yes	no	yes	no	same as above; w/o viscous dissip.; the drop surface defined to be at the crit point; C_D calc.
	[59]	2D mix. layer w. drops^{e}	LO_x drops in H_2; H_2	0.1-40; 1000	yes	no	yes	yes	LES w. subcrit. SGS; Lagrangian drop tracking; above C_D used
	[95]	2D mix. layer w. drops^{co}	LO_x drops in H_2; H_2	10; n.a.	yes	no	yes	yes	same as above

Table 4: Cont'd.

p_e, MPa	T_e, K	K (μg)	K (normal g)	K_{ap}	$K_{ap}/K_{data,\mu g}$
0.1	470	0.116 (Nom)	0.22 (Mor)	0.135	1.16
0.1	655	0.306 (Nom)	0.45 (Mor)	0.280	0.92
0.1	745	0.390 (Nom)	0.56 (Mor)	0.350	0.90
0.5	470	0.117 (Nom)		0.135	1.15
0.5	655	0.356 (Nom)		0.320	0.90
0.5	745	0.437 (Nom)		0.390	0.89
1.0	470	0.138 (Nom)		0.135	0.98
1.0	655	0.424 (Nom)		0.330	0.78
2.0	445	0.097 (Sat)	0.14 (Sat)	0.0935	0.97
2.0	452	0.096 (Nom)			
2.0	655	0.475 (Nom)		0.360	0.76
2.0	745	0.4 - 1.7 (Nom)		0.450	—
5.0	495	0.2 - 0.13 (Nom)		0.140	0.70 - 1.08

Table 5: Maximum regression rate of the maximum density gradient location, K in mm^2/s, obtained from the current model (ap), Nomura et al.'s, 1996, microgravity experimental data (Nom), Sato's, 1993, microgravity and normal gravity experimental data (Sat), and Morin et al.'s, 1999, normal gravity data (Mor). The Nomura et al.'s and Morin et al.'s data were provided by the authors, and Sato's values were read on their graph following the directions given in their paper. In the simulations $T_d^0 = 300$ K and $d^0 = 0.7$ mm, while Nomura et al.'s d^0 was 0.6 - 0.8 mm, Sato's was 1mm, and Morin et al.'s was 1 - 1.5 mm.

Figure Captions

Figure 1 Correlation of a jet, mixing layer or spray angle versus the ratio of the chamber fluid density by the injected fluid density.

Figure 2 Fractal dimension versus reduced pressure for jets.

Figure 3 Molecular weight dependency of the first order term in the expansion of the thermal diffusion factor as a function of temperature according to the Sutherland model. The second species is air.

Figure 4 Heptane/Nitrogen: High temperature comparisons. $R_d^0 = 0.35$ mm; $R_e^0 = 4$ mm, $Y_e^0 = 0$ and $T_{d,b}^0 = 300$ K. In the far field T_e and p_e are specified as in the experiments. Simulations at $T_e = 745$ K and p_e: 0.1MPa, $\alpha_{IK} = 0.01$——; 0.1MPa, $\alpha_{BK} = 0.01$—o—; 0.5MPa, $\alpha_{IK} = 0.01$ - - - -; 0.5MPa, $\alpha_{BK} = 0.01$ - - o - -; 2MPa $-\cdot-$. Data: 741 K and 0.1MPa ■; 749 K and 0.5MPa ▲; 746K and 2MPa ▼.

Figure 5 Heptane/Nitrogen: Intermediary temperature comparisons at 2MPa. $R_d^0 = 0.35$ mm; $R_e^0 = 4$ mm, $Y_e^0 = 0$ and $T_{d,b}^0 = 300$ K. Simulations at 655 K; $\alpha_{IK} = 0.01$ ——; 0.3 - - - ; - 0.3 $-\cdot-$; - 0.6 $-\cdot\cdot-$;0.6 — —; $\alpha_{BK} = 0.01$ —o—. Data at 656 K: ■.

Figure 6 Heptane/Nitrogen: Intermediary temperature comparisons. $R_d^0 = 0.35$ mm; $R_e^0 = 4$ mm, $Y_e^0 = 0$ and $T_{d,b}^0 = 300$ K. Simulations at 655 K: 0.1MPa ——; 0.5MPa - - - -; 1MPa $-\cdot-$; 2MPa — —. Data: 648 K and 0.1MPa ■; 655 K and 0.5MPa ▲; 669 K and 1MPa▼; 656 K and 2MPa •.

Figure 7 Heptane/Nitrogen: Low temperature comparisons. $R_d^0 = 0.35$ mm except at 445K where $R_d^0 = 0.5$ mm; $R_e^0 = 4$ mm, $Y_e^0 = 0$ and $T_{d,b}^0 = 300$ K. Simulations at 470 K: 0.1 MPa —— ; 0.5 MPa - - - ; 1 MPa $-\cdot-$; at 445 K and 2 MPa — —; at 495 K and 5 MPa $-\cdot\cdot-$. Data: 471 K and 0.1 MPa ■; 468 K and 0.5 MPa ▲; 466 K and 1 MPa ▼; 445 K and 2 MPa ◇; 452 K and 2MPa ▶; 493 K and 5 MPa •.

Figure 8 Heptane/Nitrogen: Classical Lewis number, Le, and effective Lewis number, Le_{eff}, at $T_e = 745$ K versus radial location at different times specified in s in the legend. $p_e = 0.1$ MPa in (a) and (b); 2 MPa in (c) and (d).

Figure 9 Heptane/Nitrogen: Classical Lewis number, Le, and effective Lewis number, Le_{eff}, versus radial location at different times specified in s in the legend. (a) and (b) $p_e = 2$ MPa and $T_e = 445$ K; (c) and (d) $p_e = 5$MPa and $T_e = 495$ K.

Jet or Spray or Mixing Layer Divergence Angle vs Chamber-to-injectant Density Ratio

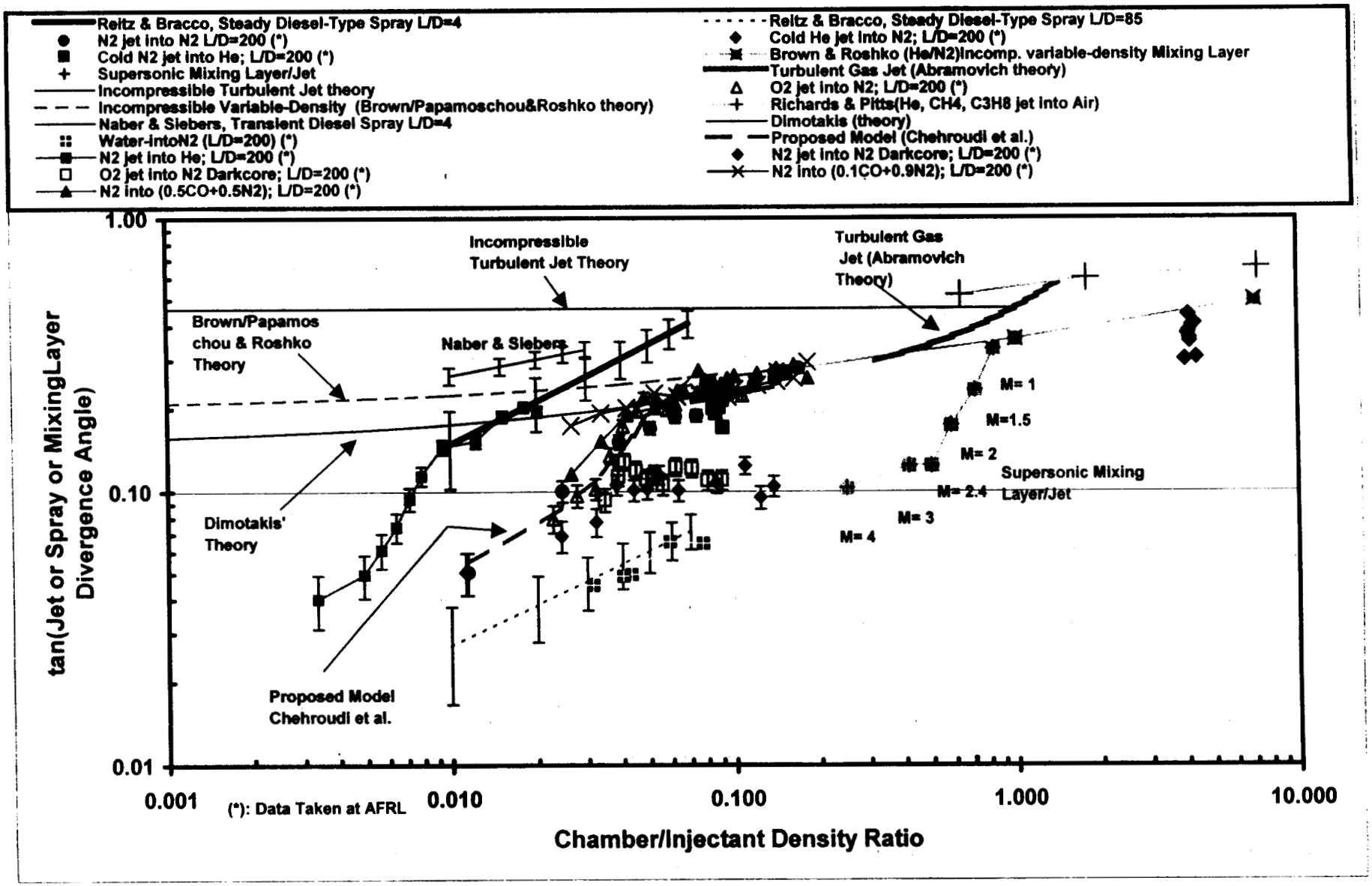

Fig. 1

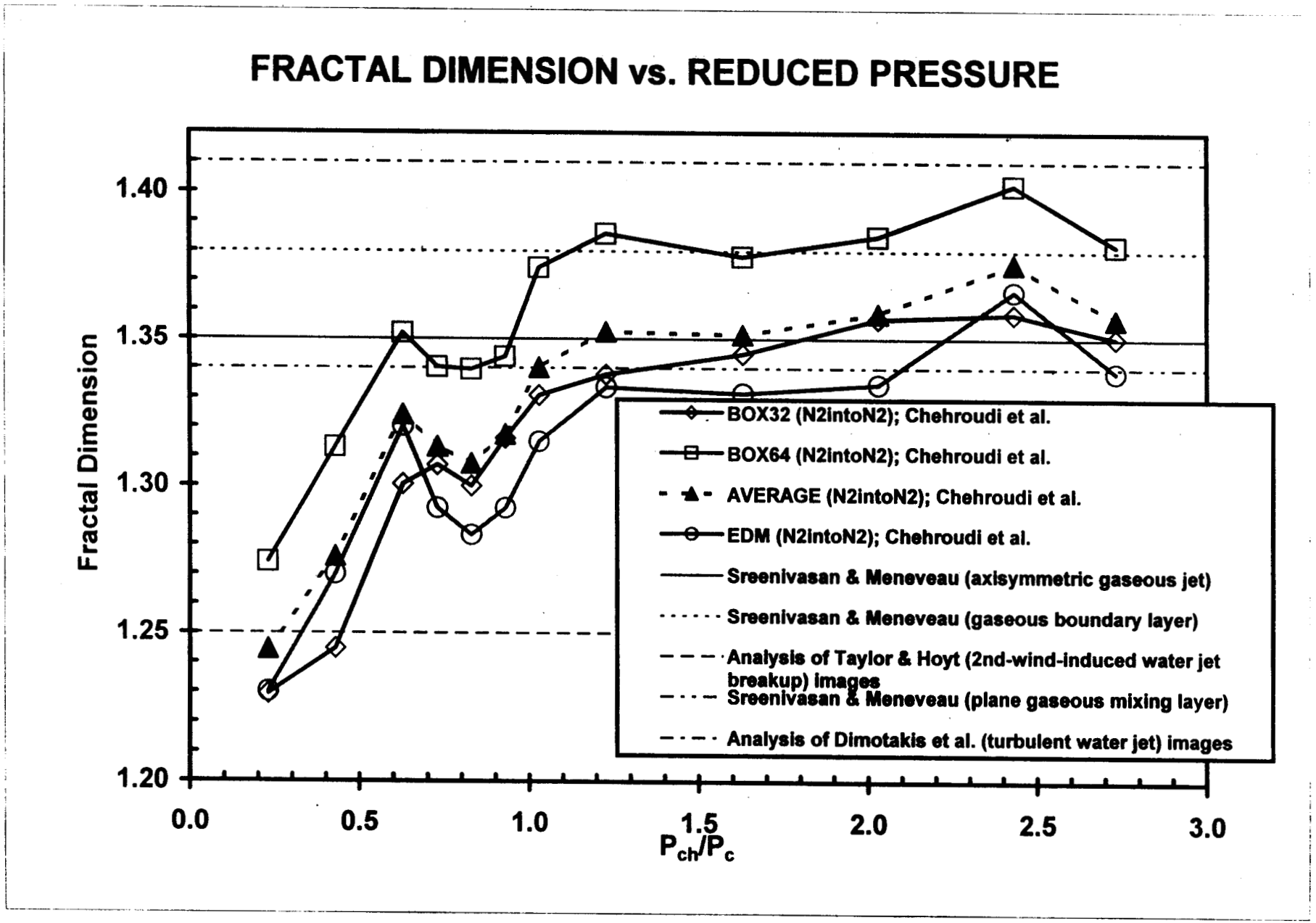
FRACTAL DIMENSION vs. REDUCED PRESSURE
Fractal Dimension
1.40
1.35
1.30
1.25
1.20
0.0
0.5
1.0
1.5
2.0
2.5
3.0
P_{ch}/P_c
BOX32 (N2intoN2); Chehroudi et al.
BOX64 (N2intoN2); Chehroudi et al.
AVERAGE (N2intoN2); Chehroudi et al.
EDM (N2intoN2); Chehroudi et al.
Sreenivasan & Meneveau (axisymmetric gaseous jet)
Sreenivasan & Meneveau (gaseous boundary layer)
Analysis of Taylor & Hoyt (2nd-wind-induced water jet breakup) images
Sreenivasan & Meneveau (plane gaseous mixing layer)
Analysis of Dimotakis et al. (turbulent water jet) images

Fig 2

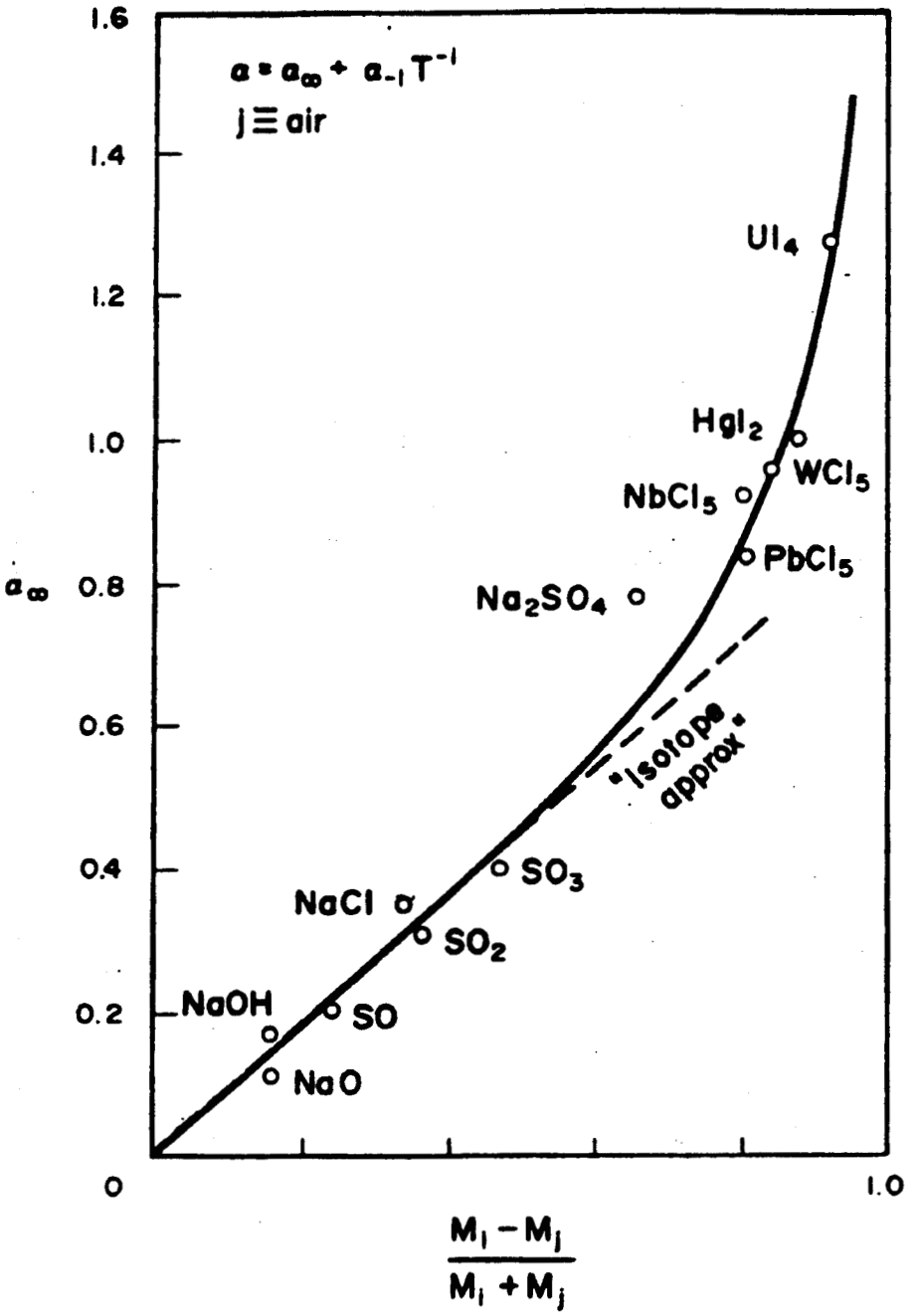
1.6
1.4
1.2
1.0
0.8
0.6
0.4
0.2
0
a_∞
$a = a_\infty + a_{-1} T^{-1}$
j ≡ air
UI_4
HgI_2
WCl_5
$NbCl_5$
$PbCl_5$
Na_2SO_4
"Isotope approx"
SO_3
NaCl
SO_2
NaOH
SO
NaO
1.0
$\frac{M_i - M_j}{M_i + M_j}$

Fig. 3

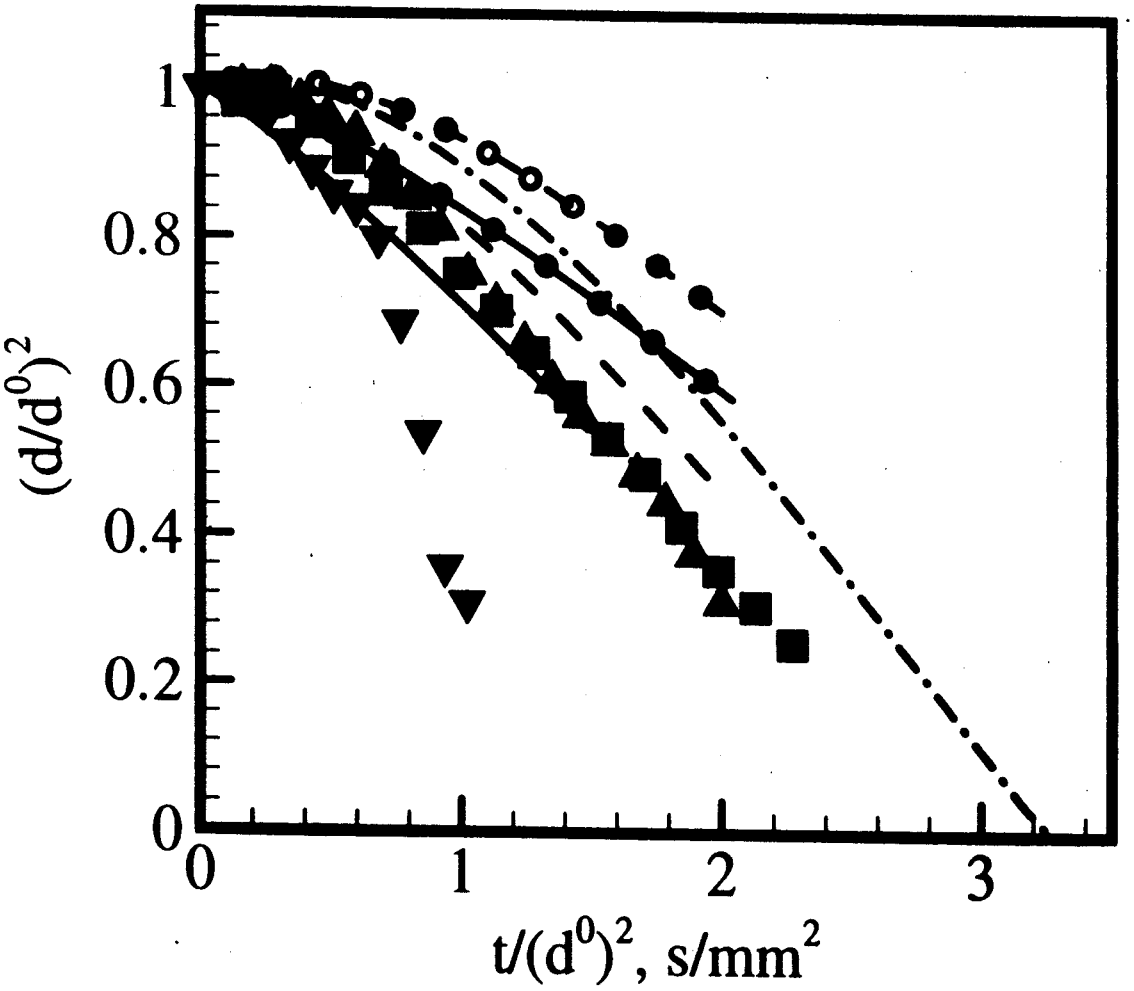

Fig 4

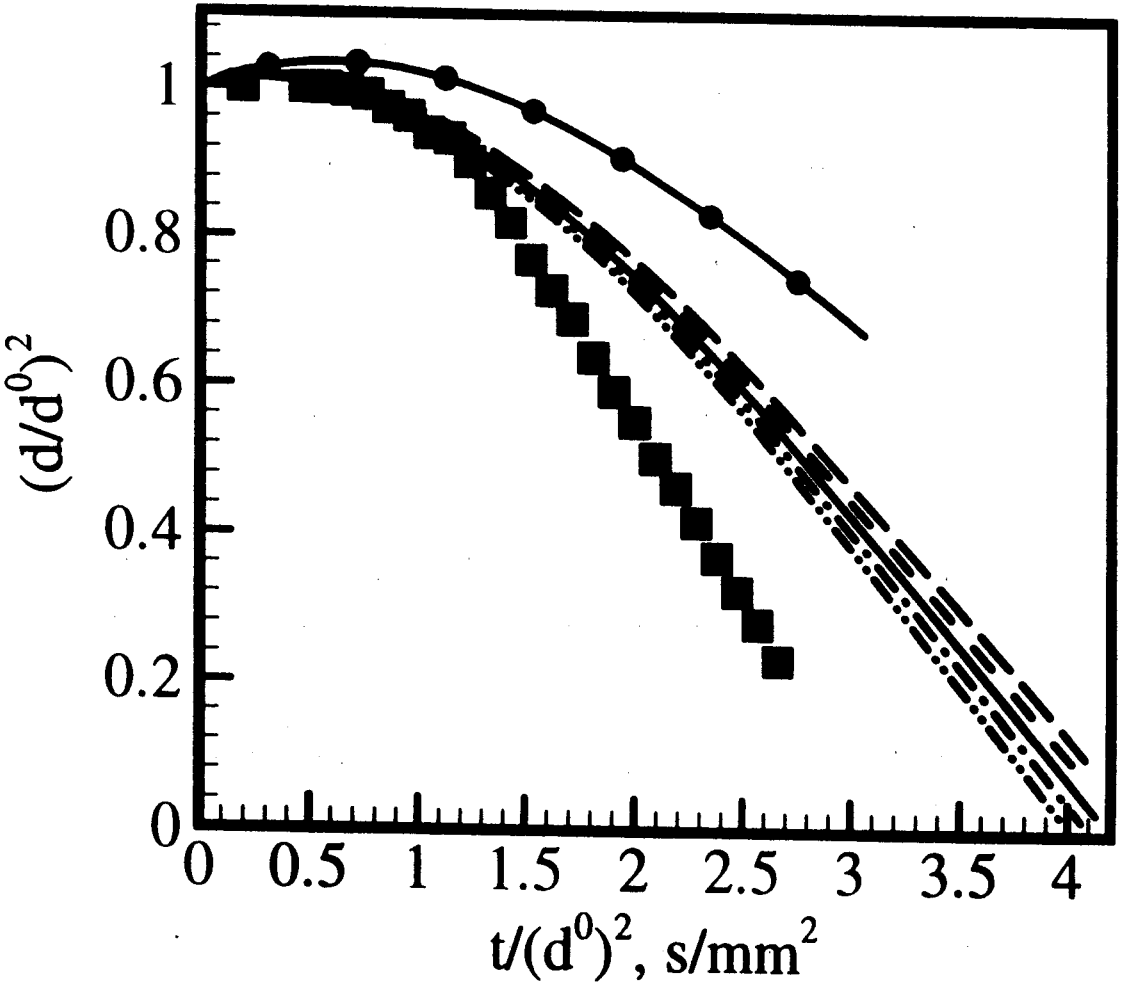

Fig 5.

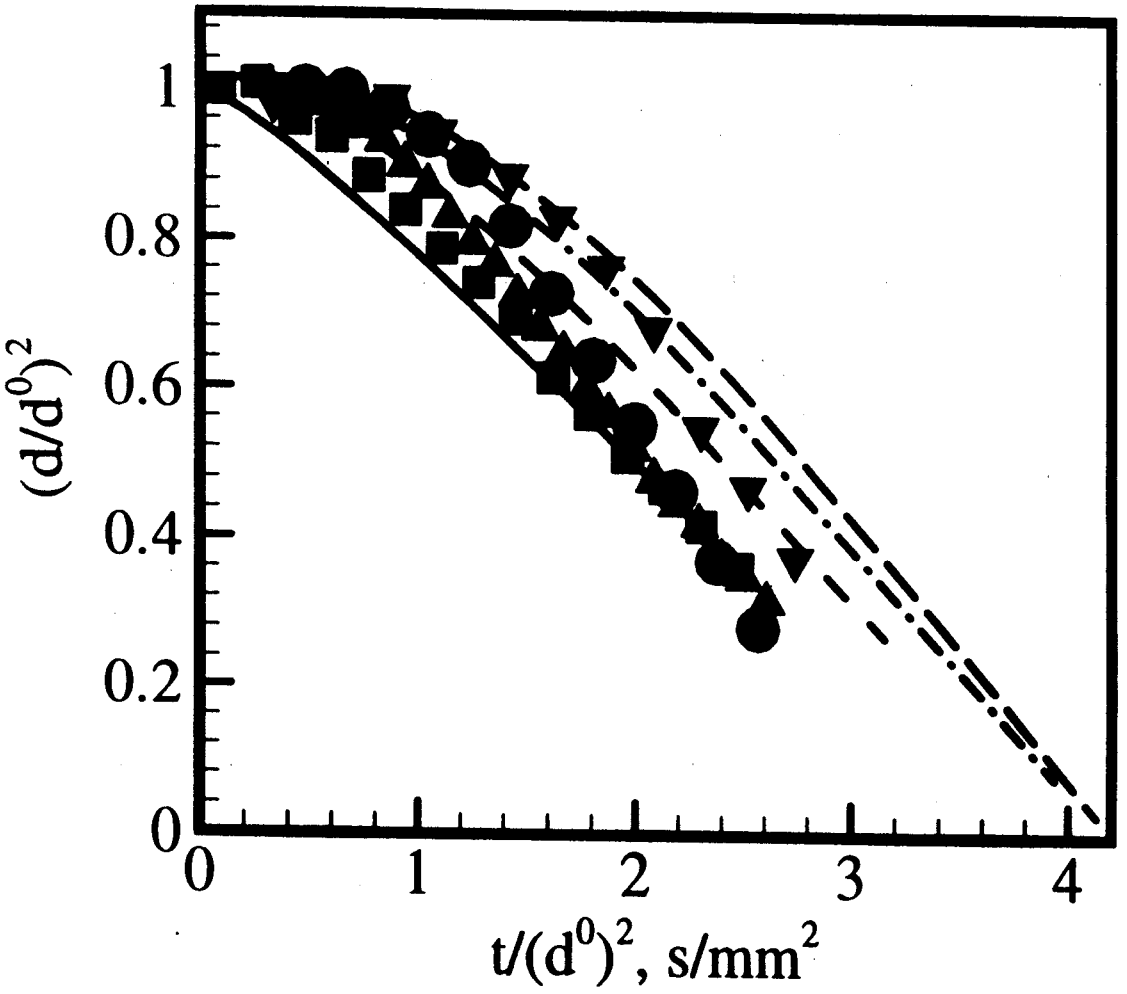

Fig 6.

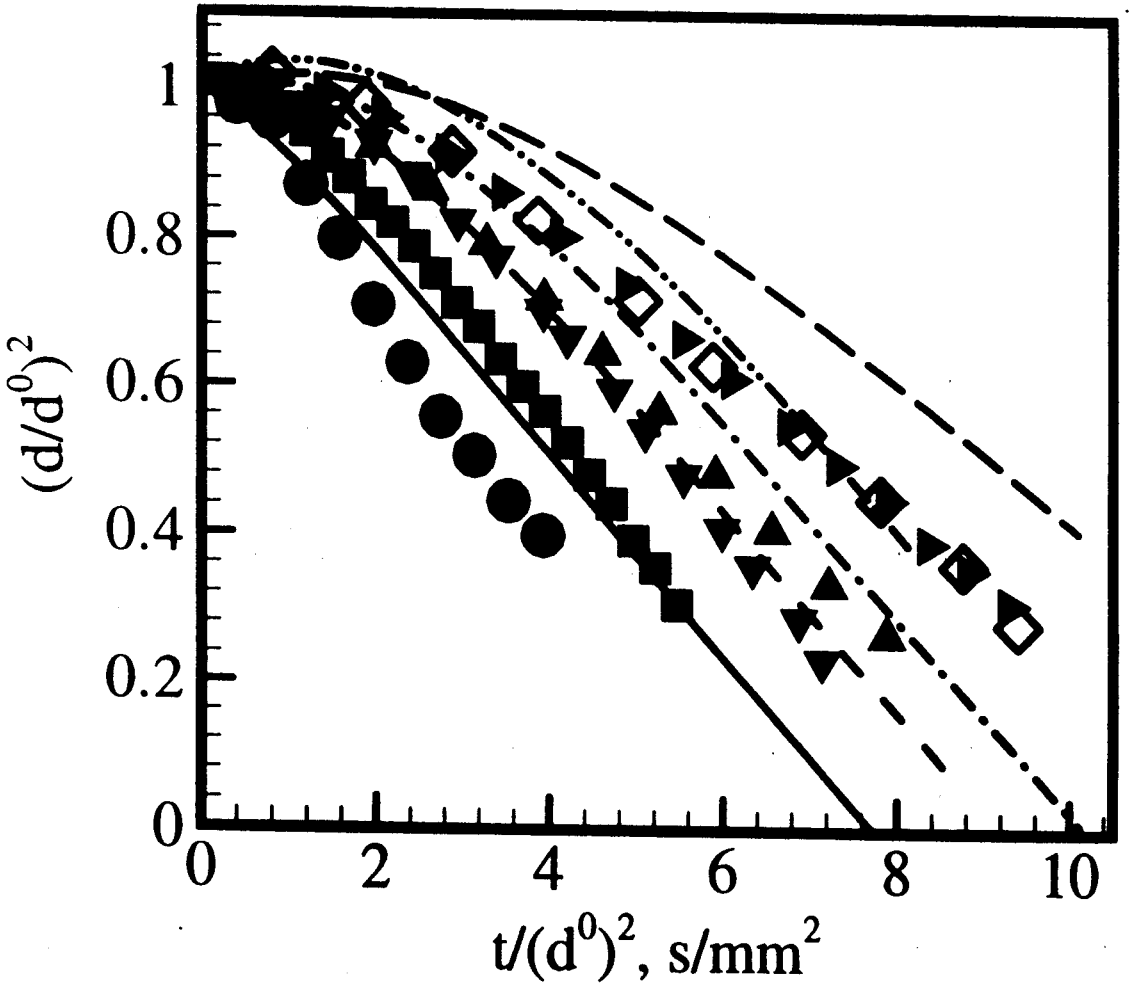

Fig 7.

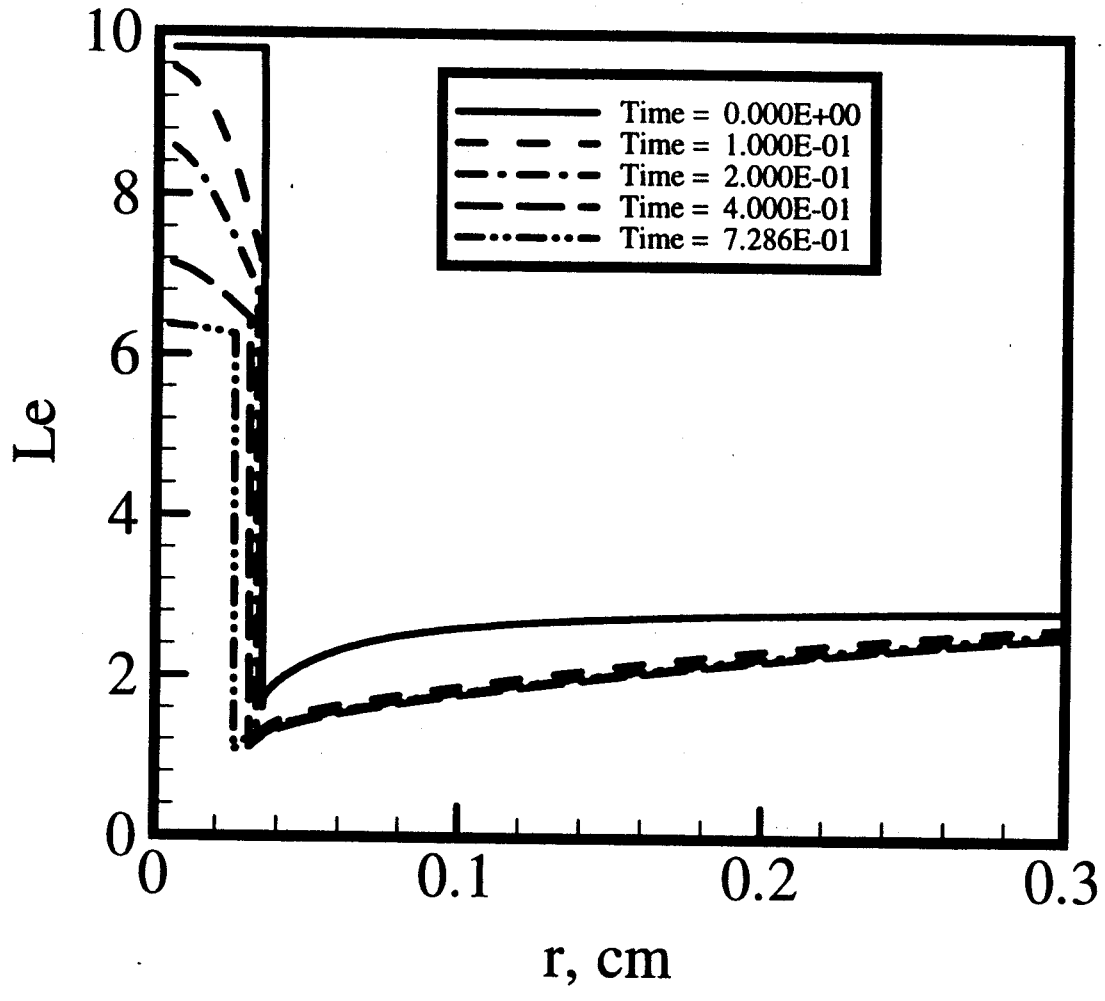
Time = 0.000E+00
Time = 1.000E-01
Time = 2.000E-01
Time = 4.000E-01
Time = 7.286E-01
Le
r, cm
0
2
4
6
8
10
0
0.1
0.2
0.3

Fig 8a

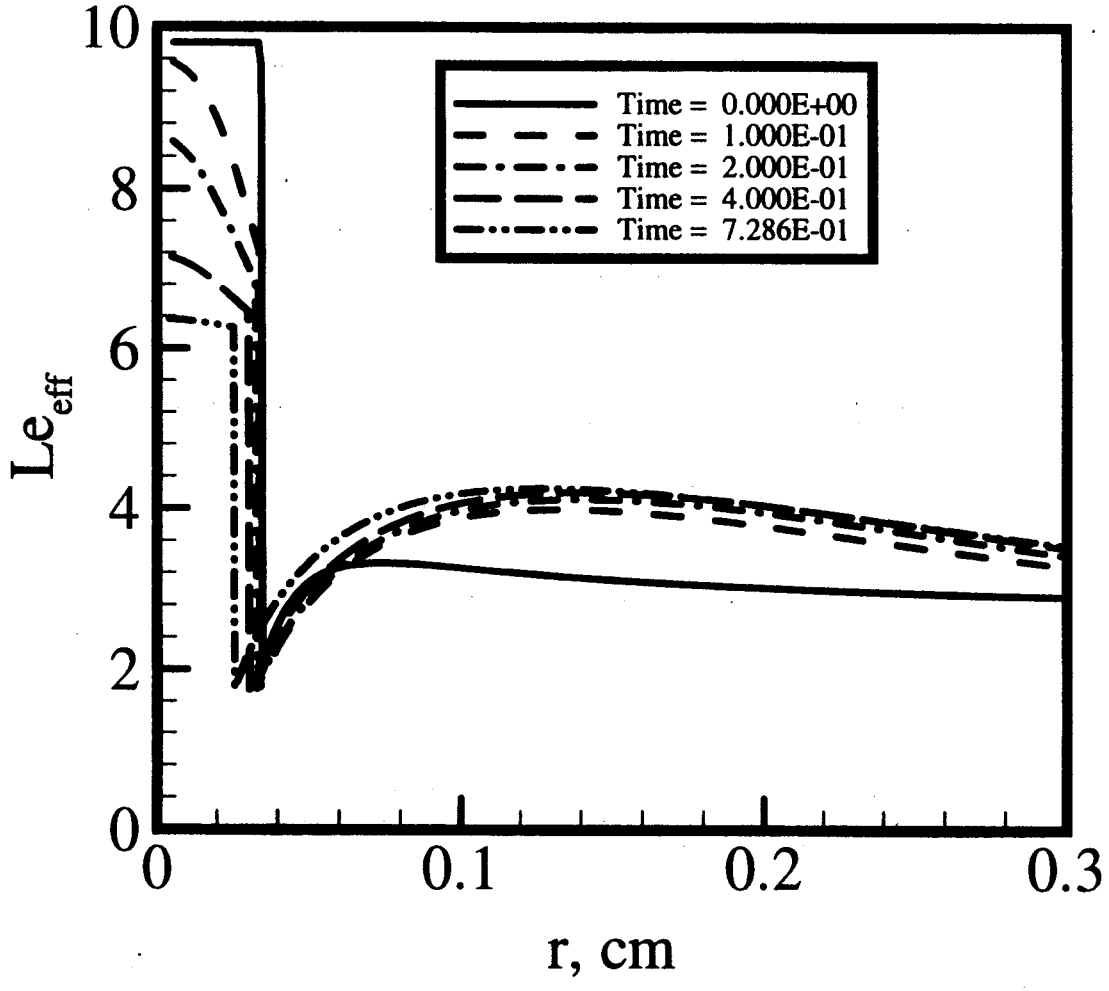
Time = 0.000E+00
Time = 1.000E-01
Time = 2.000E-01
Time = 4.000E-01
Time = 7.286E-01
Le_eff
r, cm
0
2
4
6
8
10
0
0.1
0.2
0.3

Fig 86

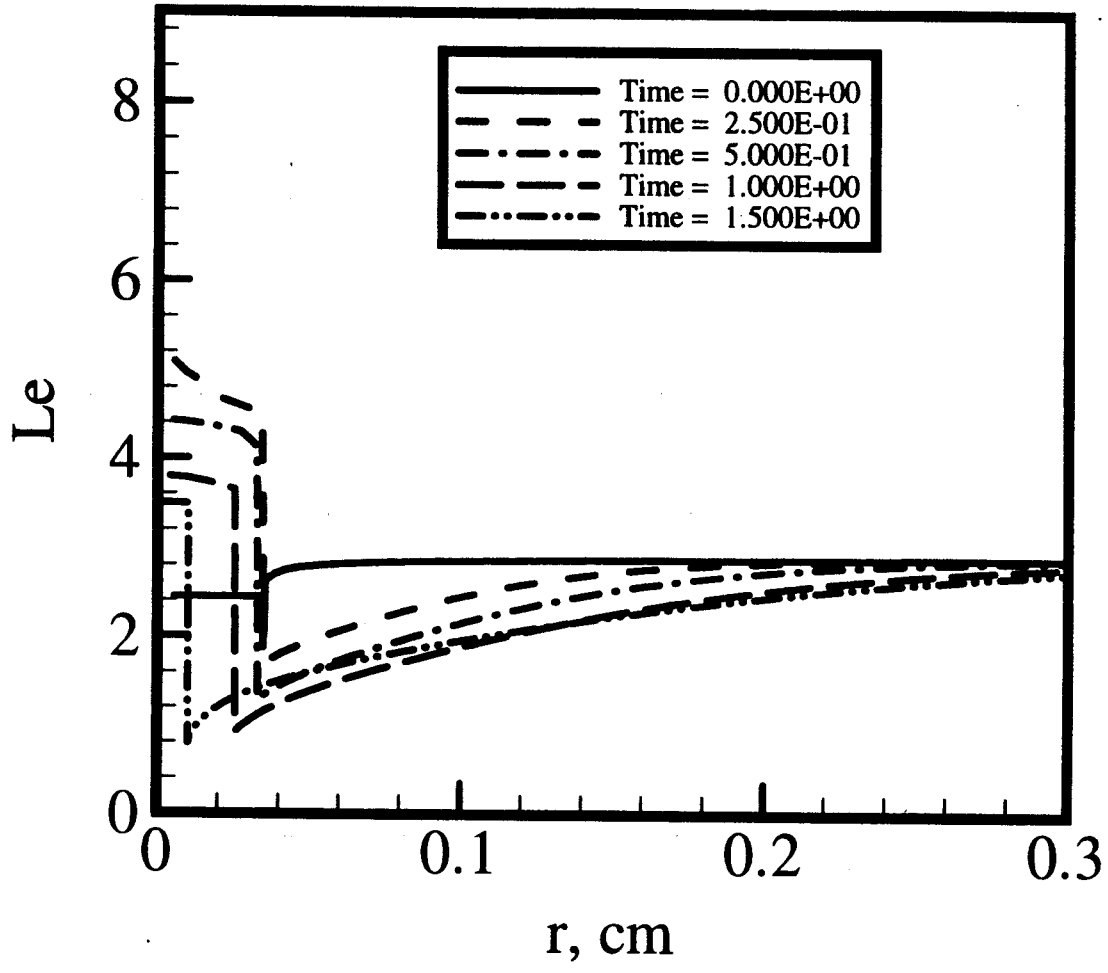
Time = 0.000E+00
Time = 2.500E-01
Time = 5.000E-01
Time = 1.000E+00
Time = 1.500E+00
Le
0
2
4
6
8
0
0.1
0.2
0.3
r, cm

Fig 8c

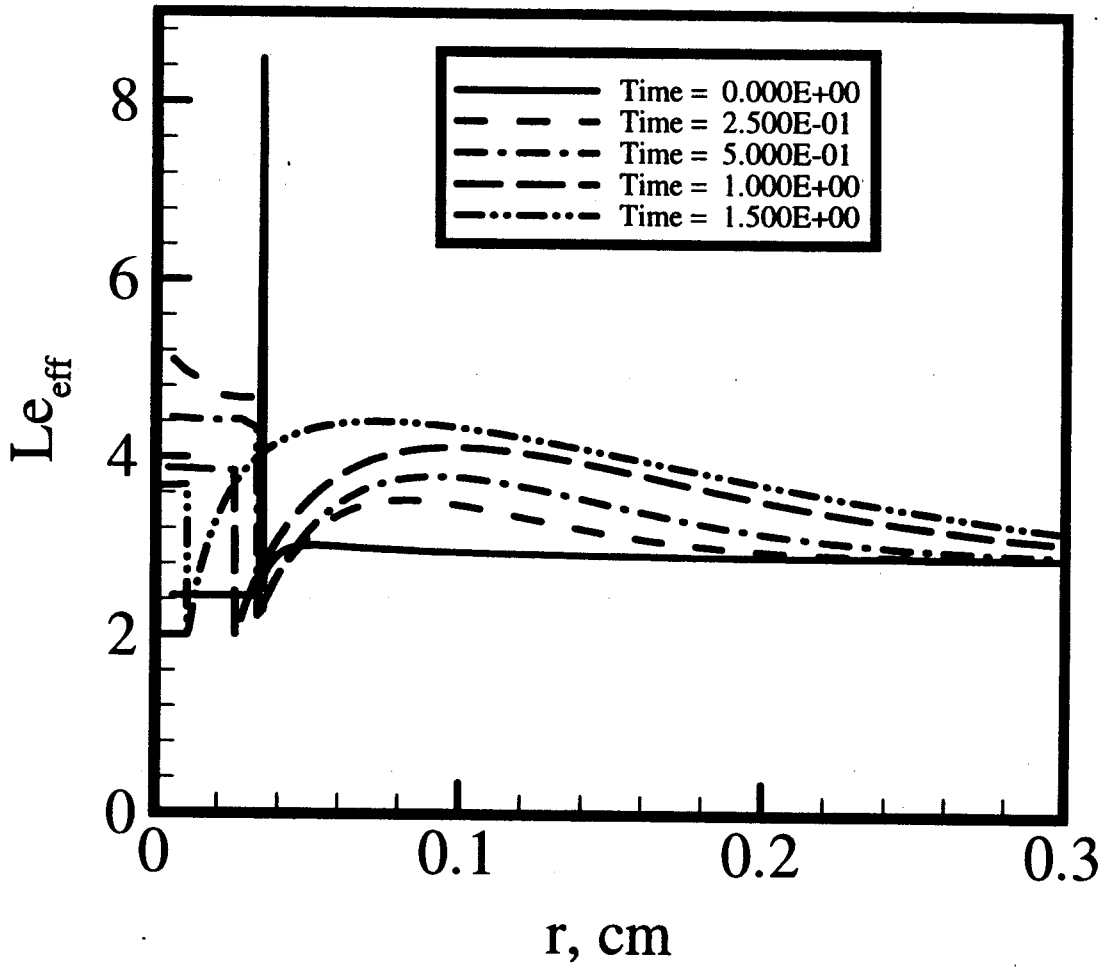
Time = 0.000E+00
Time = 2.500E-01
Time = 5.000E-01
Time = 1.000E+00
Time = 1.500E+00
Le_eff
0
2
4
6
8
0
0.1
0.2
0.3
r, cm

Fig 8d

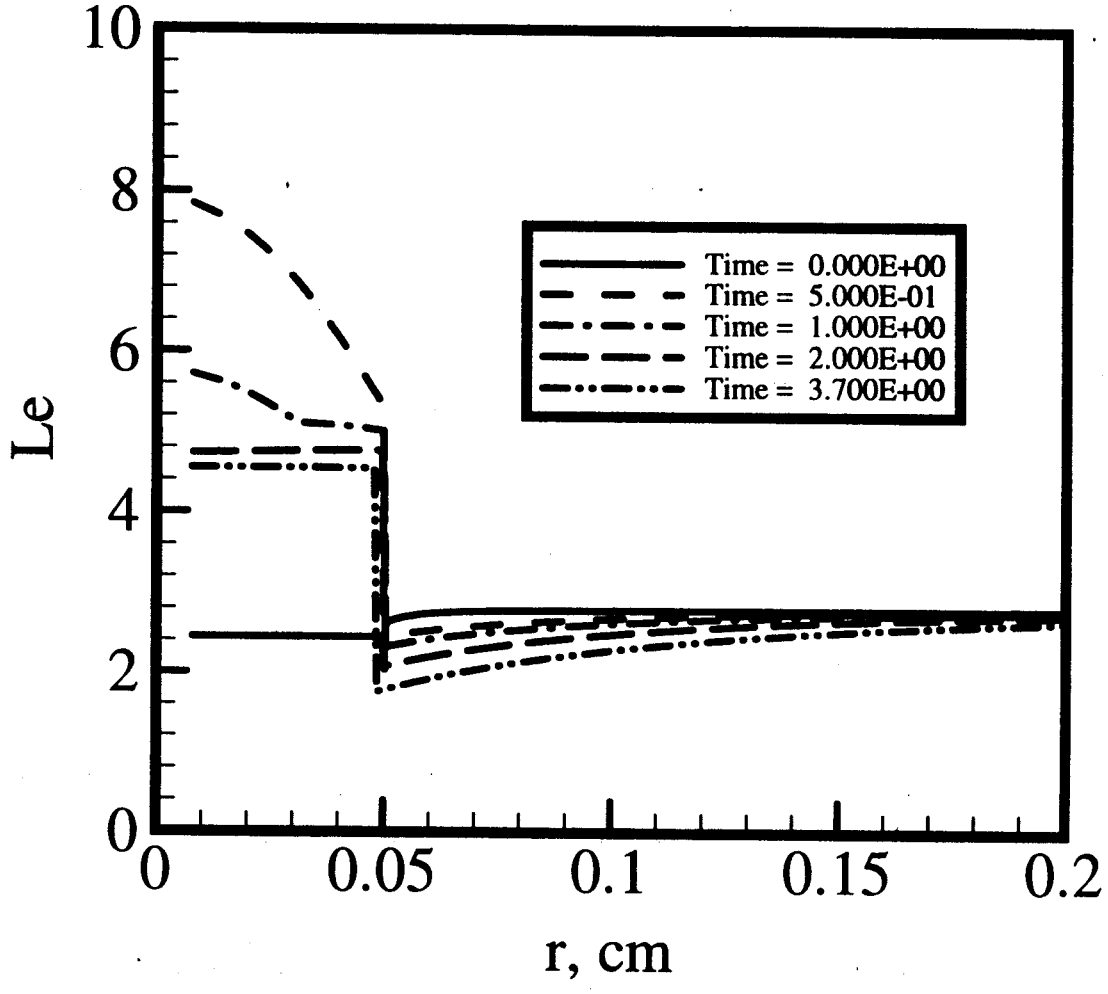
10
8
6
4
2
0
Le
0
0.05
0.1
0.15
0.2
r, cm
Time = 0.000E+00
Time = 5.000E-01
Time = 1.000E+00
Time = 2.000E+00
Time = 3.700E+00

Fig 9a

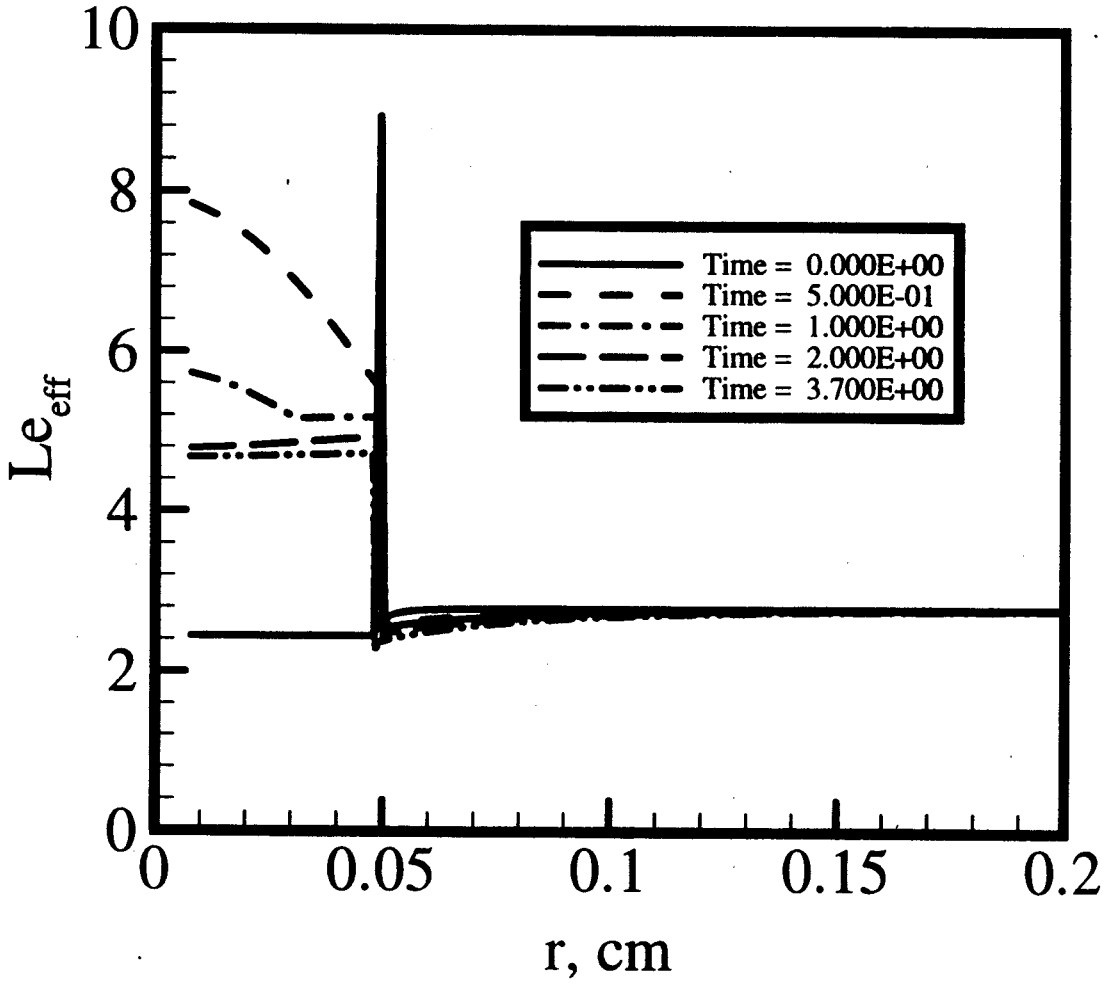
10
8
6
4
2
0
0
0.05
0.1
0.15
0.2
Le_{eff}
r, cm
Time = 0.000E+00
Time = 5.000E-01
Time = 1.000E+00
Time = 2.000E+00
Time = 3.700E+00

Fig 96

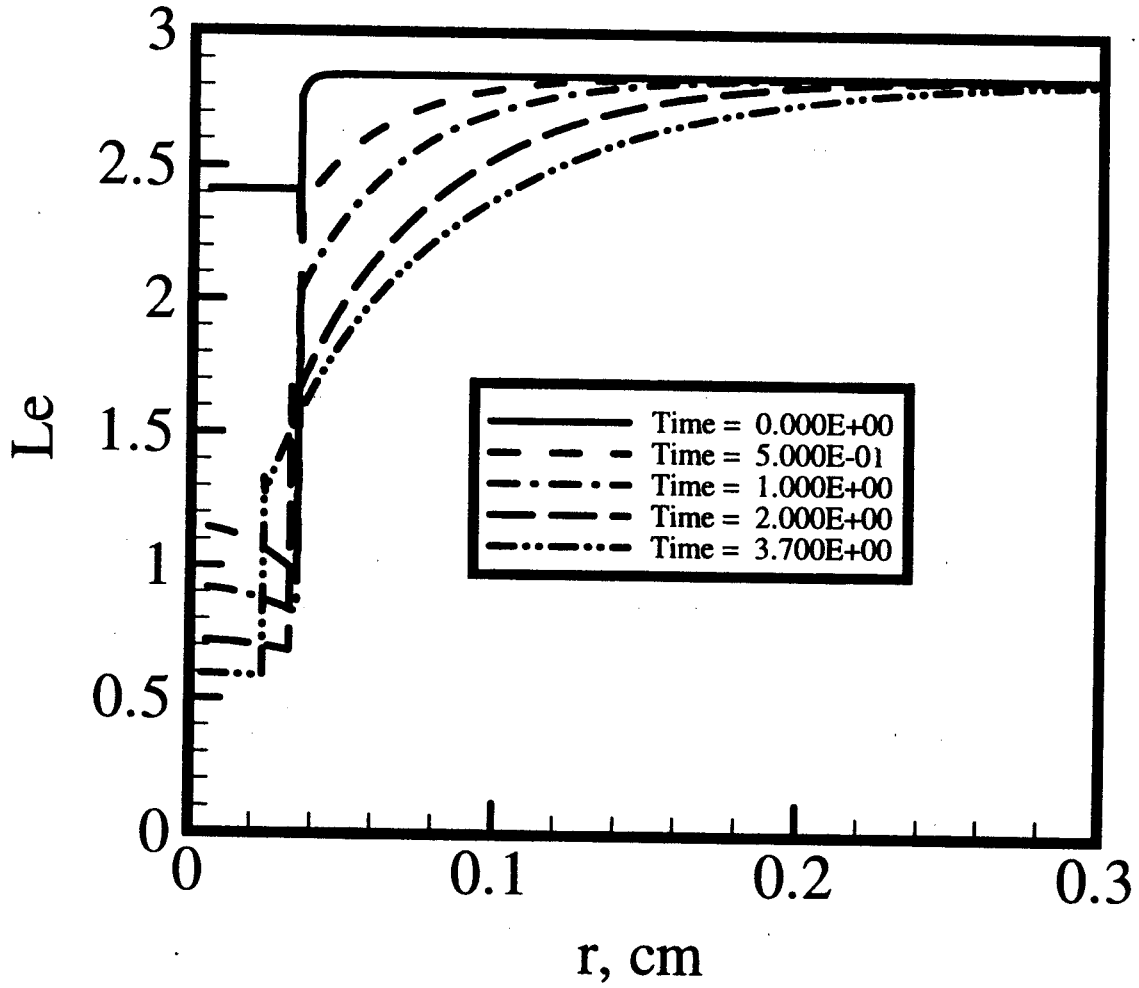
Le
r, cm
0
0.5
1
1.5
2
2.5
3
0
0.1
0.2
0.3
Time = 0.000E+00
Time = 5.000E-01
Time = 1.000E+00
Time = 2.000E+00
Time = 3.700E+00

Fig 9c